VARIATIONS

doi: 10.5065/6n20-pe38

Spring 2022 • Vol. 20, No. 2

Table of Contents

US CLIVAR VARIATIONS

Editors:
Jennie Zhu, Sam Coakley, Alyssa Cannistraci, and Mike Patterson
US CLIVAR Project Office
www.usclivar.org

Needs and prospects for advancing tropical Pacific observations of the ocean and atmosphere

Guest editors:
Charlotte DeMott[1] and Aneesh Subramanian[2]

[1]Colorado State University
[2]University of Colorado

Welcome to this issue of the US CLIVAR *Variations* focused on the Tropical Pacific Observing System (TPOS) and related process studies, where we spotlight emerging science and evolving needs in tropical Pacific observations critical for advancing Earth system predictions.

The tropical Pacific Ocean drives global climate variability, weather extremes, and ecosystem dynamics. This collection of articles highlights the forefront of observational and modeling science aimed at improving our understanding and prediction of key coupled ocean-atmosphere processes, and the observations needed to achieve these objectives.

We begin with Kumar et al., who provide a broad perspective on the critical observational needs for initializing Earth system models and reducing persistent biases. They emphasize two key components: the need for sustained observations on subseasonal-to-seasonal (S2S) and subseasonal-to-decadal (S2D) timescales and targeted process studies of phenomena like upper ocean mixing and barrier layer formation.

Jauregui and Chen delve into the intricate interactions between the Madden-Julian Oscillation (MJO) and El Niño-Southern Oscillation (ENSO), focusing on how MJO-driven oceanic and atmospheric processes modulate the timing of El Niño onset via ocean Kelvin waves and freshwater jets. They present detailed ocean-atmosphere diagnostics of processes relevant to the variability of the eastern edge of the West Pacific Warm Pool.

Building on the theme of ocean-atmosphere coupling, Eddebar et al. explore the equatorial Pacific cold tongue, a region vital to climate variability and marine ecosystems. Their paper outlines the urgent need for more comprehensive turbulence and tracer observations to better resolve the processes driving biogeochemical dynamics and ocean heat uptake.

Turning to atmospheric observations, Wolding et al. question whether the current and planned marine boundary layer observations are sufficient to support initiatives like the "Decade of Convection." They stress that systematic errors in models often stem from limited measurements in key convective regimes of the tropical Pacific.

Drushka et al. highlight the strengths and gaps in satellite-based observing capabilities, particularly the challenge of resolving fine-scale variability and the vertical structure of coupled marine boundary layers.

Complementing these observational studies, Fujii et al. illustrate how adjoint sensitivity methods can diagnose the spatial-temporal value of observations and identify gaps. Their analysis underscores the importance of existing systems, like the TPOS array and Argo, while pointing to critical areas for enhanced monitoring.

Finally, Thompson et al. provide a comprehensive review of the operational in-situ observing system across the tropical Pacific, showing how the current network—from moorings to drifters—is the backbone for advancing research and operational forecasting.

Together, these papers articulate a vision for the next generation of tropical Pacific observations, blending sustained monitoring with targeted process studies to reduce uncertainties and unlock new predictive capabilities for the Earth system.

We hope this issue sparks further dialogue and collaboration as we advance towards a more integrated and impactful observing system.

Tropical Pacific observing needs for Earth system predictions

Arun Kumar[1], Magdalena Balmaseda[2], Antonietta Capotondi[3], and Terence O'Kane[4]

[1]NOAA Climate Prediction Center
[2]European Centre for Medium–Range Weather Forecasts
[3]NOAA Physical Sciences Laboratory and University of Colorado / Cooperative Institute for Research in Environmental Sciences
[4]Commonwealth Scientific and Industrial Research Organisation, Oceans and Atmosphere

The consequences of weather and climate variability intersect with large swaths of society. Prolonged droughts and flash floods, along with many other extremes, all have substantial impacts on the economy, while posing further threats to loss of life and property. To ameliorate adverse consequences or to benefit from favorable climate conditions, decision makers can benefit from knowing the future weather and climate conditions. One approach for providing outlooks for the evolution of the current climate is based on Earth System prediction models.

The basic premise of dynamical Earth System prediction methods is the specification of the initial state for various model components (e.g., the initialization) followed by the forward integration of equations of motion. Although dynamical models work to incorporate physical processes that occur in the Earth System components, inadequate understanding of physical processes and approximations involved in their representation in the models results in biases in the models' depiction of observed climate variability.

The requirements that (i) dynamical models need to be initialized and (ii) observational data is needed to understand and reduce model biases guide requirements for the observing system needs. In this article, needs for the Tropical Pacific Observing System (TPOS), in the context of Earth System prediction, are discussed.

Needs for TPOS: Sustained observations

The needs for TPOS can be separated into two categories: (i) sustained observations and (ii) process studies which will collect observations for improved understanding of processes that govern aspects of climate variability to improve their representation in prediction models.

The need for sustaining real-time weather and climate predictions requires an infrastructure of sustained observations and these requirements differ for predictions for weather, subseasonal to seasonal (S2S), and decadal time scales. Unique features of climate variability in the tropical Pacific that include El Niño-Southern Oscillation (ENSO), the Madden-Julian Oscillation (MJO), and tro-

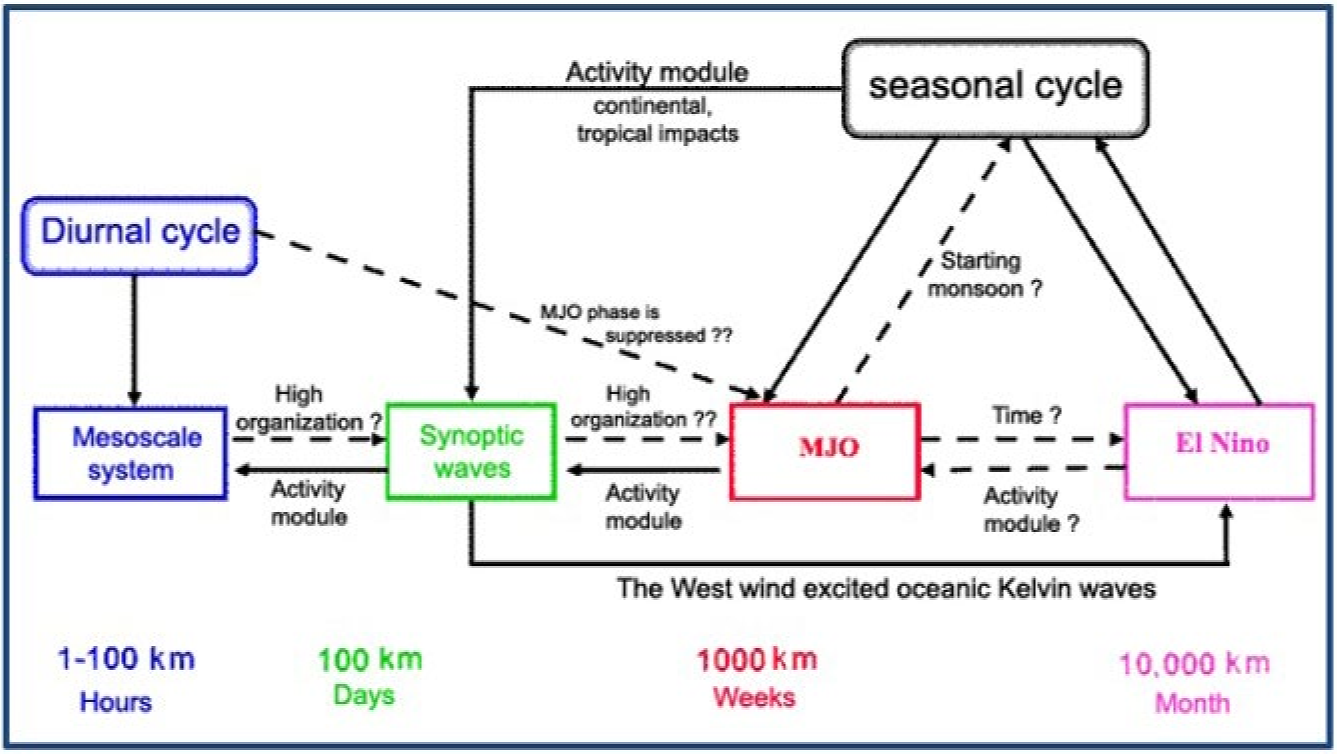

Figure 1. Physical processes on different spatial and temporal scales that are of importance in the tropical Pacific and that govern the multi-scale interactions in ocean-atmospheric boundary layer. TPOS needs to sample relevant spatial and temporal scales to improve understanding, modeling, and prediction. Skill in predicting phenomenon like ENSO and MJO is the underlying source of predictability on longer timescales (Slingo et al. 2006).

pical instability waves (TIW) also place distinctive requirements for the TPOS (Figure 1).

Sustained observations are needed for the estimation of the ocean state and the atmosphere when using data assimilation (DA) techniques. The most critical observations to capture are variables needed for the initial conditions for forward integration. These variables in the ocean temperature, salinity, and currents; and atmospheric temperature, humidity, and winds. Additional variables that are used in DA are surface pressure and sea surface heights.

Spatial and temporal requirements for observations in support of S2S predictions depend on the phenomena that are important sources of predictability. The importance of ENSO on seasonal prediction requires spatial and temporal sampling that can adequately resolve features that are important for ENSO evolution and these may depend on the decorrelation scales of variables to be observed. The spatial design of the TAO array relied on the spatial decorrelation scales of the surface zonal and meridional wind in the equatorial Pacific because of their importance in modulating ENSO variability (Harrison and Luther 1990; Wen and Kumar 2020). Similarly, the westerly wind events associated with the MJO in the western Pacific are important for ENSO so observing requirements over that region must take these corresponding scales of variability into account.

The surface fluxes of heat, momentum, and precipitation from atmospheric reanalyses have large errors, and it is believed that the large part of the uncertainty is not related to the bulk formulation, but to the poor knowledge of state variables, such as directional surface wind, skin temperature, and 2 m temperature (Cronin et al. 2019). Reference in-situ measurements of these variables will greatly help their retrievals at a global scale from satellite instruments, which will indirectly translate into improving ocean initialization and facilitate model and DA developments.

On decadal timescales, the observables of interest are related to the representation of the large-scale teleconnections and their phases (e.g., ENSO, North Atlantic Oscillation (NAO), and the Atlantic Meridional Overturning Circulation (AMOC)) (Harries and O'Kane 2021). In decadal prediction, the challenge is to detect the trends associated with the occurrence and frequency of particular phases of the low frequency modes of variability while limiting the impact of rapidly growing errors due to the fastest spatio-temporal scales (weather) in the system. This is a classic signal to noise problem but one where the signal, although weak, is often highly predictable in certain regions but requires large ensemble forecasts to capture (Smith et al. 2019; 2020).

Decadal predictions require observations relevant to the many processes within the broader Earth system that can influence large scale variations in the TPOS because of the wide range of timescales involved (O'Kane et al. 2014). Hence, a globally heterogeneous observing system of the atmosphere, oceans, land, and sea ice that enables quality-controlled observations to be interpolated through space and time with sufficient spatial and temporal density to provide accurate estimates of the evolution of the major climate teleconnections is required. Such a system has only been in existence for the oceans over the most recent decades such that we only have a largely climatological stationary estimate of the subtropical upper oceans prior to the early 2000's, with the deep ocean remaining largely unobserved. That said, with the advent of "deep Argo" and increasingly accurate satellite observations of sea surface height, total water storage and the geoid from GRACE and SMOS, there are now additional observational constraints to be exploited for DA and forecast system design.

Ancillary practices need to be in place to monitor that collected observations are being adequately utilized. As multiple operational centers are engaged in analysis and predictions (Graham et al. 2011), coordinated efforts to monitor what observational data is received in real-time and how it is used in the DA systems need to be put in place. Similarly, methods to monitor the efficacy of observations in constraining the state of the ocean and atmosphere, along with the relative utility of different observing platforms on subsequent forecasts, are also essential.

Needs for TPOS: Process studies

Although variables that are ingested in the DA systems are the most critical to sustaining prediction systems, observations of other non-assimilated variables on the observation platforms of opportunity can play a critical, supportive role. The inclusion of instruments that provide measurements of radiative fluxes, rainfall, and covariances on the tropical moored array can provide important constraints in validating corresponding variables that are produced as part of DA thereby providing an assessment of model biases.

A challenge in our efforts to reduce model biases is our inadequate understanding of some phenomena. Examples include but are not limited to diurnal variability at the ocean-atmosphere boundary layers, vertical mixing in the ocean (Figure 2), and processes that govern the

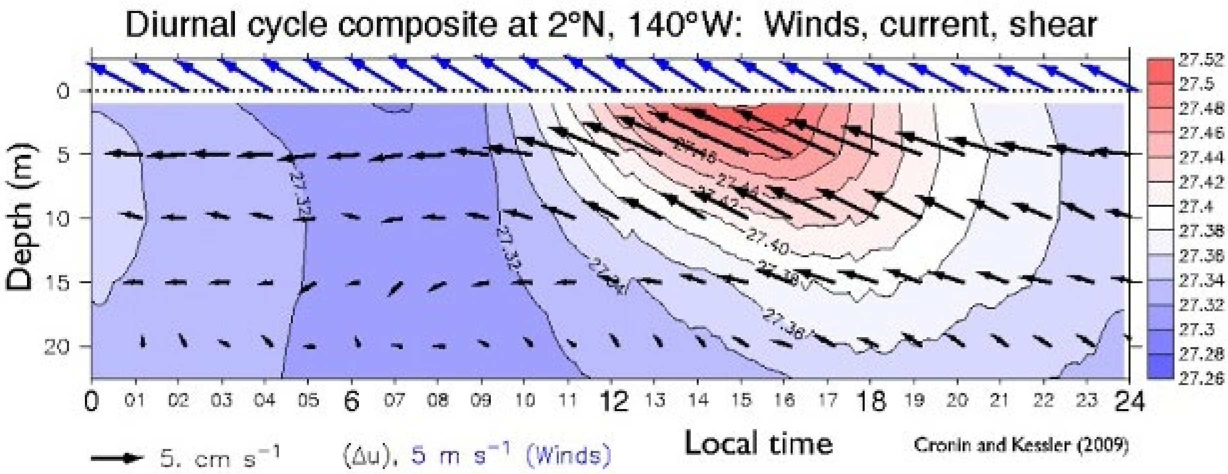

Figure 2. A composite analysis of diurnal variability at the ocean-atmosphere interface in the equatorial eastern Pacific. Blue vectors represent surface wind, color shading represents ocean temperature, and black vectors are ocean currents (relative to at 25-meter depth). In response to the diurnal variability, heating and ocean currents propagate downward through the evening. The influence of diurnal variability can rectify in constraining the mean climate and needs to be correctly represented in Earth System models (Cronin and Kessler 2009; Cravatte et al. 2016). © American Meteorological Society. Used with permission.

evolution of barrier layers in the western Pacific. Improved simulation of these phenomena in the prediction models requires a period of intensive observations targeting (often non-traditional) variables that are deemed of importance for specific phenomenon and associated interactions (Figure 1). Such highly targeted field programs aim to provide observations at a much higher spatial and temporal scale.

Determining what process studies are of high importance requires the close interaction of the modeling and the observational communities. Following this approach, TPOS 2020 recommended process studies including one to better understand mixing physics in the regions of equatorial upwelling. Best practices for process studies are discussed by Cronin et al. (2009) and Sprintall et al. (2020).

TPOS needs for evolving requirements

In order for the TPOS to serve the evolving prediction needs, planning for the evolution in the observing system and platforms should be cognizant of (i) evolving prediction requirements, (ii) deficiencies in the prediction skill of some important features of climate variability, and (iii) possible changes in characteristics of the key phenomenon of climate variability.

Coupled data assimilation (CDA) systems are rapidly developing and are expected to play an essential role in advancing numerical weather prediction (NWP), S2S, and decadal forecasting systems (Penny et al. 2019). CDA refers to the assimilation of observational data using a coupled forecast model. Weakly coupled DA (WCDA) (Saha et al. 2010; 2014) does not allow for observations to exert information across domains within the analysis cycle. For example, an ocean observation will only directly influence ocean state variables while indirectly influencing the atmosphere via ocean-atmosphere fluxes at the interface in posterior cycles in a WCDA system. Strongly coupled DA (SCDA) (Sandery et al. 2020; O'Kane et al. 2021a and 2021b) allows observations from one domain to directly influence the state estimation and model initialization in another via a cross-domain covariance. For example, high-frequency measurements of the ocean mixed layer along the equator are allowed to make corrections to the estimated atmospheric surface winds via known correlations in forecast errors in a SCDA system. There is also the multi-incremental formulation with successive iterations followed by the European Centre for Medium-Range Weather Forecasts (ECMWF) which allows for observational information to propagate across domains during the analysis cycle without the need for covariances. Examples of applications following this approach are coupled reanalyses like CERA-20C (Laloyaux et al. 2018) and CERA-SAT (Schepers et al. 2018). As CDA methods are being developed, there will be an increased need for concurrent observations across the ocean-atmosphere interface, including measurements of air-sea fluxes.

The current generation of S2S and decadal prediction systems mostly focus on the prediction of physical variables. As societal needs evolve, meeting requirements for the prediction of biogeochemical processes will become more important. TPOS needs to be forward-looking and start considering the development of cost-effective observational technologies and changes in sensors on existing observational platforms to meet requirements for the prediction of the biogeochemical variables (Kessler et al. 2019; Kessler et al. 2021).

Emerging requirements also include addressing changes in ENSO characteristics and improving the prediction of different ENSO flavors. ENSO events exhibit a large diversity in spatial patterns and temporal evolution. In particular, whether the largest sea surface temperature (SST) anomalies in the tropical Pacific occur in the Eastern (EP; Figure 3a) or Central (CP; Figure 3c) equatorial Pacific appears to affect ENSO's global impact (Larkin and Harrison 2005; Capotondi et al. 2019; Patricola et al. 2020). Thus, skillful predictions of different ENSO types are critical for decision-making. Unfortunately, current state-of-the-art operational forecast systems have difficulty in differentiating between EP and CP El Niño events at lead times longer than 2-3 months (Hendon et al. 2009; Kirtman et al. 2014; Ren et al. 2019).

Recent studies have also identified different precursors for EP and CP events which may improve models' prediction skill, if they are properly represented in the models' initialization. The zonal slope of the thermocline, for example, appears to play a key role in controlling the type of a developing El Niño event: an enhanced zonal thermocline slope favors CP-type events, while a reduced zonal thermocline slope is more conducive to EP events 2–3 seasons later (Capotondi and Sardeshmukh 2015). This is consistent with the predominance of CP El Niños during decadal periods characterized by La Niña-like background conditions, as seen in observations from recent decades (McPhaden et al. 2011; Figure 3e-f). Thus, initialization of the upper-ocean density structure and zonal thermocline slope is a necessary condition for the models' ability to differentiate between El Niño flavors.

In addition to local precursors in the equatorial Pacific, off-equatorial SST and wind conditions, especially those associated with the North and South Pacific Meridional Modes (Chiang and Vimont 2004; Zhang et al. 2014), play an important role in the development of CP events. The development of EP events, on the other hand, appears to be primarily controlled by equatorial processes (Capotondi and Ricciardulli 2021; Vimont et al. 2022). Thus, the TPOS should capture both equatorial and off-equatorial wind and SST precursors for advancing the understanding, modeling, validation, and prediction of ENSO diversity.

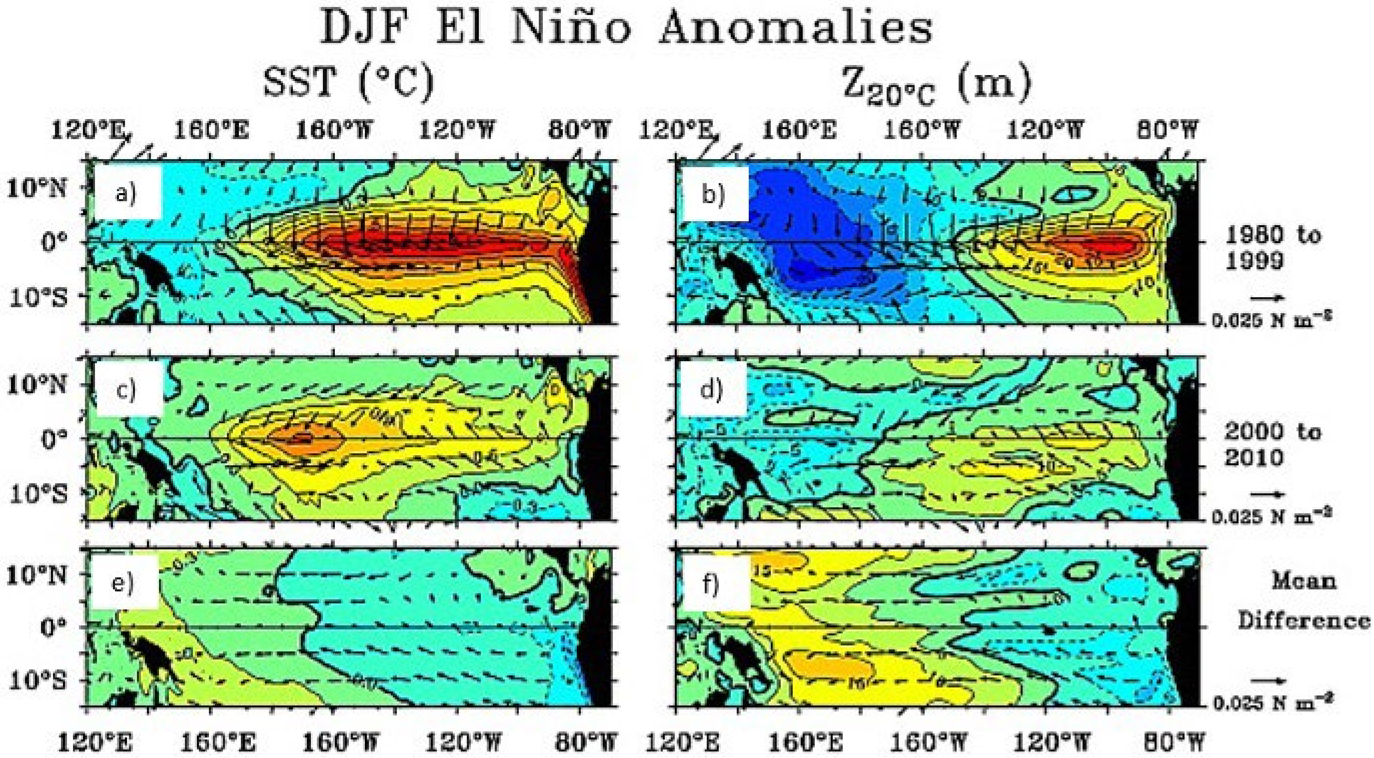

Figure 3. Composites of (a) SST (in °C) and (b) Z20 (in m) for December-February (DJF) of El Niño years during 1980–1999 with zonal wind stress (in N m−2) overplotted on both. (c and d) Same as Figures 3a and 3b but for 2000–2010. Decadal mean differences (2000–2010 minus 1980–1999) of (e) SST (in °C) and (f) Z20 (in m). Z20 is the depth of 20 °C isotherm, used as a proxy for thermocline depth. Adapted from McPhaden et al. (2011).

Unresolved issues

In the context of the sustained TPOS to support predictions in a cost-effective manner, spatial and temporal sampling requirements need to be carefully assessed. This assessment needs to consider the current capabilities of DA systems and their future evolution. For example, most of the ocean data assimilation systems used daily average data from moorings, thus filtering the high-frequency signal. Studies are required to quantify observations on what temporal frequency may be adequate in the determination of the ocean state that can be resolved by the current capabilities of DA systems. Similar considerations exist for the retention of observations during the early stages of the forecast. For instance, the correct initialization of the ocean and atmospheric boundary layers is challenging, and often the observational information is not retained correctly in the forecast. The mixed layer impacts the coupled processes at the early stages of the forecast. For instance, Yao et al. (2021) found that errors in the initialization of the upper ocean significantly degrade the extended range predictions of the MJO. Focused experiments targeting the initialization of the mixed layer would help to tackle this problem. Any efforts targeting this topic will be hampered without good-quality reference verification datasets. Currently, reference datasets for verification of mixed layer variability are lacking.

The status of TPOS evolution towards meeting Earth System prediction needs

Readers interested in the evolution of the TPOS towards meeting and sustaining requirements for Earth System predictions are invited to consult reports from the TPOS 2020 Project (Cravatte et al. 2016; Kessler et al. 2019; Kessler et al. 2021). While TPOS 2020 has come to an end and is moving into an implementation phase, similar exercises need to be repeated on a periodic basis to understand the evolution in the requirement for the TPOS because of advances in prediction systems, societal priorities, and changes in observational technologies.

References

Capotondi, A., and L. Ricciardulli, 2021: The influence of Pacific winds on ENSO diversity. *Sci. Rep.*, **11**, 18672, https://doi.org/10.1038/s41598-021-97963-4.

Capotondi, A., and P. D. Sardeshmukh, 2015: Optimal precursors of different types of ENSO events. *Geophys. Res. Lett.*, **42**, 9952-9960, https://doi.org/10.1002/2015GL066171.

Capotondi, A., P. D. Sardeshmikh, E. Di Lorenzo, A. C. Subramanian, and A. J. Miller, 2019: Predictability of US West Coast ocean temperatures is not solely due to ENSO. *Sci. Rep*., **9**, https://doi.org/10.1038/s41598-019-47400-4.

Chiang, J. C. H., and D. J. Vimont, 2004: Analogous Pacific and Atlantic meridional modes of tropical atmosphere–ocean variability. *J. Clim.*, **17**, 4143–4158, https://doi.org/10.1175/JCLI4953.1.

Cravatte, S., and Coauthors, 2016: First Report of TPOS 2020. GOOS-215, 200 pp, https://tropicalpacific.org/tpos2020-project-archive/reports/.

Cronin, M. F., and Coauthors, 2019: Air-sea fluxes with a focus on heat and momentum. *Front. Mar. Sci.*, **6**, https://doi.org/10.3389/fmars.2019.00430.

Cronin, M. F., and W. S. Kessler, 2009: Near-surface shear flow in the tropical Pacific cold tongue front. *J. Phys. Oceanogr*., **39**, 1200–1215, https://doi.org/10.1175/2008JPO4064.1.

Cronin, M. F., S. Legg, and P. Zuidema, 2009: Climate research: Best practices for process studies. *Bull. Amer. Meteor. Soc.*, **90**, 917-918, https://doi.org/10.1175/2009BAMS2622.1.

Graham, R., and Coauthors, 2011: Long-range forecasting and global framework for climate services. *Clim. Res.*, **47**, 47-55, https://doi.org/10.3354/cr00963.

Harries, D., and T. J. O'Kane, 2021: Dynamic Bayesian networks for evaluation of Granger causal relationships in climate reanalyses. *J. Adv. Model. Earth Syst.*, **13**, https://doi.org/10.1029/2020MS002442.

Harrison D. E., and D. S. Luther, 1990: Surface winds from tropical Pacific islands—climatological statistics. *J. Climate*, **3**, 251–271, https://doi.org/10.1175/1520-0442(1990)003<0251:SWFTPI>2.0.CO;2.

Hendon, H. H., E. Lim, G. Wang, O. Alves, and D. Hudson, 2009: Prospect for predicting two flavors of El Niño. *Geophys. Res. Lett.*, **36**, https://doi.org/10.1029/2009GL040100.

Kessler, W. S., and Coauthors, 2019: Second Report of TPOS 2020. GOOS-234, 265 pp, https://tropicalpacific.org/tpos2020-project-archive/reports/.

Kessler, W. S., and Coauthors, 2021: Final Report of TPOS 2020. GOOS-268, 83 pp, https://tropicalpacific.org/tpos2020-project-archive/reports/.

Kirtman, B. P., and Coauthors, 2014: The North American multi-model ensemble. *Bull. Amer. Meteor. Soc.*, **95**, 585-601, https://doi.org/10.1175/BAMS-D-12-00050.1.

Laloyaux, P., and Coauthors, 2018: Cera-20c: A coupled reanalysis of the twentieth century. *J. Adv.Model. Earth Syst.*, **10**, 1172–1195, https://doi.org/10.1029/2018MS001273.

Larkin, N. K., and D. E. Harrison, 2005: On the definition of El Niño and associated seasonal average U.S. weather anomalies. *Geophys. Res. Lett.*, **32**, https://doi.org/10.1029/2005GL022738.

McPhaden, M. J., T. Lee, and D. McClurg, 2011: El Niño and its relationship with changing background conditions in the tropical Pacific Ocean. *Geophys. Res. Lett.*, **38**, https://doi.org/10.1029/2011GL048275.

O'Kane, T. J., and Coauthors, 2021a: CAFE60v1: A 60-year large ensemble climate reanalysis. Part I: System design, model configuration and data assimilation. *J. Climate*, **34**, 5153-5169, https://doi.org/10.1175/JCLI-D-20-0974.1.

O'Kane, T. J., and Coauthors, 2021b: CAFE60v1: A 60-year large ensemble climate reanalysis. Part II: Evaluation, *J. Climate*, **34**, 5171-5194, https://doi.org/10.1175/JCLI-D-20-0518.1.

O'Kane, T. J., R. Matear, M. Chamberlain, and P. Oke, 2014: ENSO regimes and the late 1970's climate regime shift: The role of synoptic weather and South Pacific ocean spiciness. *J. Comp. Phys.*, **271**, https://doi.org/10.1016/j.jcp.2013.10.058.

Patricola, C., and Coauthors, 2020: Maximizing ENSO as a source of western US hydroclimate predictability. *Clim. Dyn.*, **54**, 351-372, https://doi.org/10.1007/s00382-019-05004-8.

Penny, S. G., and Coauthors, 2019: Observational needs for improving ocean and coupled reanalysis, S2S prediction, and decadal prediction. *Front. Mar. Sci*., **6**, https://doi.org/ https://doi.org/10.3389/fmars.2019.00391

Ren, H. L., and Coauthors, 2019: Seasonal predictability of winter ENSO types in operational dynamical model prediction. *Clim. Dyn.*, **52**, 3869-3890, https://doi.org/10.1007/s00382-018-4366-1.

Saha, S., and Coauthors, 2010: The NCEP climate forecast system reanalysis. *Bull. Amer. Meteor. Soc.*, **91**, 1015–1057, https://doi.org/10.1175/2010BAMS3001.1.

Saha, S., and Coauthors, 2014: The NCEP climate forecast system version 2 journal of climate. *J. Clim.*, **27**, 2185-2208, https://doi.org/10.1175/JCLI-D-12-00823.1.

Sandery, P. A., T. J. O'Kane, V. Kitsios, and P. Sakov, 2020: Climate model state estimation using variants of EnKF coupled data assimilation. *Mon. Wea. Rev.*, **148**, 2411-2431, https://doi.org/10.1175/MWR-D-18-0443.1.

Schepers, D., E. de Boisseson, R. Eresmaa, C. Lupu, and P. de Rosnay, 2018: CERA-SAT: A coupled satellite-era reanalysis. ECMWF Newsletter, **155**, 32-37, https://doi.org/10.21957/sp619ds74g.

Slingo, J. F. Molteni, M. Moncrieff, and M. Shapiro, 2006: Organisation and maintenance of tropical convection and the Madden Julian Oscillation. THORPEX/ WCRP/ ICTP Workshop, 13 pp, https://usclivar.org/sites/default/files/documents/2015/TriesteReport.pdf.

Smith, D. M., and Coauthors, 2019: Robust skill of decadal climate predictions. *Clim. Atmos. Sci.*, **2**, https://doi.org/10.1038/s41612-019-0071-y.

Smith, D. M., and Coauthors, 2020: North Atlantic climate far more predictable than models imply. *Nature*, **583**, 796-800, https://doi.org/10.1038/s41586-020-2525-0.

Sprintall, J., V. J. Coles, K. A. Reed, A. H. Butler, G. R. Foltz, S. G. Penny, and H. Seo, 2020: Best practice strategies for process studies designed to improve climate modeling. *Bull. Amer. Meteor. Soc.*, **101**, 1842-1850, https://doi.org/10.1175/BAMS-D-19-0263.1.

Vimont, D. J., M. Newman, D. S. Battisti, and S. -I. Shin, 2022: The role of seasonality and the ENSO mode in central and east Pacific ENSO growth and evolution. *J. Clim.*, **35**, https://doi.org/10.1175/JCLI-D-21-0599.1.

Yao, J., F. Vitart, M. A. Balmaseda, T. Wu, and X. Liu, 2021: The impact of coupled data assimilation on Madden–Julian Oscillation predictability initialized from coupled satellite-era reanalysis. *Mon. Wea. Rev.*, **149**, 2897-2912, https://doi.org/10.1175/MWR-D-20-0360.1.

Wen, C., A. Kumar, and Y. Xue, 2020: Quantifying horizontal length scales for surface wind variability in the Tropical Pacific based on reanalysis. *Clim. Dyn.*, **55**, 1697-1709, https://doi.org/10.1007/s00382-020-05342-y.

Zhang, H., A. Clement, and P. P. Di Nezio, 2014: The south Pacific meridional mode: A mechanism for ENSO-like variability. *J. Climate*, **27**, 769-783, https://doi.org/10.1175/JCLI-D-13-00082.1.

Multiscale air-sea interaction processes contributing to the Warm Pool Eastward Extension (WPEE)

Yakelyn R. Jauregui[1] and Shuyi S. Chen[1]

[1]University of Washington

The Pacific atmosphere is coupled to the ocean on a broad range of temporal and spatial scales. The coupling occurs through different mechanisms, which lead to different climate regimes. The trade winds blowing westward affect the equatorial ocean upwelling resulting in a deep thermocline in the west and a shallow one in the east. The sloped thermocline results in warmer sea surface temperature (SST) in the west than in the east. The resulting basin-scale zonal gradient in temperature strengthens the zonal winds and determines the spatial distribution of SST and precipitation. The tropical Pacific mean climate condition is maintained by the feedback between the zonal component of the trade winds and the basin-wide temperature zonal gradient, known as the Bjerknes feedback. The western Pacific warm pool (WP) is characterized by waters above 28°C, weak winds, intense precipitation, and lower sea surface salinity (SSS). In contrast, the central Pacific is characterized by strong trade winds and upwelling that bring deep, colder and saltier waters to the surface. Thus, the eastern edge of the WP marks the boundary where large-scale winds converge to form deep convection, and the equatorial cold tongue water to the east, where trade winds prevail. The confluence of these two water masses generates a sharp zonal salinity front (34.6 PSU).

The most dominant tropical phenomena that affect global high-impact weather (tropical cyclones, extreme precipitation and drought, heat waves, and severe storm outbreaks) occur on various spatial and temporal timescales. The Madden-Julian Oscillation (MJO) and the El Niño-Southern Oscillation (ENSO) dominate the variability of the intraseasonal (30–90 days) and interannual (2–7 years) timescales, respectively (e.g., McPhaden et al. 2006; Zhang 2013), and the WP and its associated large-scale fields migrate in association with these large-scale oscillations. However, these large-scale changes result from physical continuum processes from small-scale and short-lived to long variations of the atmosphere and the ocean.

Despite extensive research on the topic of the MJO-ENSO connection in observations (Lau and Chan 1988; Kessler et al. 1995; Anderson et al. 1996; Bergman et al. 2001; Zhang and Gottschalck 2002; Maes et al. 2002, 2006; Bosc et al. 2009), and modeling studies (McPhaden and Yu 1999; Kessler and Kleeman 2000; Suzuki and Takeuchi 2000; Lengaigne et al. 2002, 2003) questions remain especially regarding the timing of the onset of El Niño. This study aims to improve the understanding of the physical mechanisms by which the MJO influences the warm pool eastward expansion (WPEE) that might lead to the onset of El Niño. Our research highlights the critical role of the MJO in upscaling the short-lived, small-scale variability where most air-sea interactions occur into a much larger atmosphere-ocean coupled phenomenon at the El Niño onset.

Model configuration

Observations alone cannot deliver a more complete picture of physical processes, modeling capabilities are needed. We use a regional atmosphere-ocean coupled model that includes full physics and yields insights into the relatively high-frequency multiscale nature of the MJO and its impact on the upper ocean. The numerical model used in this study is the Unified Wave INterface–Coupled Model (UWIN-CM; Chen et al. 2013; Chen and Curcic 2016), which allows for interactive coupling between atmosphere and ocean circulation models. The atmospheric component is the Weather Research and Forecasting (WRF V3.9) model and is constrained by reanalysis and reinitialized daily. In contrast, the ocean component (HYbrid Coordinate Ocean Model – HYCOM V2.3.0) evolves continuously and is fully coupled with the atmosphere every three minutes. We examine the period January–August 2018. Consecutive MJO events over the western Pacific were observed during the La Niña condition and were followed by a WPEE that led to El Niño 2018 onset in September 2018.

The model domain covers the entire tropical Pacific Ocean (Figure 3 in Kerns and Chen 2021). The initial and lateral boundary conditions for the atmosphere and ocean are from ECMWF ERA5 and HYCOM global analysis. The WRF model is configured with 12 km of horizontal grid spacing with 43 vertical levels and HYCOM with a uniform grid spacing of 0.08° and 41 vertical levels. Details about the UWIN-CM configuration are described in Kerns and Chen (2021). The model includes the rain/fresh water-induced salinity changes and therefore captures the formation and maintenance of the upper ocean stratification. The overall good agreement between the simulation and satellite and in-situ observations (Figure 1) gives confidence in studying the processes responsible for the WPEE. This helps us assess the observational needs that would help model development.

Mechanisms that connect the MJO(s) occurrence and El Niño initiation

The MJO's local and remote effects on the Pacific upper ocean are well known. The MJO is a planetary-scale, eastward-propagating intraseasonal convective envelope that often initiates in the Indian Ocean and propagates eastward into the Western Pacific at slow speeds (Zhang 2005). They can be considered "external forcing" to the Pacific. The multiscale nature of the MJO affects the atmosphere and ocean on timescales from days to several weeks (Kikuchi et al. 2018).

The La Niña conditions in 2017 transitioned to El Niño onset in August 2018 associated with the WPEE, which occurred only after the intense and consecutive 3 MJO events observed from January to May 2018 (Kerns and Chen 2021). Locally, each MJO-induced westerly wind burst cools the sea surface through intense evaporation and vigorous upper-ocean mixing. Westerly winds bursts (WWBs) along the equator excite Kelvin and Rossby oceanic waves. Kelvin waves propagate eastward, recognizable to the east of the forcing; during its propagation, they deepen the thermocline and induce changes in the surface and subsurface temperature and salinity fields (Figure 2). Warmer

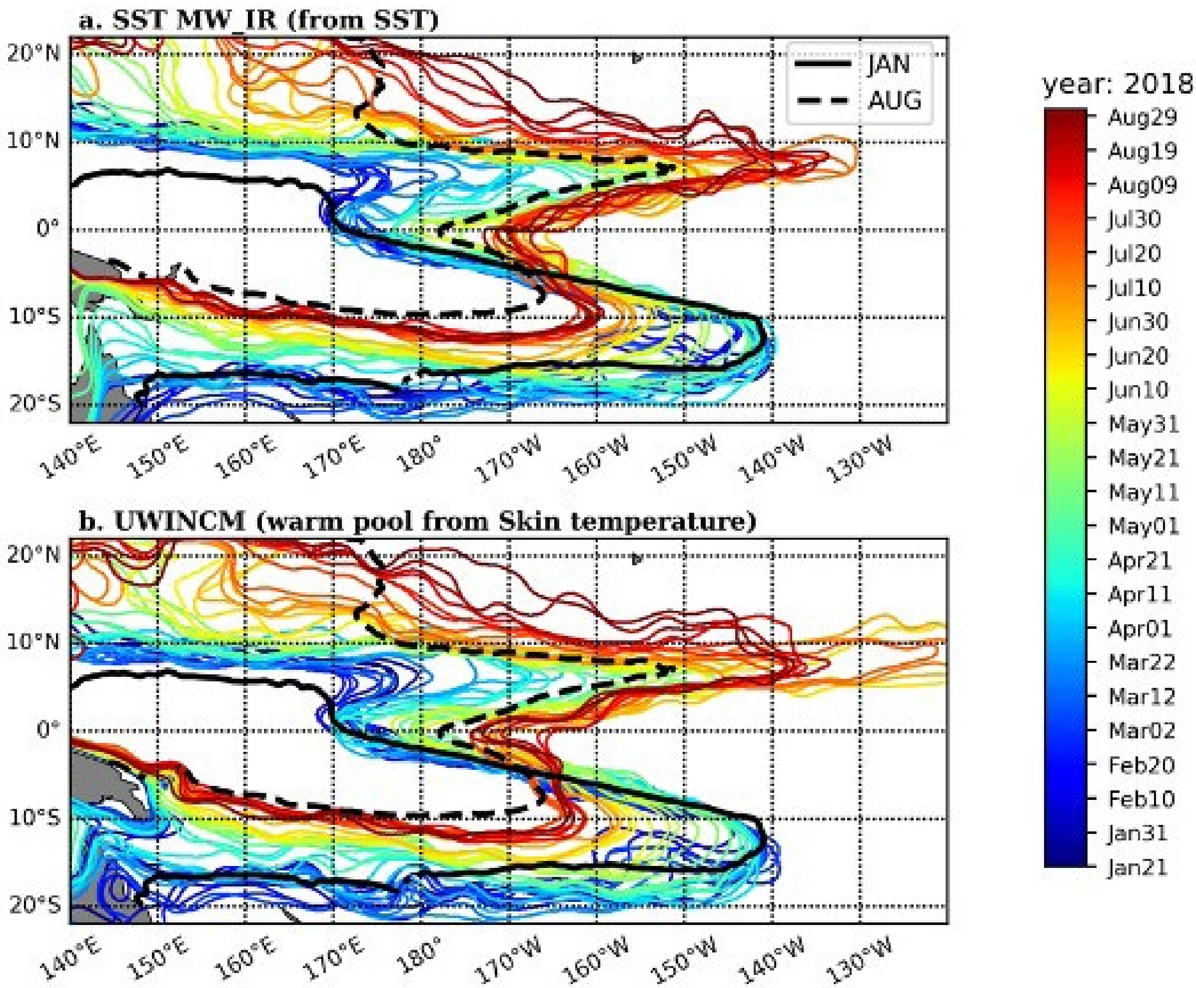

Figure 1. The warm pool (28.5°C) evolution from January 21 to August 31 color coded by dates. Contour lines indicate the climatological warm pool during January and August from 1981–2010, respectively. Courtesy of Yakelyn R. Jauregui.

waters reached Niño 3.4 region, leaving a much weaker large-scale zonal SST gradient in June–August after the third MJO event (Figure 2). The WPEE led up to the large-scale zonal SST gradient weakening (Figure 2) that favored El Niño onset in August in the same year.

It is often assumed that the upper-ocean adjustment to direct wind forcing occurs mostly through these waves by redistributing water masses and affecting surface and subsurface temperatures along the equator. The large-scale namely the dynamics of WWB-oceanic Kelvin wave namely the dynamics of WWB-oceanic and the upper ocean stratification development, act together to reduce the east-west temperature gradient, and subsequent convection and westerly winds can occur further east. Over time, if these favorable

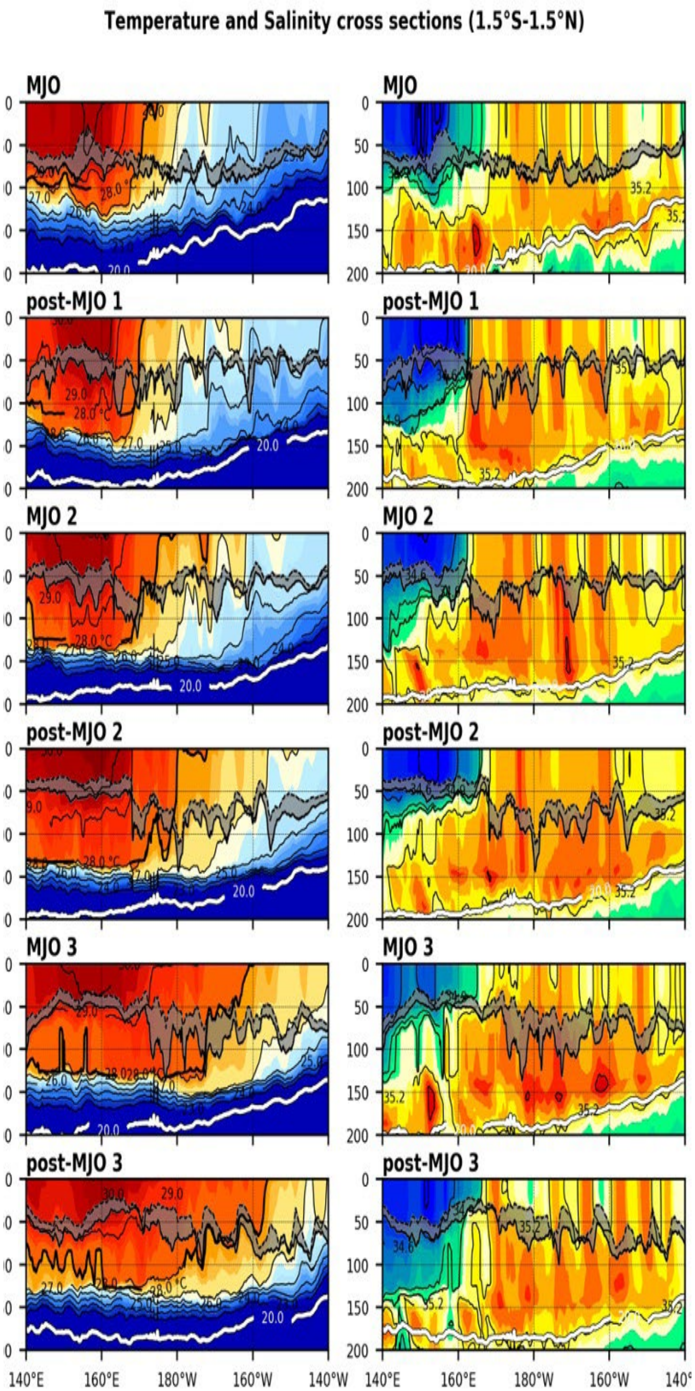

Figure 2. The equatorial (1.5°S–1.5°N) upper evolution of temperature and salinity at specific days during and after the MJO. The gray shading indicates the barrier layer, the mixed layer and isothermal depths are computed following Sprintall and Tomczak (1992), with a reference temperature at 10 m and a temperature step of -0.25°C. Courtesy of Yakelyn R. Jauregui.

adjustment is often observed as a propagating thermocline signal that affects the oceanic zonal large-scale gradient and suppresses entrainment in the central and eastern Pacific (Boulanger et al. 2004; Chen et al. 2015; Chiodi et al. 2014; Kessler et al. 1995; Kessler and Kleeman 2000). The MJO's net effect is observed on the SST warming in the central and eastern Pacific as observed in Figure 2 and widely studied in observations (McPhaden et al. 1988; Seiki and Takayabu 2007; Zhang and Gottschalck 2002).

This warming has been explained mainly through the intraseasonal ocean dynamical processes associated with MJO events. However, the ocean's response to MJO forcing is quite complex. The equatorial Pacific ocean's subsurface temperature and salinity response to the MJOs forcing (Figure 2) are observed as the expansion of a warm and fresh pool eastward caused by a combination of continuum processes. We highlight one other process that occurs immediately after the passage of the MJO; in calm wind and clear sky conditions, the presence of barrier layers (BL) maintains a warmer SST. BLs were first analyzed around 30 years ago, using observations from the tropical west Pacific (Godfrey and Lindstrom 1989; Lukas and Lindstrom 1991). These initial studies showed that the ocean mixed layer (defined by near-constant density) can be vertically separated from the top of the thermocline by a near isothermal but salt-stratified layer—the BL. Figure 2 highlights BLs in gray shading, the region of the most substantial temperature stratification (top of the thermocline) is located between 50–100 m. The region of increased density stratification is located on the top 50 m over the warm pool but can reach 100 m over the central Pacific. Since the atmosphere can respond to SST forcing much more rapidly, new deep convection and further WWBs can be triggered by these warmer waters. If the positive loop continues, the two air-sea interactive processes associated with the MJO, namely the dynamics of WWB-oceanic Kelvin waves and the upper ocean stratification development, act together to reduce the east-west temperature gradient, and subsequent convection and westerly winds can occur further east. Over time, if these favorable conditions prevail and if the loop continues, these relatively high frequency convective events shift eastward as the warm SST expands during the onset and growth stage of El Niño (McPhaden and Picaut 1990; Delcroix et al. 1994; Fink and Speth 1997; Kessler and Kleeman 2000; Lengaigne et al. 2003).

MJO-induced fresh equatorial jets

The maintenance of warmer waters over the central Pacific is crucial to the onset of El Niño. The presence and strength of BLs are of particular importance to achieve that. Kerns and Chen (2021) used the same full physics UWIN-CM simulation and compared it to another simulation that did not include the freshwater fluxes effect on the upper ocean. They found a strong density current that resembles the fresh equatorial jets observed and described for the first time by Roemmich et al. (1994). These fresh equatorial jets transport warm waters eastward maintaining the BLs and are observed in the absence of convection after the passage of the MJO convective phase and when the trade winds dominate the warm pool area (Kerns and Chen 2021). Figure 3 illustrates the vertical structure of equatorial zonal currents and salinity during and after the MJO convective phase. The combination of the MJO westerly to the west, easterly winds to the east of the WP eastern edge, and the rainfall-induced freshwater fluxes form a

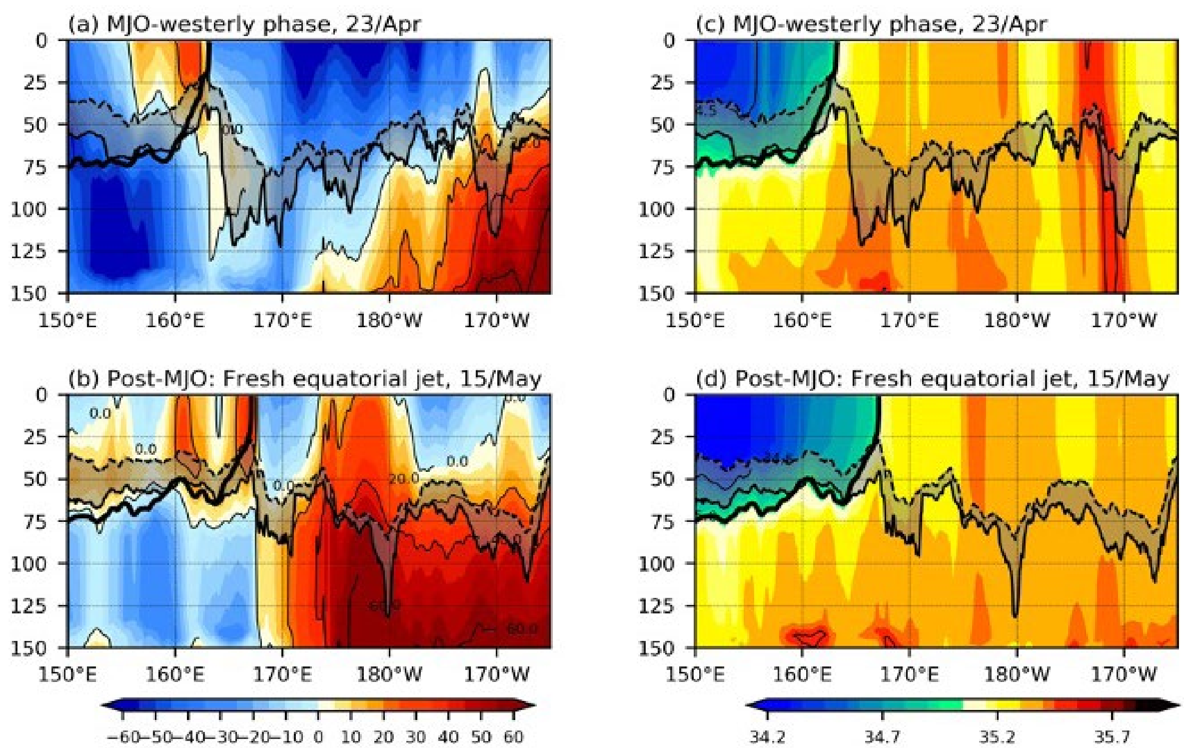

Figure 3. The equatorial (1.5°S–1.5°N) zonal currents (a, b) and salinity (c, d) in colors on April 23 and May 15, in cm/s and PSU, respectively. Black tick lines highlight the 35PSU in all panels. The gray shading indicates the barrier layer similar to Figure 2. Courtesy of Yakelyn R. Jauregui.

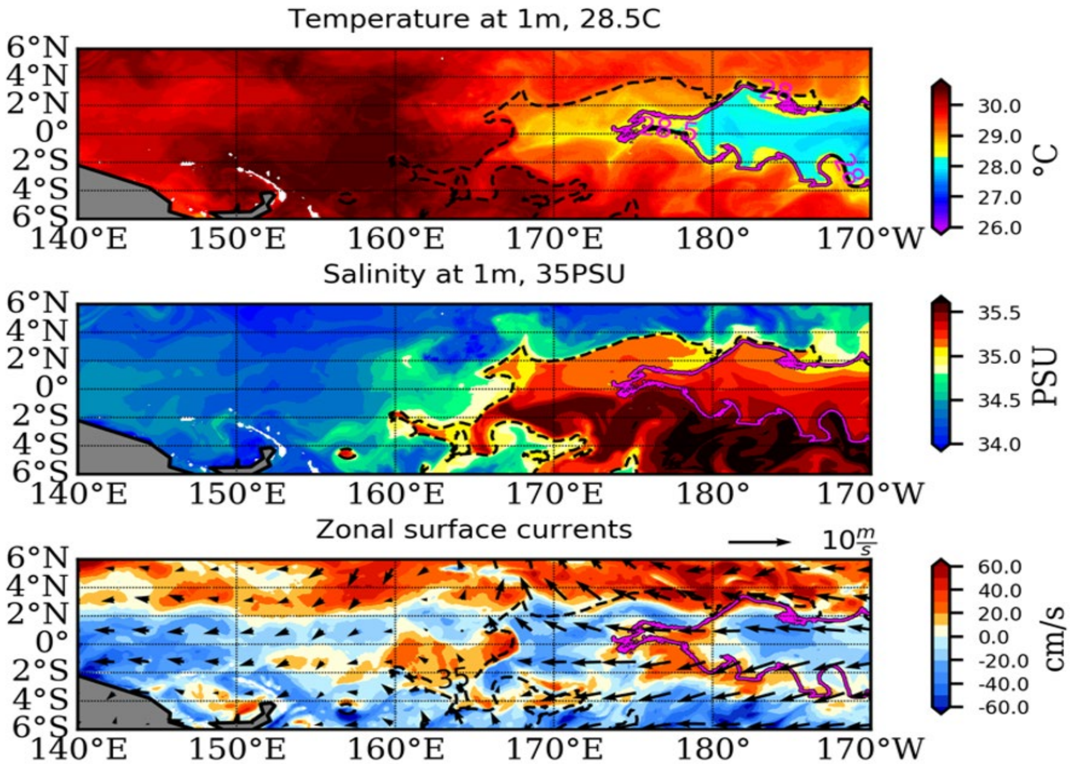

Figure 4. Temperature (top panel), salinity (middle), and zonal currents (in colors, bottom panel) at the first model level (1 m) on May 15. Winds vectors are shown in the bottom panel, the dashed black contours indicate the 35PSU and the magenta tick contour indicate the warm pool (28.5°C) in all panels. Courtesy of Yakelyn R. Jauregui.

shallower mixed layer depth to the west of the fresh pool. In contrast, deeper mixed layers are observed on the east side of the fresh pool. Beneath this mixed layer, a very thick barrier layer is found, and they persist up to 40 days after the MJO convective phase has ended.

On May 15, 22 days later, in the absence of convection and under prevailing trade winds, a fresh equatorial jet is observed confined to the uppermost 75 meters with a strong peak across the salinity front. These fresh and warm waters maintained by the presence of BLs absorb large amounts of solar radiation at the surface while being transported eastward by these jets. Jauregui and Chen (2024a) used the theory of fresh equatorial jets described in Roemmich et al. (1994). They found that these jets are driven by a strong horizontal pressure gradient force set up by the strong positive buoyancy flux over the western side of the warm pool's eastern edge. Figure 4 illustrates that several processes occur at the same time. The impact of MJO-induced rainfall on ocean dynamics is observed as fresh equatorial jets that can last beyond ten days. They are confined within 3°S–0, 160°E–168°E over the fresh pool while the MJO-induced oceanic Kelvin waves affect the eastward currents associated as they passage of across the warm pool from 175°E–180°.

Conclusions

Using over 20 years of satellite observations, Jauregui and Chen (2021) showed that consecutive MJO events occurred before the onset of each

El Niño event from 1999–2019 and have found evidence that MJO events can indeed contribute to the onset of El Niño by warming a large portion of the Niño 3.4 region (170°E–160°W, 5°S–5°N) with anomalies above 0.5°C. These prior-to-the-El Niño-onset MJO events were particularly strong in precipitation and westerly wind bursts (WWBs) and often occurred as consecutive events. The two air-sea interactive processes associated with the MJO, namely the dynamics of WWB-oceanic Kelvin waves identified by Kessler et al. (1995) and the upper ocean stratification via rainfall-induced development of BL which maintains warm SST as observed by Anderson et al. (1996), are key to understand this MJO-ENSO interaction. Together they act to reduce the east-west temperature gradient, which allows a further shift of the warm pool eastward during the onset of El Niño. The MJO impact on the upper ocean dynamics and thermodynamics favors the WPEE and maintenance of warm SSTs over the central Pacific helped by fresh equatorial jets that could last from several days to weeks (Jauregui and Chen 2022).

A more comprehensive analysis of these processes associated with the MJO-induced WPEE is currently in preparation by Jauregui and Chen (2022 a, b) and will provide a better understanding and quantitative assessment of possible sources of the ENSO prediction that is still a significant challenge in numerical models.

Acknowledgments

We are grateful to the NOAA CVP and NASA FINESST support through the grants NA18OAR4310401 (Chen) and 80NSSC21K1590 (Jauregui), respectively.

References

Anderson, S. P., R. A. Weller, and R. B. Lukas, 1996: Surface buoyancy forcing and the mixed layer of the western Pacific warm pool: Observations and 1D model results. *J. Climate*, **9**, 3056–3085, https://doi.org/10.1175/1520-0442(1996)009<3056:SBFATM>2.0.CO;2.

Bergman, J. W., H. H. Hendon, and K. M. Weickmann, 2001: Intraseasonal air–sea interactions at the onset of El Niño. *J. Climate*, **14**, 1702–1719, https://doi.org/10.1175/1520-0442(2001)014<1702:IASIAT>2.0.CO;2.

Bosc, C., T. Delcroix, and C. Maes, 2009: Barrier layer variability in the western Pacific warm pool from 2000 to 2007. *J. Geophys. Res.*, **114**, C06023, https://doi.org/10.1029/2008JC005187.

Chen, S. S., and M. Curcic, 2016: Ocean surface waves in Hurricane Ike (2008) and Superstorm Sandy (2012): Coupled model predictions and observations. *Ocean Model.*, **103**, 161–176, https://doi.org/10.1016/j.ocemod.2015.08.005.

Chen, S. S., W. Zhao, M. A. Donelan, and H. L. Tolman, 2013: Directional wind-wave coupling in fully coupled atmosphere-wave-ocean models: Results from CBLAST-hurricane. *J. Atmos. Sci.*, **70**, 3198–3215, https://doi.org/10.1175/JAS-D-12-0157.1.

Chiodi, A. M., D. E. Harrison, and G. A. Vecchi, 2014: Subseasonal atmospheric variability and El Niño waveguide warning: Observed effects of the Madden-Julian Oscillation and Westerly Wind Events. *J. Climate*, **27**, 3619–3642, https://doi.org/10.1175/JCLI-D-13-00547.1

Delcroix, T., J. P. Boulanger, F. Masia, and C. Menkes, 1994: Geosat-derived sea level and surface current anomalies in the equatorial Pacific during the 1986–1989 El Niño and La Niña. *J. Geophys. Res. Oceans*, **99**, 25093–25107, https://doi.org/10.1029/94JC02138.

Fink, A., and S. Speth, 1997: Some potential forcing mechanisms of the year-to-year variability of the tropical convection and its intraseasonal (25–70-day) variability. *Int. J. Climatol.*, **17**, 1513–1534, https://doi.org/10.1002/(SICI)1097-0088(19971130)17:14<1513::AID-JOC210>3.0.CO;2-U.

Godfrey, J. S., and E. J. Lindstrom, 1989: The heat budget of the equatorial western Pacific surface mixed layer. *J. Geophys. Res. Oceans*, **94**, 8007–8017, https://doi.org/10.1029/JC094iC06p08007.

Jauregui, Y. R., and S. S. Chen, 2024a: MJO-induced warm pool eastward extension prior to the onset of El Niño: Observations from 1998-2019. *J. Climate*, **37**, 855-873, https://doi.org/10.1175/JCLI-D-23-0234.1.

Jauregui, Y. R., and S. S. Chen, 2024b: Ocean density currents induced by MJO precipitation: A key player in warm pool eastward extension during onset of El Niño. *J. Geophys. Res.: Oceans*, **129**, https://doi.org/10.1029/2023JC020424.

Kerns, B. W., and S. S. Chen, 2014: ECMWF and GFS model forecast verification during DYNAMO: Multiscale variability in MJO initiation over the equatorial Indian Ocean. *J. Geophys. Res.: Atmos.*, **119**, 3736–3755, https://doi.org/10.1002/2013JD020833.

Kerns, B. W., and S. S. Chen, 2016: Large-scale precipitation tracking and the MJO over the Maritime Continent and Indo-Pacific warm pool. *J. Geophys. Res.: Atmos*., **121**, 8755–8776, https://doi.org/10.1002/2015JD024661.

Kerns, B. W., and S. S. Chen, 2021: Impacts of precipitation-evaporation-salinity coupling on upper ocean stratification and momentum over the tropical pacific prior to onset of the 2018 El Niño. *Ocean Model.*, **168**, https://doi.org/10.1016/j.ocemod.2021.101892.

Kessler, W. S., M. J. McPhaden, and K. M. Weickmann, 1995: Forcing of intraseasonal Kelvin waves in the equatorial Pacific. *J. Geophys. Res*., **100**, 10613, https://doi.org/10.1029/95JC00382.

Kessler, W. S. and R. Kleeman, 2000: Rectification of the Madden–Julian Oscillation into the ENSO cycle. *J. Climate*, **13**, 3560-3575, https://10.1175/1520-0442(2000)013<3560:ROTMJO>2.0.CO;2.

Kikuchi, K., G. N. Kiladis, J. Dias, and T. Nasuno, 2018: Convectively coupled equatorial waves within the MJO during CINDY/DYNAMO: Slow Kelvin waves as building blocks. *Clim. Dyn*., **50**, 4211–4230, https://doi.org/10.1007/s00382-017-3869-5.

Lau, K. -M., and P. H. Chan, 1988: Intraseasonal and interannual variations of tropical convection: A possible link between the 40–50 day oscillation and ENSO? *J. Atmos. Sci.*, **45**, 506–521, https://doi.org/10.1175/1520-0469(1988)045<0506:IAIVOT>2.0.CO;2.

Lengaigne, M., J. Boulanger, C. Menkes, S. Masson, G. Madec, and P. Delecluse, 2002: Ocean response to the March 1997 Westerly Wind Event. *J. Geophys. Res.: Oceans*, **107**, 8015, https://doi.org/10.1029/2001JC000841.

Lengaigne, M., J. P. Boulanger, C. Menkes, G. Madec, P. Delecluse, E. Guilyardi, and J. Slingo, 2003: The March 1997 westerly wind event and the onset of the 1997/98 El Niño: Understanding the role of the atmospheric response. *J. Climate*, **16**, 3330–3343, https://doi.org/10.1175/1520-0442(2003)016<3330:TMWWEA>2.0.CO;2.

Lukas, R., and E. Lindstrom, 1991: The mixed layer of the western equatorial Pacific Ocean. *J. Geophys. Res.: Oceans*, **96**, 3343-3357, https://doi.org/10.1029/90JC01951.

Madden, R. A., and P. R. Julian, 1971: Detection of a 40–50 day oscillation in the zonal wind in the Tropical Pacific. *J. Atmos. Sci.*, **28**, 702–708, https://doi.org/10.1175/1520-0469(1971)028<0702:DOADOI>2.0.CO;2.

Madden, R. A., and P. R. Julian, 1972: Description of global-scale circulation cells in the tropics with a 40–50 day period. *J. Atmos. Sci.*, **29**, 1109–1123, https://doi.org/10.1175/1520-0469(1972)029<1109:DOGSCC>2.0.CO;2.

Maes, C., J. Picaut, and S. Belamari, 2002: Salinity barrier layer and onset of El Niño in a Pacific coupled model. *Geophys. Res. Lett.*, **29**, 2206, https://doi.org/10.1029/2002GL016029.

Maes, C., K. Ando, T. Delcroix, W. S. Kessler, M. J. McPhaden, and D. Roemmich, 2006: Observed correlation of surface salinity, temperature and barrier layer at the eastern edge of the western Pacific warm pool. *Geophys. Res. Lett*., **33**, https://doi.org/10.1029/2005GL024772.

McPhaden, M. J., and J. Picaut, 1990: El Niño-Southern Oscillation displacements of the Western Equatorial Pacific Warm Pool. *Science*, **250**, 1385-1388, https://doi.org/10.1126/science.283.5404.950.

McPhaden, M. J., and X. Yu, 1999: Equatorial waves and the 1997–98 El Niño. *Geophys. Res. Lett.*, **26**, 2961-2964, https://doi.org/10.1029/1999GL004901.

McPhaden, M. J., 1999: Genesis and evolution of the 1997–98 El Niño. *Science*, **283**, 950-954, https://doi.org/10.1126/science.283.5404.950.

McPhaden, M. J., S. E. Zebiak, and M. H. Glantz, 2006: ENSO as an integrating concept in earth science. *Science*, **314**, 1740–1745, https://doi.org/10.1126/science.1132588.

Roemmich, D., M. Morris, W. R. Young, and J. R. Donguy, 1994: Fresh equatorial jets. *J. Phys. Oceanogr*., **24**, 540-558, https://doi.org/10.1175/1520-0485(1994)024<0540:FEJ>2.0.CO;2.

Seiki, A., and Y. N. Takayabu, 2007: Westerly wind bursts and their relationship with intraseasonal variations and ENSO. Part I: Statistics. *Mon. Wea. Rev.*, **135**, 3325-3345, https://doi.org/10.1175/MWR3477.1.

Sprintall, J., and M. Tomczak, 1992: Evidence of the barrier layer in the surface layer of the tropics. *J. Geophys. Res.*, **97**, 7305-7316, https://doi.org/10.1029/92JC00407.

Suzuki, T., and K. Takeuchi, 2000: Response of Equatorial Pacific mean temperature field to intraseasonal wind forcing. *J. Oceanogr*., **56**, 485-494, https://doi.org/10.1023/A:1011140708962.

Zhang, C., 2005: Madden-Julian Oscillation. *Rev. Geophys*., **43**, https://doi.org/10.1029/2004RG000158.

---, 2013: Madden–Julian Oscillation: Bridging weather and climate. *Bull. Amer. Meteor. Soc.*, **94**, 1849-1870, https://doi.org/10.1175/BAMS-D-12-00026.1.

Zhang, C., and J. Gottschalck, 2002: SST anomalies of ENSO and the Madden–Julian Oscillation in the Equatorial Pacific. *J. Climate*, **15**, 2429–2445, https://doi.org/10.1175/1520-0442(2002)015<2429:SAOEAT>2.0.CO;2.

Upwelling and mixing in the Equatorial Pacific Cold Tongue: Biogeochemical implications, dynamics, and observing needs

Yassir Eddebbar[1], Anna-Lena Deppenmeier[2], Deepak A. Cherian[2], and Daniel B. Whitt[3]

[1]University of California, San Diego / Scripps Institution of Oceanography
[2]NSF National Center for Atmospheric Research
[3]NASA Ames Research Center

The equatorial Pacific ocean's cold tongue is a dynamically and biogeochemically fascinating region. Cold thermocline waters upwell along the equator, resulting in intense ocean heat uptake (Holmes et al. 2019), with profound implications for air-sea interactions and global climate. The high nutrient load of these upwelled waters fuels a productive community of plankton (Strutton et al. 2001), attracting marine life across the trophic ladder (e.g., Ryan et al. 2017) and sustaining a lucrative tuna fishery (Barrange et al. 2018). The cold tongue is also a region of intense carbon outgassing as remineralized carbon-rich waters are upwelled and warmed at the surface, making it the largest oceanic source of carbon dioxide (CO2) to the atmosphere (Takahashi et al. 1997). Below the mixed layer, the transport of oxygen (O2) by the energetic circulation maintains an equatorial oxygenated tongue that extends well into the thermocline (Stramma et al. 2010), providing valuable habitable space amidst the hypoxic conditions of the eastern tropical Pacific. Untangling the pathways and processes governing the upwelling and mixing of heat and biogeochemical properties in this region (Figure 1) is of paramount importance to understanding climate and ecosystem dynamics.

The dynamical regime in the cold tongue is unique: persistent strong shear between the eastward equatorial undercurrent (EUC) and south equatorial current (SEC) acts against the stratifying effects of solar heating and upwelling and maintains a flow state near marginal instability below the mixed layer (e.g., Smyth and Moum 2013). A diurnal cycle in shear turbulence arises driven by solar irradiance effects on stratification and shear, cooling the sea surface and entraining heat downward into the upper thermocline (e.g., Gregg et al. 1985), driving an intense ocean heat uptake along the equator (see Moum et al. 2022 for a detailed review). Though turbulent mixing processes act on relatively small (< meters) and fast (< minutes) scales, they contribute to the large-scale structure and variability of upper ocean properties and air-sea interactions from diurnal to interannual timescales (Moum et al. 2013), including the Bjerknes feedbacks that

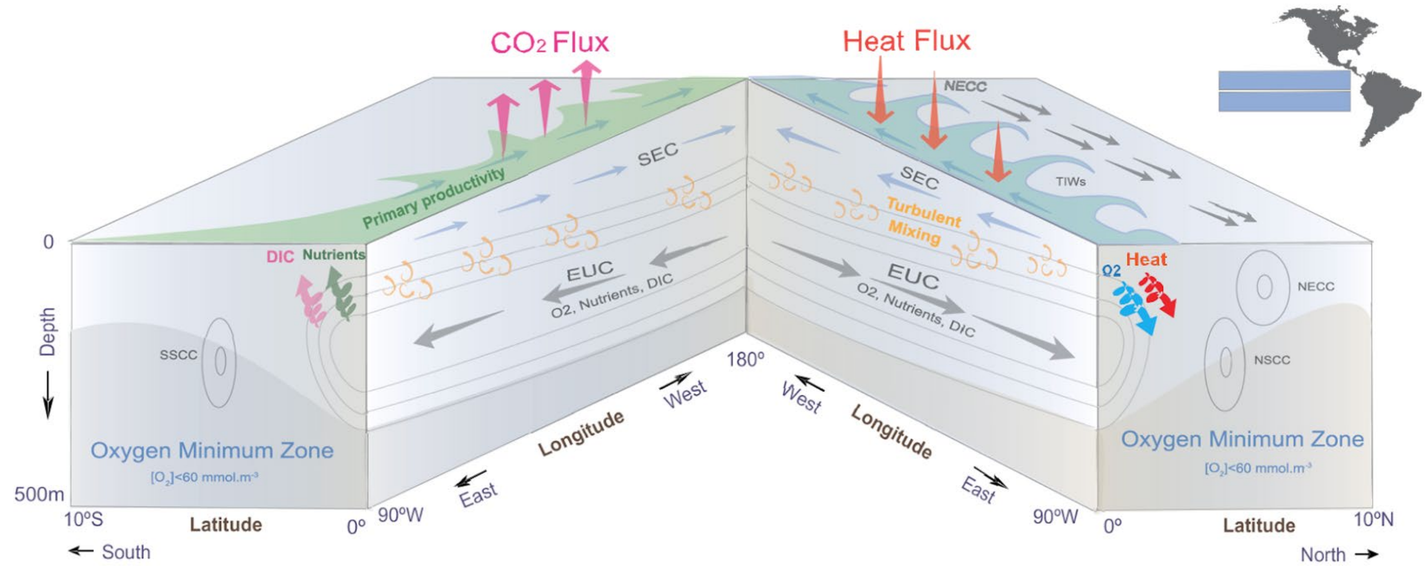

Figure 1. A split view simplified illustration of select processes governing the vertical exchange of heat, carbon, oxygen, and nutrients along the equatorial Pacific cold tongue. Features not to scale. Courtesy of Yassir Eddebbar.

govern the El Niño Southern Oscillation (ENSO) (Warner and Moum 2019). High-resolution simulations of the equatorial Pacific reveal substantial spatial and temporal variability in mixing with far-reaching consequences for the heat budget and biogeochemical cycles. Here, we describe emerging insights and knowledge gaps from these modeling studies and discuss observing the need to test these model-derived hypotheses in the real ocean.

Biogeochemical implications

Poor ventilation by the subtropical gyres and microbial consumption at depth give rise to the tropical Pacific Oxygen Minimum Zones (OMZs) (Sverdrup 1938; Wyrtki 1962). These OMZs are expanding (Stramma et al. 2008). An explanation for this expansion remains limited by poor understanding of ventilation processes in the equatorial Pacific (Oschlies et al. 2018; Cabré et al. 2015). Recent studies indicate the EUC and mesoscale eddies may both dictate the extent and variability of the equatorial oxygenated tongue, a deep feature of oxygenated waters in the thermocline that ventilate OMZs (Figure 1). The EUC in particular has been suggested to play a central role in shaping the O2 field in the tropical Pacific thermocline and its interannual variability associated with ENSO (Busecke et al. 2019). Recent high resolution simulations also reveal that Tropical Instability Vortices (TIVs) induce a seasonal oxygenation of the upper thermocline, depressing the northern equatorial boundary of the OMZ from summer through winter as TIVs propagate westward (Eddebbar et al. 2021). This oxygenation is driven by a combination of TIV advective effects, including isopycnal displacement, lateral stirring, eddy trapping, and subduction by submesoscale fronts, as well as TIV intensification of turbulent mixing of O2 below the mixed layer (Eddebbar et al. 2021; Holmes et al. 2014).

These advective and mixing processes may also regulate nutrient supply and primary productivity. In this high-nitrate low-chlorophyll region, phytoplankton growth is strongly dependent on the zonal advection of iron (Fe) from the western Pacific by the EUC and its vertical supply through upwelling and mixing (Ryan et al. 2006). The intense upwelling, downwelling, and turbulent mixing associated with TIVs, and the Tropical Instability Waves (TIWs) they are embedded in may play a key role in the vertical supply of Fe to the euphotic layer. Indeed, chlorophyll enrichment along TIW cold cusps has been observed in satellite and hydrographic measurements (Yoder et al. 1994; Archer et al. 1997; Strutton et al. 2001; 2011). Whether these cusps of chlorophyll reflect new production or simply outline a redistribution of biomass by TIW circulation is unclear. An early model study argued that TIWs weaken primary production by leaking Fe out of the equatorial Pacific (Gorgues et al. 2005). Other models suggest that TIWs intensify primary production through enhanced upwelling of Fe that is sensitive to the depth of the nutricline (Vichi et al. 2008). This intensified production may feed back on physical processes by suppressing the penetration of shortwave irradiance, increasing stratification, and reducing vertical mixing (Tian et al. 2018). These simulated effects of TIWs on productivity reflect a subtle balance between large opposing fluxes of Fe driven by transport processes that are likely poorly represented by these relatively coarse (~0.5º) models (e.g., TIW submesoscale dynamics; See Marchesiello et al. 2011).

These process-oriented modeling studies raise numerous questions and targets for future observing campaigns. A thematic motivating goal here is the need to identify the pathways by which biogeochemical tracers are exchanged between the mixed layer and the thermocline. Specifically, what are the contributions of advective (e.g., submesoscale fronts) vs turbulent mixing processes in the vertical exchange of O2, nutrients, and carbon? What biogeochemical feedbacks arise from these simultaneous exchanges? How do these processes influence the mean structure and temporal variability of upper-ocean nutrients, biological productivity and composition, oxygen ventilation, and carbon export from diurnal to multidecadal timescales?

Mixing heat and underlying dynamics

Clues to the answers for many of these questions may be found in studies of another tracer: heat. Discussions of equatorial upwelling typically give an impression of colder water moving across the thermocline towards the surface. This picture is overly simplified (Bryden and Brady 1985). Much of upwelling is associated with the eastward flow of the EUC along upward-sloping isotherms (Meinen et al. 2001) and is thus adiabatic. Up to a third of the total upwelling is accounted for by its diabatic component: water parcels undergo water mass transformation and cross isopycnals while moving upwards, for example by changing their temperature due to solar radiation or mixing (Bryden and Brady 1985; Meinen et al. 2001; Huguenin et al. 2019; Deppenmeier et al. 2021). The sun heats water parcels at and near the surface, while mixing cools the near-surface layer (~ top 25 m) and warms water in the upper flanks of the EUC (Ray et al. 2018; Huguenin et al. 2020; Deppenmeier et al. 2021). Mixing influences O2 similarly: it reduces oxygen in the near-surface waters and increases it in the upper thermocline (Eddebbar et al. 2021). In this way, vertical mixing exchanges heat and other properties between the thermocline and the near-surface ocean.

This elegant conceptual idea of upwelling and mixing only approximately describes the mean behavior of a system characterized by vigorous spatio-temporal variability that is not fully understood. The intensity of vertical mixing and diabatic upwelling varies over a wide range of magnitudes on many timescales. The turbulent heat flux regularly varies by up to hundreds of W/m^2 each day due to the diurnal cycle (e.g., Gregg et al. 1985) and by up to about 100 W/m^2 from peak to trough of the seasonal cycle on the equator (Moum et al. 2013; Pham et al. 2017; Whitt et al. 2022). Daily mean heat fluxes range over 2–3 orders of magnitude up to perhaps 500 W/m^2 (Smyth et al. 2021; Whitt et al. 2022). Subseasonal variability is forced by variations in the wind stress (Moum and Caldwell 1985; Whitt et al. 2022) as well as vertical shear and stratification (e.g., by TIWs and Kelvin waves; Lien et al. 1995; Moum et al. 2009; Cherian et al. 2021; Whitt et al. 2022; Deppenmeier et al. 2022). Interannual variability is also large, with mixing playing an active role in ENSO feedbacks (Warner and Moum 2019; Huguenin et al. 2020; Deppenmeier et al. 2021).

This characterization of turbulent mixing has been possible only through multiple intensive process-study campaigns combined with long time series from mooring-based mixing observations (Moum and Nash 2009), and analysis of high resolution simulations. Most long-term observations come from one mooring centered at 0ºN, 140ºW. Thus, most knowledge of off-equatorial mixing

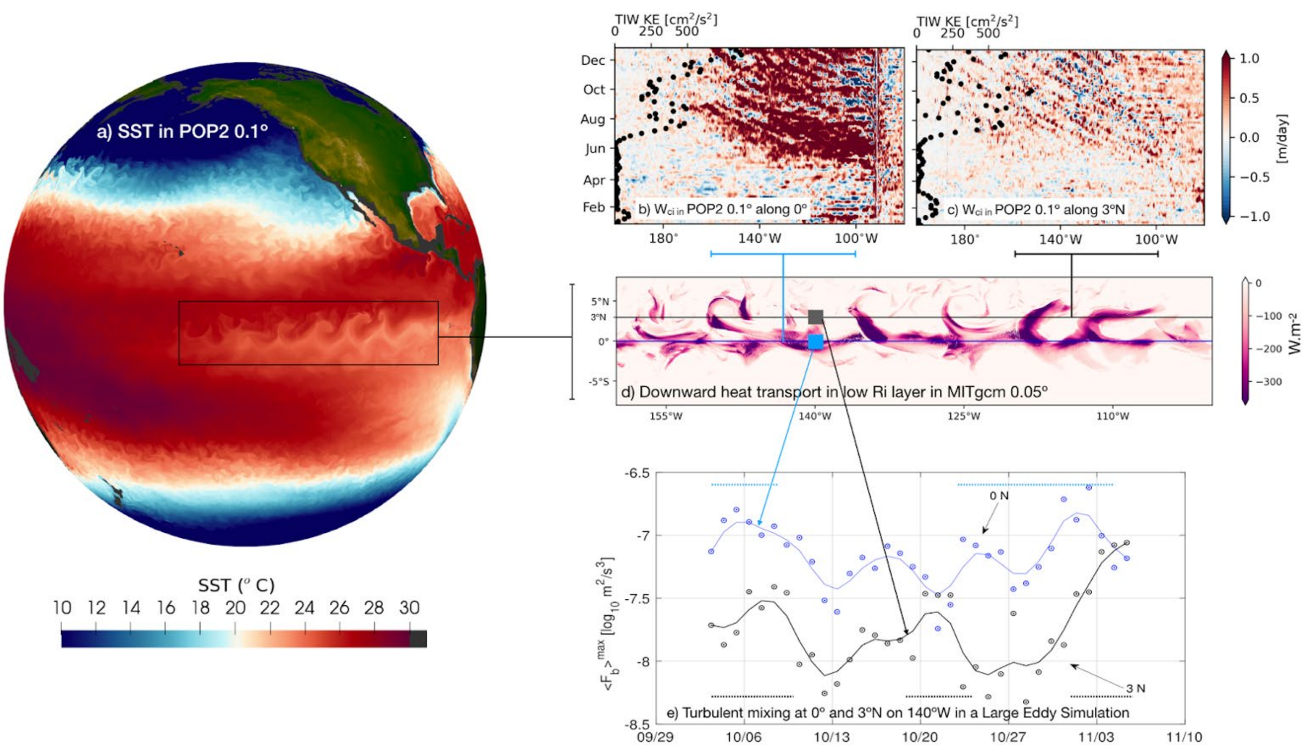

Figure 2. Temporal and spatial scales of turbulent mixing inferred from models. (a) Snapshot of SST in an eddy-resolving hindcast simulation of POP2 at 0.1°, TIWs are outlined by cold cusps along the equator (Eddebbar et al. 2021). (b) Hovmöller plot of the cross-isothermal velocity (Wci)—the diabatic component of upwelling—averaged over the 20–22ºC isotherms along 0ºN and TIW EKE (dots) at 0º, 125ºW in POP2 (Deppenmeier et al. 2022). (c) same as (b) but for Wci along 3ºN and TIW EKE (dots) at 3º, 125ºW. (d) Downward heat flux in the low Richardson number (Ri) layer below the mixed layer and above the EUC in a simulation of MITgcm at 1/20º (Cherian et al. 2021). (e) Time series of the maximum (over depth) of the daily-mean downward turbulent buoyancy flux at 0º, 140ºW and 3ºN, 140ºW in a large eddy simulation, with dotted lines indicating periods of enhanced shear by TIWs (Whitt et al. 2022).

geography and variability is derived from model simulations except for a few cross-equatorial sections (Hebert et al. 1991; Moum et al. 2022). Models show that mixing causes water mass transformation and carries heat from the mixed layer to the upper-thermocline at an average rate of 10–100 W/m^2 throughout the cold tongue (Deppenmeier et al. 2021; Whitt et al. 2022). However, these time-mean turbulent heat fluxes integrate over logarithmic temporal intermittency, which is particularly prominent off the equator due to the mesoscale ocean variability, e.g., associated with TIVs/TIWs (Figure 2; Cherian et al. 2021; Whitt et al. 2022; Deppenmeier et al. 2022). With pronounced vertical gradients in the upper thermocline similar to that of temperature, we hypothesize that the spatio-temporal variability in turbulence is also expressed in the variability of carbon, oxygen, and nutrients in the upper equatorial Pacific.

Outlook: Observing needs and opportunities

Extensive observations of turbulence and its covariation with momentum, heat, and biogeochemical tracers across a variety of timescales on and off the equator are necessary to test these model-based hypotheses and interrogate the representation of mixing and its consequences in forecast and Earth system models. Model based process-studies imply that TIWs and TIVs, through their 3-dimensional circulation and modulation of turbulent mixing, strongly control the exchange of tracers between the thermocline and the ocean surface. Due to their sensitivity to large scale forcing (e.g., winds and equatorial current shear) and modulation of small scale processes (shear-driven turbulence and submesoscale fronts), we hypothesize that TIVs occupy a central role in coupled interactions across scales (Figure 3).

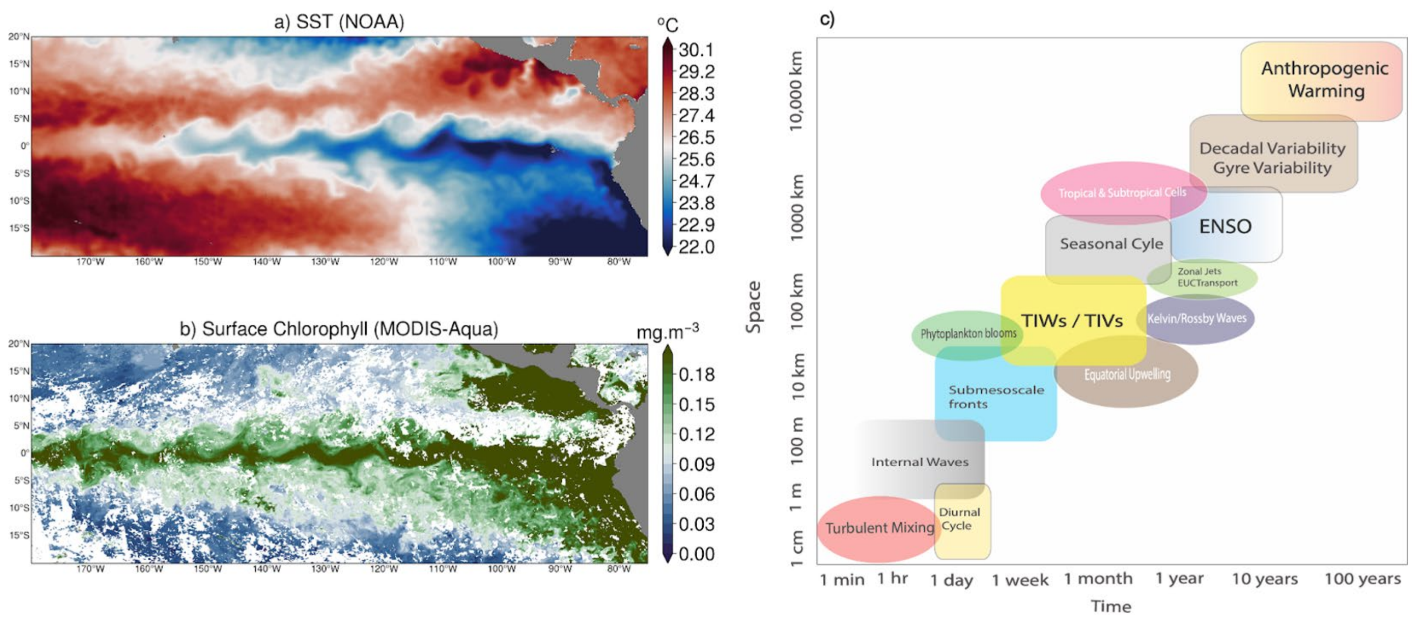

Figure 3. 8-day composites of (a) SST and (b) surface chlorophyll from the NOAA 0.25 OISST Analysis product and MODIS Aqua (9 km resolution) Level 3 product, respectively, centered on December 14, 2016. (c) Temporal and spatial scales of physical and biogeochemical variability in the cold tongue. Strong interactions across scales and processes characterize this region. SST and Chlorophyll data were accessed and are freely available on the NOAA repository and NASA Ocean Color Data repository.

Future process field studies should prioritize characterizing the full 3-dimensional circulation of TIVs/TIWs, biological and chemical structures, and variability. Measurements are needed to specify the meridional and vertical extent of deep cycle turbulence off the equator and its imprints on gradients and fluxes of heat, O2, carbon, and nutrients (e.g., nitrate, iron, and silicate). Observations are also needed to explore submesoscale motions, including their role in the downwelling and upwelling of these properties along the leading and trailing edges of TIVs, respectively. Satellite (Figure 3) and ship-based observations (e.g., Archer et al. 1997; Kennan and Flament 2000; Menkes et al. 2002) and model studies (Holmes et al. 2014; Cherian et al. 2021; Eddebbar et al. 2021) reveal remarkable 3-D physical and biogeochemical complexity that would benefit greatly from the use of fleets of autonomous surface and underwater vehicles (e.g., Saildrones and gliders) that can simultaneously transect large scale TIV structures and sample their fine scale motions (Meinig et al. 2019; Mahadevan 2020). These synergistic observations would be highly beneficial to both physical and biogeochemical communities, as biological changes can feed back on physical processes (Tian et al. 2018) while biogeochemical gradients can provide independent constraints on rates and pathways of upwelling and mixing.

Long-term measurements are needed to characterize the spatio-temporal variability of mixing and its interaction with larger scale processes (Figure 3). In particular, observations are needed to assess the meridional variations of temporally intermittent mixing predicted by models and its biogeochemical consequences. To capture both meridional and temporal variability, enhancing the mooring array along and off the equator with chipods for turbulence estimates and biogeochemical sensors (surface pCO2 and subsurface O2) should be considered in future adjustments of the tropical Pacific Observing Network (TPON; Kessler et al. 2021). Observing these interactions and underlying dynamics is critical to predicting and preparing for anthropogenic warming impacts on the cold tongue and their global consequences.

Acknowledgments

We would like to acknowledge the organizers and participants of the TPON meeting in May 2021, where many fruitful discussions inspired the content of this article. YE would like to acknowledge funding support from NSF under award OCE # 1948599. We would also like to acknowledge high-performance computing support from Cheyenne provided by NCAR's Computational and Information Systems Laboratory, sponsored by the National Science Foundation. DBW was supported by NASA's physical oceanography and ocean biology and biogeochemistry programs. ALD and DAC acknowledge support from the NOAA Climate Variability and Predictability Program (NA18OAR4310399, NA18OAR4310408).

References

Archer, D., and Coauthors, 1997: A meeting place of great ocean currents: Shipboard observations of a convergent front at 2°N in the Pacific. *Deep Sea Res., Part II*, **44**, 1827–1849, https://doi.org/10.1016/S0967-0645(97)00031-3.

Barange, M., T. Bahri, M. C. Beveridge, K. L. Cochrane, S Funge-Smith, F. Poulain, 2018: Impacts of climate change on fisheries and aquaculture: synthesis of current knowledge, adaptation and mitigation options. FAO Fisheries and Aquaculture Technical Paper, 654 pp, http://www.fao.org/3/i9705en/I9705EN.pdf.

Bryden, H. L., and E. C. Brady, 1985: Diagnostic Model of the Three-Dimensional Circulation in the Upper Equatorial Pacific Ocean. *J. Phys. Oceanogr.*, **15**, 1255–1273, https://doi.org/10.1175/1520-0485(1985)015%3C1255:DMOTTD%3E2.0.CO;2.

Busecke, J. J. M., L. Resplandy, and J. P. Dunne, 2019: The Equatorial Undercurrent and the Oxygen Minimum Zone in the Pacific. *Geophys. Res. Lett.*, **46**, 6716–6725, https://doi.org/10.1029/2019GL082692.

Cabré, A., I. Marinov, R. Bernardello, and D. Bianchi, 2015: Oxygen minimum zones in the tropical Pacific across CMIP5 models: Mean state differences and climate change trends. *Biogeosciences*, **12**, 5429–5454, https://doi.org/10.5194/bg-12-5429-2015.

Cherian, D. A., D. B. Whitt, R. M. Holmes, R. -C. Lien, S. D. Bachman, and W. G. Large, 2021: Off-equatorial deep-cycle turbulence forced by Tropical Instability Waves in the equatorial Pacific. *J. Phys. Oceanogr*., **51**, 1575-1593, https://doi.org/10.1175/jpo-d-20-0229.1.

Christian, J. R., M. A. Verschell, R. Murtugudde, A. J. Busalacchi, and C. R. McClain, 2002: Biogeochemical modelling of the tropical Pacific Ocean. I: Seasonal and interannual variability, *Deep Sea Res., Part II*, **49**, 509-543, https://doi.org/10.1016/S0967-0645(01)00110-2.

Deppenmeier, A. L., F. O. Bryan, W. S. Kessler, and L. Thompson, 2021: Modulation of cross-isothermal velocities with ENSO in the tropical Pacific cold tongue. *J. Phys. Oceanogr*., **51**, 1559-1574, https://doi.org/10.1175/JPO-D-20-0217.1.

Deppenmeier, A. -L., F. O. Bryan, W. S. Kessler, and L. Thompson, 2022: Diabatic Upwelling in the tropical Pacific: seasonal and subseasonal variability. *J. Phys. Oceanogr*., **52**, 2657-2668, https://doi.org/10.1175/JPO-D-21-0316.1.

Eddebbar, Y. A., A. C. Subramanian, D. B. Whitt, M. C. Long, A. Verdy, M. R. Mazloff, and M. A. Merrifield, 2021: Seasonal Modulation of Dissolved Oxygen in the Equatorial Pacific by Tropical Instability Vortices. *J. Geophys. Res.: Oceans*, **126**, https://doi.org/10.1029/2021JC017567.

Gorgues, T., C. Menkes, O. Aumont, J. Vialard, Y. Dandonneau, and L. Bopp, 2005: Biogeochemical impact of tropical instability waves in the equatorial Pacific. *Geophys. Res. Lett*., **32**, L24615, https://doi.org/10.1029/2005GL024110.

Gregg, M. C., H. Peters, J. C. Wesson, N. S. Oakey, and T. J. Shay, 1985: Intensive measurements of turbulence and shear in the equatorial undercurrent. *Nature*, **318**, 140–144, https://doi.org/10.1038/318140a0.

Hebert, D., J. N. Moum, and D. R. Caldwell, 1991: Does ocean turbulence peak at the equator?: Revisited. *J. Phys. Oceanogr*., **21**, 1690-1698, https://doi.org/10.1175/1520-0485(1991)021<1690:DOTPAT>2.0.CO;2.

Holmes, R. M., L. N. Thomas, L. Thompson, and D. Darr, 2014: Potential Vorticity Dynamics of Tropical Instability Vortices. *J. Phys. Oceanogr*., **44**, 995–1011, https://doi.org/10.1175/JPO-D-13-0157.1.

Holmes, R. M., J. D. Zika, and M. H. England, 2019: Diathermal Heat Transport in a Global Ocean Model. *J. Phys. Oceanogr*., **49**, 141–161, https://doi.org/10/gfs9z9.

Huguenin, M. F., R. M. Holmes, and M. H. England, 2020: Key role of diabatic processes in regulating warm water volume variability over ENSO events. *J. Climate*, **33**, 9945-9964, https://doi.org/10.1175/JCLI-D-20-0198.1.

Kennan, S. C., and P. J. Flament, 2000: Observations of a tropical instability vortex. *J. Phys. Oceanogr.*, **30**, 2277–2301, https://journals.ametsoc.org/view/journals/phoc/30/9/1520-0485_2000_030_2277_ooativ_2.0.co_2.pdf

Kessler, W. S., and Coauthors, 2021: Final Report of Tropical Pacific Observing System 2020. Global Ocean Observing System-268, 83 pp, https://doi.org/10.13140/RG.2.2.19282.68802.

Kosaka, Y., and S. -P. Xie, 2016: The tropical Pacific as a key pacemaker of the variable rates of global warming. *Nat. Geosci*., **9**, 669–673, https://doi.org/10/f84j6s.

Lien, R. -C., E. A. D'Asaro, and C. E. Menkes, 2008: Modulation of equatorial turbulence by tropical instability waves. *Geophys. Res. Lett*., **35**, L24607, https://doi.org/10/fcvdgw.

Mahadevan, A., A. Pascual, D. L. Rudnick, S. Ruiz, J. Tintoré, and E. D'Asaro, 2020: Coherent pathways for vertical transport from the surface ocean to interior. *Bull. Amer. Meteor. Soc*., **101**, E1996-E2004, https://doi.org/10.1175/BAMS-D-19-0305.1.

Marchesiello, P., X. Capet, C. Menkes, and S. C. Kennan, 2011: Submesoscale dynamics in tropical instability waves. *Ocean Modelling*, **39**, 31–46, https://doi.org/10/dgx7rx.

Margolskee, A., H. Frenzel, S. Emerson, and C. Deutsch, 2019: Ventilation pathways for the north Pacific oxygen deficient zone. *Global Biogeochem. Cycles*, **33**, 875–890, https://doi.org/10.1029/2018gb006149.

Meinen, C. S., M. J. McPhaden, and G. C. Johnson, 2001: Vertical Velocities and Transports in the Equatorial Pacific during 1993–99. *J. Phys. Oceanogr*., **31**, 11, 3230–3248, https://doi.org/10/c6q8pj.

Meinig, C., and Coauthors, 2019: Public–private partnerships to advance regional ocean-observing capabilities: A saildrone and NOAA-PMEL case study and future considerations to expand to global scale observing. *Front. in Mar. Sci*., **448**, https://doi.org/10.3389/fmars.2019.00448.

Menkes, C., and Coauthors, A whirling ecosystem in the equatorial Atlantic. *Geophys. Res. Lett*., **29**, https://doi.org/10.1029/2001GL014576

Moum, J. N., and D. R. Caldwell, 1985: Local influences on shear-flow turbulence in the equatorial ocean. *Science*, **230**, 315-316, https://doi.org/10.1126/science.230.4723.315.

Moum, J. N., and J. D. Nash, 2009: Mixing measurements on an equatorial ocean mooring. *J. Atmos. Oceanic Technol*., **26**, 317–336, https://doi.org/10.1175/2008JTECHO617.1.

Moum, J. N., R. -C. Lien, A. Perlin, J. D. Nash, M. C. Gregg, and P. J. Wiles, 2009: Sea surface cooling at the Equator by subsurface mixing in tropical instability waves. *Nat. Geosci*., **2**, 761–765, https://doi.org/10.1038/ngeo657.

Moum, J. N., A. Perlin, J. D. Nash, and M. J. McPhaden, 2013: Seasonal sea surface cooling in the equatorial Pacific cold tongue controlled by ocean mixing. *Nature*, **500**, 64–67, https://doi.org/10.1038/nature12363.

Moum, J. N., A. Natarov, K. J. Richards, E. L. Shroyer, and W. D. Smyth, 2022: Mixing in equatorial oceans. In Ocean Mixing. Ocean Mixing, M. Meredith and A. N. Garabato, Elsevier, 257-273, https://doi.org/10.1016/B978-0-12-821512-8.00017-7.

Oschlies, A., P. Brandt, L. Stramma, and S. Schmidtko, 2018: Drivers and mechanisms of ocean deoxygenation. *Nat. Geosci*., **11**, 467–473, https://doi.org/10.1038/s41561-018-0152-2.

Pham, H. T., W. D. Smyth, S. Sarkar, and J. N. Moum, 2017: Seasonality of deep cycle turbulence in the eastern equatorial Pacific. *J. Phys. Oceanogr*., **47**, 2189-2209, https://doi.org/10.1175/JPO-D-17-0008.1.

Ray, S., A. T. Wittenberg, S. M. Griffies, and F. Zeng, 2018: Understanding the equatorial Pacific cold tongue time-mean heat budget. Part I: Diagnostic framework. *J. Climate*, **31**, 9965-9985, https://doi.org/10.1175/JCLI-D-18-0152.1.

Ryan, J. P., I. Ueki, Y. Chao, H. Zhang, P. S. Polito, and F. P. Chavez, 2006: Western Pacific modulation of large phytoplankton blooms in the central and eastern equatorial Pacific. *J. Geophys. Res*., **111**, G02013, https://doi.org/10.1029/2005JG000084.

Ryan, J. P., J. R. Green, E. Espinoza, A. R. Hearn, 2017: Association of whale sharks (Rhincodon typus) with thermo-biological frontal systems of the eastern tropical Pacific. *PLoS ONE*, **12**, https://doi.org/10.1371/journal.pone.0182599.

Smyth, W. D., and J. N. Moum, 2013: Marginal instability and deep cycle turbulence in the eastern equatorial Pacific Ocean. *Geophys. Res. Lett*., **40**, 6181–6185, https://doi.org/10.1002/2013GL058403.

Smyth, W. D., S. J. Warner, J. N. Moum, H. T. Pham, and S. Sarkar, 2021: What controls the deep cycle? Proxies for equatorial turbulence. *J. Phys. Oceanogr*., **51**, 2291-2302, https://doi.org/10.1175/JPO-D-20-0236.1.

Stramma, L., G. C. Johnson, E. Firing, and S. Schmidtko, 2010: Eastern Pacific oxygen minimum zones: Supply paths and multidecadal changes. *J. Geophys. Res.: Oceans*, **115**, https://doi.org/10.1029/2009JC005976.

Stramma, L., G. C. Johnson, J. Sprintall, and V. Mohrholz, 2008: Expanding oxygen-minimum zones in the tropical oceans. *Science*, **320**, 655–658, https://doi.org/10.1126/science.1153847.

Strutton, P. G., A. P. Palacz, R. C. Dugdale, F. Chai, A. Marchi, A. E. Parker, V. Hogue, and F. P. Wilkerson, 2011: The impact of equatorial Pacific tropical instability waves on hydrography and nutrients: 2004-2005. *Deep Sea Res., Part II*, **58**, 284–295, https://doi.org/10/c9b3qc.

Strutton, P. G., J. P. Ryan, and F. P. Chavez, 2001: Enhanced chlorophyll associated with tropical instability waves in the equatorial Pacific. *Geophys. Res. Lett*., **28**, 2005-2008, https://doi.org/10.1029/2000GL012166.

Sverdrup, H., 1938: On the explanation of the oxygen minima and maxima in the oceans. *ICES Journal of Marine Science*, **13**, 163–172, https://doi.org/10.1093/icesjms/13.2.163.

Takahashi, T., R. A. Feely, R. F. Weiss, R. H. Wanninkhof, D. W. Chipman, S. C. Sutherland, and T. T. Takahashi, 1997: Global air-sea flux of CO2: An estimate based on measurements of sea–air pCO2 difference. *Proc. Natl. Acad. Sci. USA*, **94**, 8292-8299, https://doi.org/10.1073/pnas.94.16.8292.

Tian, F., R. H. Zhang, and X. Wang, 2018: A coupled ocean physics-biology modeling study on tropical instability wave-induced chlorophyll impacts in the Pacific. *J. Geophys. Res.: Oceans*, **123**, 5160-5179, https://doi.org/10.1029/2018JC013992.

Vichi, M., S. Masina, and F. Nencioli, 2008: A process-oriented model study of equatorial Pacific phytoplankton: The role of iron supply and tropical instability waves. *Prog. in Oceanography*, **78**, 147-162, https://doi.org/10.1016/j.pocean.2008.04.003.

Warner, S. J., and J. N. Moum, 2019: Feedback of mixing to ENSO phase change. *Geophys. Res. Lett*., **46**, 13920-13927, https://doi.org/10.1029/2019GL085415.

Whitt, D. B., D. A. Cherian, R. M. Holmes, S. D. Bachman, R. C. Lien, W. G. Large, and J. N. Moum, 2022: Simulation and scaling of the turbulent vertical heat transport and deep-cycle turbulence across the equatorial Pacific cold tongue. *J. Phys. Oceanogr*., **52**, 981-1014, https://doi.org/10.1175/JPO-D-21-0153.1.

Wyrtki, K., 1962: The oxygen minima in relation to ocean circulation. *Deep-Sea Res. Oceanogr. Abstr*., **9**, 11-23, https://doi.org/10.1016/0011-7471(62)90243-7.

Yoder, J. A., S. G. Ackleson, R. T. Barber, P. Flament, and W. M. Balch, 1994: A line in the sea. *Nature*, **371**, 689–692. https://doi.org/10/cpc6t3.

Will we have the marine atmospheric boundary layer observations necessary to realize the "Decade of Convection" in the tropics?

Brandon Wolding[1,2], Scott W. Powell[3], Kathleen Schiro[4], Rachel Storer[5], Tong Lee[5], and Raghavendra Krishnamurthy[6]

[1]University of Colorado
[2] NOAA Earth System Research Laboratory
[3]Naval Postgraduate School
[4]University of Virginia
[5]NASA Jet Propulsion Laboratory
[6]Pacific Northwest National Laboratory

The decade of convection

In 2028, three radar equipped SmallSats orbiting in quick succession will use a novel time-differencing technique to begin providing the first ever tropics-wide measurements of convective mass flux (CMF) as part of Investigation of Convective Updrafts (INCUS), a recently funded NASA Earth Venture 3 initiative. The following year, a constellation of three satellites comprising NASA's Atmosphere Observing System (AOS) will begin using a wide array of active and passive instruments to collect measurements optimized for identifying the links between aerosols, clouds, convection, and precipitation. INCUS and AOS will offer an unprecedented opportunity to characterize tropical convection and convectively-coupled processes within the atmosphere and ocean, ushering in what some anticipate will come to be known as the "Decade of Convection." Yet the tropical air-sea "transition zone," a region encompassing the marine atmospheric boundary layer (MABL), air-sea interface, and upper-ocean, remains sparsely observed, posing significant challenges to process-level studies of convection and air-sea coupling. With the Decade of Convection rapidly approaching, we must ask: "What observations will be needed to characterize tropical convection and convectively-coupled processes within the atmosphere and ocean"?

In alignment with companion articles in this edition of *Variations*, we believe that routine, simultaneous, and coincident measurements of the air-sea transition zone collected across representative convective regimes of the tropical Pacific rank amongst primary observing needs. This article will suggest that emerging ocean-surface autonomous observing platform technologies provide unique prospects for addressing this need. This article adopts a necessarily limited scope, focusing primarily on the "needs and prospects" for expanding thermodynamic observations of a single component of the tropical air-sea transition zone, namely the MABL. Companion articles in this edition of *Variations* focused on spaced-based observations of the air-sea transition zone, observational "Supersites," and Earth system prediction compliment this contribution.

Process studies highlight critical need for MABL observations

What is the state of the system? **How** is the state of the system changing? **Why** is the state of the system changing? These questions represent a hierarchy of understanding, each one becoming considerably more difficult to answer than the previous. Ideally, we want to know the answers to these questions across a range of scales, over large and varied geographical regions, over extended periods of time and, in the case of convection and convectively-coupled processes, at different stages of convective development. Each observational platform and approach, having distinctive strengths and weaknesses, contributes to this hierarchy of understanding in unique ways and, just as advances in our understanding are often borne from advances in these platforms and approaches, critical gaps in our understanding often reflect critical gaps in these platforms and approaches.

Recent process studies of convection and air-sea coupling highlight that observing and understanding MABL thermodynamic variability remains a longstanding critical gap (Zadra et al. 2018; Yasunaga et al. 2019; Ren et al. 2021; Wolding et al. 2022). To better understand the observational origins of this critical gap, and the limitations it imposes on model development, we will consider how observations of tropospheric humidity are routinely collected, used in concert with models and assimilation systems to produce (re)-analyses, and then used by process studies requiring uniform sampling across broad spatio-temporal scales and/or diverse geographical regions.

Routinely collected humidity observations over remote tropical oceans, where in-situ measurements are relatively sparse, are predominantly provided by spaced-based platforms falling into two general categories: passive multi- or hyperspectral soundings and Global Navigation Satellite System (GNSS) Radio Occulations (RO) (Pincus et al. 2017; Hersbach et al. 2020). Passive infrared and microwave sounders exploit the absorption and emission characteristics of water vapor to make coarsely resolved estimates of its vertical distribution and, when used in concert, provide relatively strong constraints on column integrated moisture. Passive infrared and microwave sounders are highly complimentary: the former having higher horizontal resolution, the latter being less impacted by the presence of clouds. GNSS ROs use time delays associated with the “bending” of active atmospheric limb soundings to retrieve high vertical resolution, coarse horizontal resolution thermodynamic profiles. As ROs are time-based measurements and are not attenuated by clouds, they offer relatively low uncertainty and unbiased estimates with unique long-term stability, providing “anchor” measurements in assimilation systems. Retrieval of moisture profiles requires a-priori estimates of temperature profiles (a.k.a. temperature-moisture ambiguity), and the rapid changes in RO bending angle that occur at the MABL top, while useful for identifying MABL depth, frequently prevent retrieval and/or assimilation of measurements from within the MABL itself (Kursinski et al. 1997; Basha and Ratnam 2009; Xie et al. 2012; Ho et al. 2020).

In an effort to produce gridded, complete (in space and time), and self-consistent “maps without gaps,” reanalyses attempt to optimally combine historical observations from hundreds of space-based and in-situ instruments using forecast models in concert with data assimilation systems (Hersbach et al. 2020). Model forecasts provide an “initial-guess” state of the atmosphere, which is then updated by concurrent and proximate (in space and time) observations using a data assimilation system seeking to minimize diff-

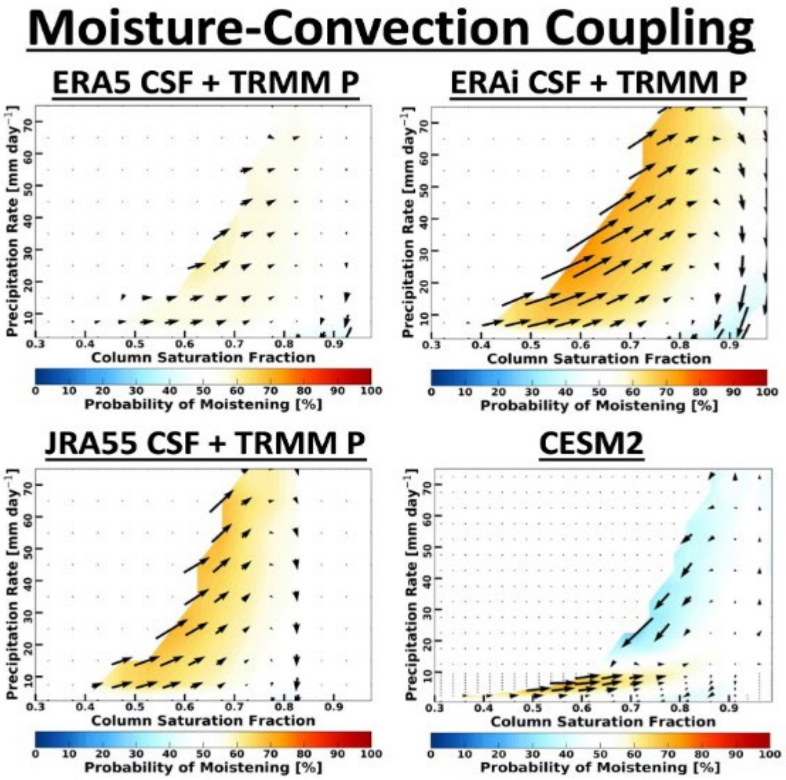

Figure 1. Moisture-convection coupling diagnostic applied to tropical (15°N–15°S) oceanic TRMM precipitation estimates and reanalysis column saturation fraction (CSF) at daily average 2.5° horizontal resolution from 1998–2015, and a pre-industrial simulation of CESM2 at daily average ~1° horizontal resolution. Vectors indicate temporal co-evolution of precipitation and CSF, calculated using bin-mean temporal center differences. Color shading indicates the probability of moistening (warm shading) or drying (cool shading), calculated as the fraction of samples within a bin having a positive moisture tendency, again using temporal centered differences. Bins containing less than 200 observations are marked with stippling. See Wolding et al. (2020) for detailed methodology. © American Meteorological Society. Used with permission.

erences amongst the forecast and all available observations, while taking their respective uncertainties into consideration. As reanalyses incorporate numerous data sources (e.g., ERA5 assimilated ~95 billion observations from 1979–2019), and estimates at a given time can be informed by coincident and proximate observations, they can be more accurate than observations from any single observing platform (Pincus et al. 2017; Hersbach et al. 2020). Yet reanalyses are susceptible to systematic errors, particularly when strong observational constraints are lacking or sampling is biased (e.g., clear versus cloudy sky conditions). This is especially true of the MABL, where the dearth of thermodynamic observations creates a large dependence on the assimilating model and its parameterized treatments of short-timescale processes impacting moisture and temperature variability (e.g., ventilation of MABL by parameterized convection) (Pincus et al. 2017).

Recent process studies illustrate how insufficient observational constraints become manifest as systematic errors in reanalyses, limit our understanding of convection, and subsequently hamper model development. Figure 1 shows a process-oriented diagnostic (POD) of moisture-convection coupling over tropical oceans (Wolding et al. 2020). Vectors indicate **how** TRMM precipitation estimates and reanalysis column saturation fraction (CSF, a column integrated measure of moisture) tend to co-evolve in time, and color shading indicates a proclivity to moisten (warm colors) or dry (cool colors). In observations/reanalyses, vectors trace a clockwise pattern in CSF-P space, indicating that cyclical increases and decreases in column moisture are coupled to the cyclical amplification and decay of convection. The Community Earth System Model version 2.0.1 (CESM2), a current generation climate model, shows a proclivity to dry (cool colors) during conditions when observations/reanalyses suggest that moistening (warm colors) should occur (Danabasoglu et al. 2020; Wolding et al. 2020). In order to guide model development, we must understand **why** CESM2 fails to reproduce aspects of observed moisture-convection coupling by, for example, using a moisture budget to identify specific moisture sources/sinks (e.g., surface fluxes/precipitation) that are behaving unrealistically. Yet, despite the comparatively strong observational constraints placed on large-scale column moisture variability by infrared and microwave sounders, considerable disagreement exists amongst the three reanalyses as to **how** CSF evolves in relation to TRMM precipitation, making it difficult to establish the clear process-level targets needed to guide model development (Schröder et al. 2016).

Such disagreements become more stark when the vertical structure of thermodynamic variations associated with these convective cycles is examined. Figure 2 compares NOAA Integrated Global Radiosonde Archive (IGRA) thermodynamic profiles from six small western Pacific islands to co-located ERA5 thermodynamic profiles over a composite convective cycle (Durre et al. 2018; Wolding et al. 2022). Moving from left to right along the X-axis is analogous to tracing a clockwise circle around Figure 1, starting/ending in the lower left corner. Systematic differences between IGRA

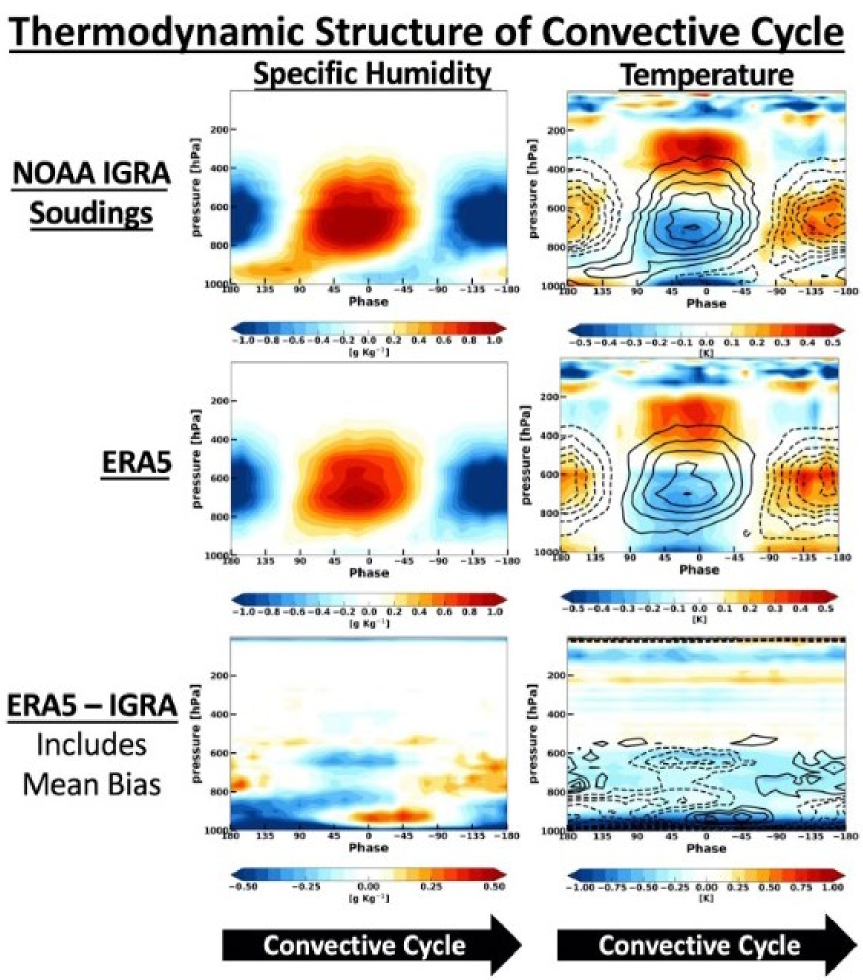

Figure 2. Vertical structure of specific humidity and temperature variations associated with composite convective cycle. Thermodynamic profiles are obtained from NOAA IGRA soundings from 6 small islands in the tropical western Pacific (Figure 3 red markers) and co-located ERA5 reanalysis at hourly 0.25° horizontal resolution. In the right column, specific humidity perturbations are contoured every 0.2 g Kg^{-1} in the top and middle row, and every 0.1 g Kg^{-1} in the bottom row, with positive values in solid contours, and negative values in dashed contours. Moving left to right along the X-axis follows a composite convective cycle, and is analogous to tracing a clockwise circle around Figure 1, starting/ending in the lower left corner. The composite convective cycle is associated with a transition from predominantly shallow, to convective, to stratiform type precipitation. Bottom row shows the difference between ERA5 and NOAA IGRA profiles, and includes mean state bias. Methodology detailed in Wolding et al. (2022). Figure adapted from Wolding et al. (2022). © American Meteorological Society. Used with permission.

and ERA5 specific humidity variations are evident in the MABL, and accompanied by compensating differences of the opposite sign in the lower free troposphere (LFT). Pincus et al. (2017) showed that the lack of observational constraints on MABL humidity, combined with the coarse vertical resolution of infrared and microwave sounders, allows analysis systems to make compensating errors in the vertical structure of humidity that approximately preserve column integrated water vapor, which is more strongly constrained by observations. Similar compensating errors are evident in climatological profiles of humidity over the warm pool in various reanalyses (see Ren et al. 2021, Figure 2h). Such systematic differences have very tangible impacts on our understanding of interactions between convection and the surrounding atmosphere and ocean. For example, Wolding et al. (2022) showed that when using reanalysis thermodynamic fields, these systematic differences cause variations in LFT humidity to appear less influential in determining the strength of convection than is suggested by observations.

Why then, despite such well-known shortcomings, are reanalyses still being used by process studies of convection and air-sea coupling? The logistical challenges of designing, establishing, and maintaining observational platforms in remote tropical oceans means that, despite being critical for the calibration/validation (cal/val) of space-based observations and identification of systematic errors in (re)analyses, in-situ observations are not routinely collected in many regions of the Pacific. While the Global Tropical Moored Buoy Array profiles upper ocean conditions, atmospheric temperature and humidity measurements are limited to the near surface (Figure 3, bottom panel). In-situ observational records from the six small islands examined in this section (Figure 3, red dots) have been utilized by numerous seminal studies of convection (e.g., Holloway and Neelin 2009; Kiladis et al. 2009), but are outliers in both their longevity and quality. Analogous records simply are not available in many regions of the tropics, leaving entire convective regimes severely under-sampled. Again, using convective cycles to illustrate this pertinent observing need, consider that while the cyclical amplification and decay of convection is ubiquitous across tropical convergence zones, the specific combination of processes supporting these cycles varies geographically. In the Indian and western Pacific oceans, regions where large-scale ascent is deep and “top-heavy” (Figure 3, cool shading), radiative and surface flux feedbacks are more important for amplifying convection than in the central Pacific, eastern Pacific, and Atlantic oceans, where shallow “bottom-heavy” large-scale ascent (Figure 3, warm shading) plays a crucial role (Inoue et al. 2021). The joint challenges posed by geographically limited in-situ records, deficiencies in space-based measurements of the MABL, and systematic errors in reanalyses conspire to limit our understanding of these different convective regimes and impede efforts to improve their model representation.

Prospects for expanding MABL observations

This section will provide a brief, non-comprehensive survey of emerging space-based and surface-based observation technologies. Interested readers are referred to Nehrir et al. (2017) and companion articles in this edition of *Variations* for more details. Readers are encouraged to consider prospects for expanding MABL observations in the context of broader observational needs for understanding convection and air-sea coupling processes.

Emerging space-based observation technologies

Differential absorption lidar (DIAL) utilizes atmospheric molecular and aerosol backscattered return signals from a pulsed laser, and has the potential to provide high accuracy high vertical

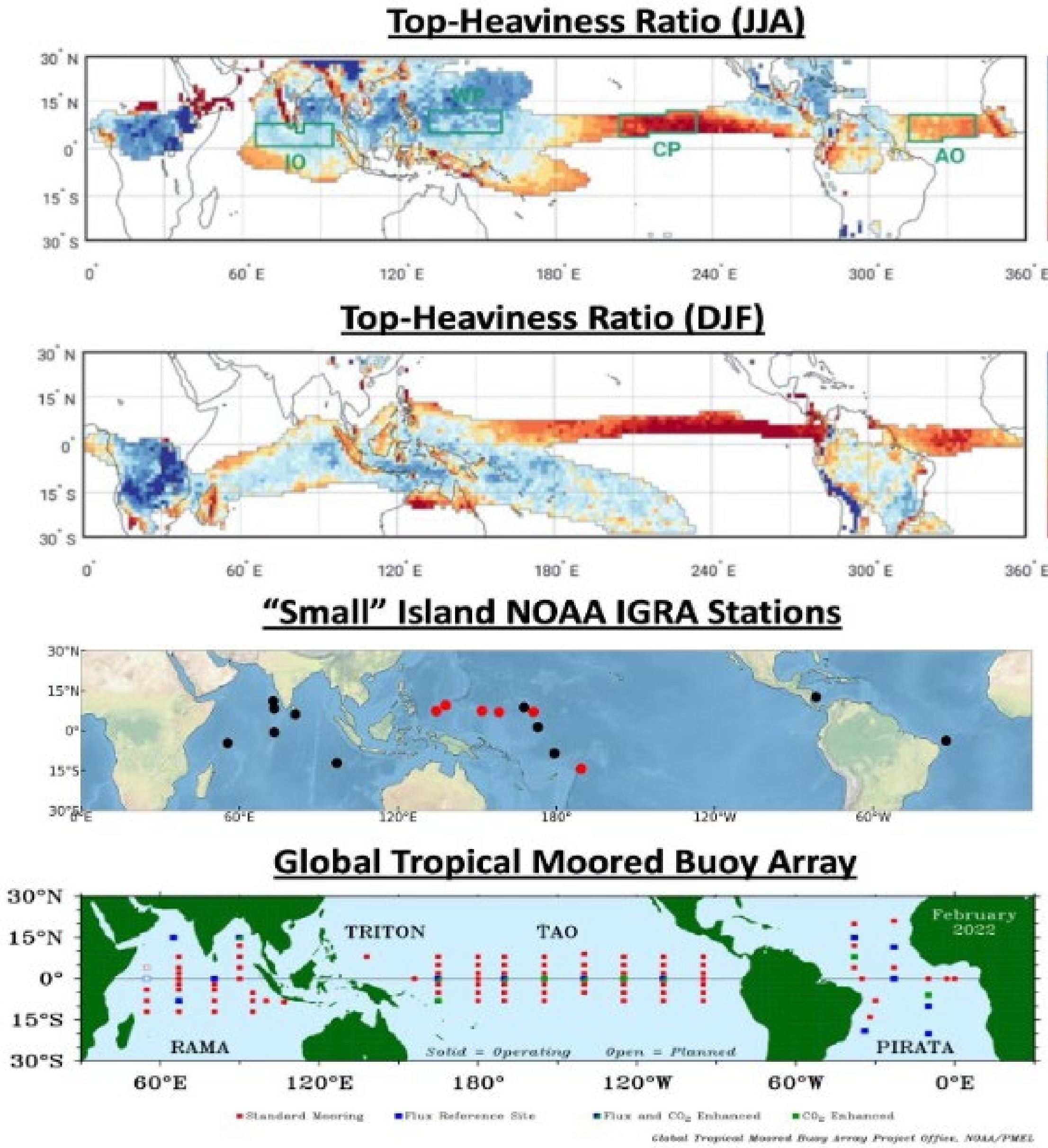

Figure 3. Upper two panels, adapted from Inoue et al. (2021), indicate regions where large-scale ascent tends to be deep and "top-heavy" (cool shading) versus shallow and "bottom-heavy" (warm shading). Third panel shows "small" islands NOAA IGRA stations, defined as stations in the tropical belt (15°N–15°S) whose nearest corresponding 0.25° ERA5 grid point has a land fraction less than 10%. Red markers indicate IGRA stations used in Figure 2. Bottom panel shows Global Tropical Moored Buoy Array as of February 2022. © American Meteorological Society. Used with permission.

resolution water vapor profiles extending to the near surface. Being relatively insensitive to surface emissivity, DIAL has the capability to profile over land and ocean, during both day and night. A weakness of DIAL is that cloudy skies, even optically thin cirrus, impact the retrieval, though its relatively small footprint (~100 m) allows retrievals to be obtained from the gaps between clouds. Comparisons with CALIPSO suggest that ~40−50% of retrievals in tropical convergence zones would be usable. See Figure 2 of Nehrir et al. (2017) for airborne DIAL retrievals from the 2015 Plains Elevated Convection At Night (PECAN) mission.

Differential absorption radar (DAR) is the radar analogue of DIAL, using cloud and precipitation scattering targets in place of clear-sky molecular and aerosol scattering (Nehrir et al. 2017). By combining the range-resolving capabilities of radar with the strong frequency dependence of atmospheric attenuation by water vapor, DAR has the potential to profile water vapor within clouds, makes it highly complementary to DIAL (Roy et al. 2018; 2020). Early versions of DAR are expected to be limited to a particular altitude range (e.g., sounding either high altitude cirrus or low altitude boundary layer clouds) by channel selection restrictions (Roy et al. 2021).

LEO-LEO Microwave Occultation (LMO) is similar to current GNSS RO technologies, but exploits both refraction and absorption signals to overcome the temperature-humidity ambiguity of RO, enabling retrievals of pressure, temperature, and humidity without a-priori information (Nehrir et al. 2017). While degraded accuracy and poor spatial resolution limit LMO capabilities in the MABL, free tropospheric LMO profiles could allow remote platforms such as DAR to be optimized for sensitivity in the lower troposphere.

These three highly complementary space-based technologies may help to characterize lower tropospheric thermodynamic variability in the coming decades, especially if implemented in concert. Yet, as detailed in a companion article led by Kyla Drushka, observing MABL thermodynamic variability from space under a range of convective conditions will continue to present considerable challenges for the foreseeable future. This suggests that expanded in-situ observations will play a critical role in addressing current MABL observing needs.

Emerging surface-based observation technologies

NASA is supporting the development of a miniaturized, upward-pointing passive microwave sounder for profiling MABL air temperature and water vapor. Development goals are targeting a light weight, low power consumption, low cost unit that could be deployed in large numbers across a range of ocean-surface autonomous platforms, including buoys and uncrewed surface vehicles. Ocean-surface upward-pointing sounders would support the cal/val of space-based MABL measurements, and could be used in combination with existing technologies to form in-situ observing systems capable of profiling the entire air-sea transition zone. While still in the initial stages of development, prototypes suitable for field deployment are expected in the next few years.

A DOE Wind Energies Technologies Office funded project has developed a wind lidar equipped buoy capable of measuring high-resolution 3-D winds from the near surface up to 250 m above sea level. The wind lidar buoy also measures upper ocean salinity, temperature, and currents, as well as near surface atmospheric temperature and relative humidity, helping relate MABL variability to sub-surface ocean processes. Buoys have been deployed at four locations along both the east and west coasts of the United States where extensive wind energy development is anticipated, and are being used for model validation in the context of wind energy applications. The wind lidar buoys will be an integral part of the 2024 Wind Forecasting Improvement 3 field campaign.

These initiatives illustrate how emerging ocean-surface autonomous platform technologies will not only help characterize **how** the MABL varies, but will also further understanding of **why** the MABL varies by simultaneously measuring processes across the air-sea transition zone.

Why "more" observations will be necessary, but insufficient

Results of a data denial experiment by Pincus et al. (2017), where dropsonde and sounding observations collected during the NOAA El-Niño Rapid Response (ENRR) field campaign were incorporated/withheld from an NCEP ensemble assimilation/forecast system, warrant brief mention. When in-situ observations were withheld, aforementioned systematic compensating biases between a too dry boundary layer and a too moist LFT were evident in the analyses. While the inclusion of in-situ observations helped ameliorate the compensating biases in the analyses, these improvements were lost within a 6-hour forecast window, in part due to systematic model errors. These results highlight that targeted model improvements will be needed if the benefits of additional observations are to be realized by forecasts. Supersites, discussed in a companion article led by Carol Anne Clayson, are an example of innovative approaches for obtaining the concentrated in-situ observations needed to support these targeted process-level model improvements.

Summary

Next-generation observations of tropical convection will offer a unique opportunity to characterize convective variability and convectively-coupled processes within the atmosphere and ocean. Realizing this opportunity will require similar advancements in our ability to collect routine, simultaneous, and coincident measurements of the air-sea transition zone across representative convective regimes. Emerging space-based technologies will help constrain free tropospheric thermodynamic variability, especially if implemented in concert. Yet, as discussed in a companion article led by Kyla Drushka, many current impediments to observing near-surface thermodynamic variability from space will remain, suggesting that a concerted effort to expand ocean-based in-situ observations will be critical to characterizing marine atmospheric boundary layer variability. Emerging ocean-surface autonomous platform technologies provide unique opportunities to bolster this critical gap in current observational capabilities. Systematic errors arising from parameterized processes with short timescales rapidly erode the potential benefits that expanded observations offer to analyses and forecasts, highlighting that "richer observational capabilities will need to be paired with systematic model improvements" (Pincus et al. 2017). Supersites, discussed in a companion article led by Carol Anne Clayson, are an example of innovative approaches for obtaining the concentrated in-situ observations needed to support these process-level model improvements.

The necessarily limited scope of this article, which focused primarily on thermodynamic observations of the MABL, has left many of the observational "needs and prospects" of the MABL unaddressed. Observations of MABL height, eddy diffusivity and viscosity, turbulent fluxes at the air-sea interface, and near-surface vertical current shear, among many others, are needed to quantify air-sea momentum fluxes, support development of eddy-diffusivity mass flux schemes in numerical models, and address other outstanding issues.

While existing observational platforms such as marine X-band radar, FLIP, and instrumentation aboard uncrewed surface vehicles are capable of obtaining these measurements, the paucity of these observations highlights a clear ongoing Need which warrants further attention (Fisher and Spiess 1963; Lund et al. 2012, 2015; Grare et al. 2021; Ortiz-Suslow et al. 2021).

Acknowledgments

Lead author Wolding extends his gratitude to Chidong Zhang and Elizabeth Thompson, whose contributions helped improve this article.

References

Basha, G., and M. V. Ratnam, 2009: Identification of atmospheric boundary layer height over a tropical station using high-resolution radiosonde refractivity profiles: Comparison with GPS radio occultation measurements. *J. Geophys. Res.: Atmos*., **114**, https://doi.org/10.1029/2008JD011692.

Danabasoglu, G., and Coauthors, 2020: The Community Earth System Model Version 2 (CESM2). *J. Adv. Model. Earth Syst*., **12**, https://doi.org/10.1029/2019MS001916.

Durre, I., X. Yin, R. S. Vose, S. Applequist, and J. Arnfield, 2018: Enhancing the data coverage in the integrated global radiosonde archive. *J. Atmos. Oceanic Technol*., **35**, 1753–1770, https://doi.org/10.1175/JTECH-D-17-0223.1.

Fisher, F. H., and F. N. Spiess, 1963: Flip-floating instrument platform. *J. Acoust. Soc. Amer*., **35**, 1633–1644, https://doi.org/10.1121/1.1918772.

Grare, L., N. M. Statom, N. Pizzo, and L. Lenain, 2021: Instrumented wave gliders for air-sea interaction and upper ocean research. *Front. Mar. Sci*., **8**, https://doi.org/10.3389/fmars.2021.664728.

Hersbach, H., and Coauthors, 2020: The ERA5 global reanalysis. Quart. *J. Roy. Meteor. Soc*., **146**, 1999–2049, https://doi.org/10.1002/qj.3803.

Ho, S. -P., and Coauthors, 2020: The COSMIC/FORMOSAT-3 radio occultation mission after 12 years: Accomplishments, remaining challenges, and potential impacts of COSMIC-2. *Bull. Amer. Meteor. Soc*., **101**, E1107–E1136, https://doi.org/10.1175/BAMS-D-18-0290.1.

Holloway, C. E., and J. D. Neelin, 2009: Moisture vertical structure, column water vapor, and tropical deep convection. *J. Atmos. Sci*., **66**, 1665–1683, https://doi.org/10.1175/2008JAS2806.1.

Inoue, K., M. Biasutti, and A. M. Fridlind, 2021: Evidence that horizontal moisture advection regulates the ubiquitous amplification of rainfall variability over tropical oceans. *J. Atmos. Sci.*, **78**, 529–547, https://doi.org/10.1175/JAS-D-20-0201.1.

Kiladis, G. N., M. C. Wheeler, P. T. Haertel, K. H. Straub, and P. E. Roundy, 2009: Convectively coupled equatorial waves. *Rev. Geophys*., **47**, https://doi.org/10.1029/2008RG000266.

Kursinski, E., G. Hajj, J. Schofield, R. Linfield, and K. R. Hardy, 1997: Observing Earth's atmosphere with radio occultation measurements using the global positioning system. *J. Geophys. Res.: Atmos*., **102**, 23429–23465, https://doi.org/10.1029/97JD01569.

Lund, B., H. C. Graber, and R. Romeiser, 2012: Wind retrieval from shipborne nautical X-band radar data. *IEEE Trans. Geosci. Remote Sens*., **50**, 3800–3811, https://doi.org/10.1109/TGRS.2012.2186457.

Lund, B., H. C. Graber, H. Tamura, C. Collins III, and S. Varlamov, 2015: A new technique for the retrieval of near-surface vertical current shear from marine X-band radar images. *J. Geophys. Res.: Oceans*, **120**, 8466–8486, https://doi.org/10.1002/2015JC010961.

Nehrir, A. R., and Coauthors, 2017: Emerging technologies and synergies for airborne and space-based measurements of water vapor profiles. *Surv. Geophys*., **38**, 1445–1482, https://doi.org/10.1007/s10712-021-09629-5.

Ortiz-Suslow, D. G., J. Kalogiros, R. Yamaguchi, and Q. Wang, 2021: An evaluation of the constant flux layer in the atmospheric flow above the wavy air-sea interface. *J. Geophys. Res.: Atmos*., **126**, https://doi.org/10.1029/2020JD032834.

Pincus, R., A. Beljaars, S. A. Buehler, G. Kirchengast, F. Ladstaedter, and J. S. Whitaker, 2017: The representation of tropospheric water vapor over low-latitude oceans in (re-) analysis: Errors, impacts, and the ability to exploit current and prospective observations. *Surv. Geophys*., **38**, 1399–1423, https://doi.org/10.1007/s10712-017-9437-z.

Ren, P., D. Kim, M. -S. Ahn, D. Kang, and H. -L. Ren, 2021: Intercomparison of MJO column moist static energy and water vapor budget among six modern reanalysis products. *J. Climate*, **34**, 2977–3001, https://doi.org/10.1175/JCLI-D-20-0653.1.

Roy, R. J., M. Lebsock, and M. J. Kurowski, 2021: Spaceborne differential absorption radar water vapor retrieval capabilities in tropical and subtropical boundary layer cloud regimes. *Atmos. Meas. Tech*., **14**, 6443–6468, https://doi.org/10.5194/amt-14-6443-2021.

Roy, R. J., M. Lebsock, L. Millán, and K. B. Cooper, 2020: Validation of a G-band differential absorption cloud radar for humidity remote sensing. *J. Atmos. Oceanic Technol*., **37**, 1085–1102, https://doi.org/10.1175/JTECH-D-19-0122.1.

Roy, R. J., M. Lebsock, L. Millán, R. Dengler, R. Rodriguez Monje, J. V. Siles, and K. B. Cooper, 2018: Boundary-layer water vapor profiling using differential absorption radar. *Atmos. Meas. Tech*., **11**, 6511–6523, https://doi.org/10.5194/amt-11-6511-2018.

Schröder, M., M. Lockhoff, J. M. Forsythe, H. Q. Cronk, T. H. Vonder Haar, and R. Bennartz, 2016: The GEWEX water vapor assessment: Results from intercomparison, trend, and homogeneity analysis of total column water vapor. *J. Appl. Meteor. Climatol*., **55**, 1633–1649, https://doi.org/10.1175/JAMC-D-15-0304.1.

Wolding, B., J. Dias, G. Kiladis, F. Ahmed, S. W. Powell, E. Maloney, and M. Branson, 2020: Interactions between moisture and tropical convection. Part I: The coevolution of moisture and convection. *J. Atmos. Sci*., **77**, 1783–1799, https://doi.org/10.1175/JAS-D-19-0225.1.

Wolding, B., S. W. Powell, F. Ahmed, J. Dias, G. Kiladis, M. Gehne, G. Kiladis, and J. D. Neelin, 2022: Tropical thermodynamic-convection coupling in observations and reanalyses. *J. Atmos. Sci*., **79**, 1781-1803, https://doi.org/10.1175/JAS-D-21-0256.1.

Xie, F., D. Wu, C. Ao, A. Mannucci, and E. Kursinski, 2012: Advances and limitations of atmospheric boundary layer observations with GPS occultation over southeast Pacific Ocean. *Atmos. Chem. Phys*., **12**, 903–918, https://doi.org/10.5194/acp-12-903-2012.

Yasunaga, K., S. Yokoi, K. Inoue, and B. E. Mapes, 2019: Space–time spectral analysis of the moist static energy budget equation. *J. Climate*, **32**, 501–529, https://doi.org/10.1175/JCLI-D-18-0334.1.

Zadra, A., and Coauthors, 2018: Systematic errors in weather and climate models: Nature, origins, and ways forward. *Bull. Amer. Meteor. Soc*., **99**, ES67–ES70, https://doi.org/10.1175/BAMS-D-17-0287.1.

Satellite measurements of the tropical Pacific coupled marine boundary layer

Kyla Drushka[1], Darren Jackson[2,3], Elizabeth Thompson[2], Gary Wick[2]

[1]University of Washington, Applied Physics Laboratory
[2]NOAA Physical Sciences Laboratory
[3]University of Colorado / Cooperative Institute for Research in Environmental Sciences

The tropical Pacific is home to energetic coupled air-sea processes on scales ranging from O(1) km to O(10,000) km. Major gaps in our understanding, observations, and prediction of these processes remain, including multi-scale interactions within the coupled ocean and atmospheric boundary layers, vertical mixing in both the ocean and the atmosphere, and turbulent fluxes across the air-sea interface. To address these gaps, the recent workshop on "Tropical Pacific Observing Needs to Advance Process Understanding and Representation in Models" identified (among other needs) a need for sustained, high-frequency, vertically resolved, and colocated observations of the upper ocean and lower atmosphere (DeMott et al. 2022).

Satellite measurements are a critical component of the tropical Pacific observing system, as they provide long-term monitoring of numerous parameters, broad spatial coverage, and reliable inputs to forecast models. This article summarizes the role of satellites in observing the oceanic and atmospheric marine boundary layers (MBLs) in the tropical Pacific, including their strengths and limitations as well as an overview of current and future capabilities. While satellites generally do a good job of characterizing daily to weekly mean properties across O(10-100) km footprints at the ocean surface (e.g., temperature, salinity, wind, radiative solar and infrared surface fluxes, and rain rate), the challenge lies in resolving these processes on finer scales, and capturing properties immediately above and below the air-sea interface (boundary layer depths, air temperature and humidity, vertical structure of properties through each boundary layer). These issues present challenges in estimating air-sea fluxes of heat, moisture, and momentum, as well as understanding the coevolution of coupled air-sea boundary layers (Figure 1).

The oceanic boundary layer

Sea surface temperature

Sea surface temperature (SST) is a fundamental boundary condition for studies of air-sea interactions and the oceanic and atmospheric boundary layers. Fortunately, satellite-based retrievals of SST are among the highest quality remotely sensed products. Infrared (IR)-based retrievals

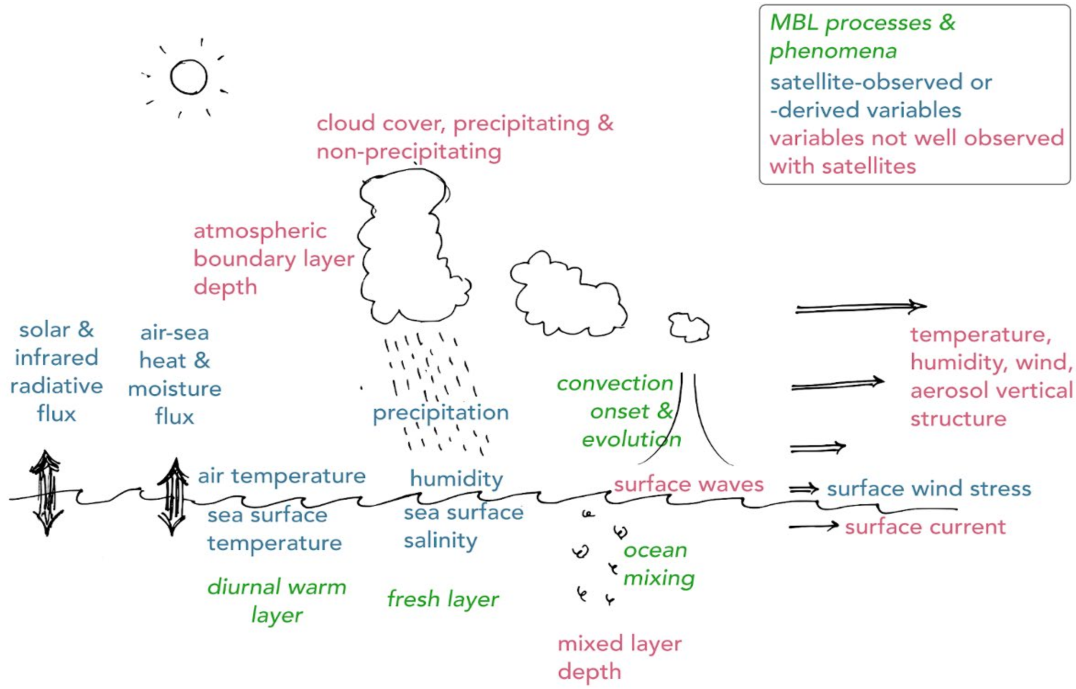

Figure 1. Illustrates the major processes and phenomena in the coupled tropical MBL (labeled in green), the variables that are observed or derived from satellite measurements (blue), and those that are not well observed using satellites (pink). Courtesy of Kyla Drushka.

provide high resolution observations (~1 km or better) under cloud-free conditions, while passive microwave data provide coarser resolution (~50 km) observations through non-precipitating clouds. The data have well-characterized uncertainties and long time records. Climate quality satellite-derived SSTs from 1981 to present are now available through the ESA Climate Change Initiative (e.g., Merchant et al. 2019). Multi-sensor analyses (see Martin et al. 2012; Dash et al. 2012; O'Carroll et al. 2019; and Vazquez-Cuervo et al. 2022) for description and comparison of many of the missions and products) take advantage of the complementary strengths of the different observation types to provide high quality daily fields of the foundation SST at spatial resolutions down to 1 km. Current generations of geostationary satellites further enable accurate sampling of diurnal SST variations (Wick and Castro 2020) and some analyses like the Operational Sea Surface Temperature and Sea Ice Analysis now provide hourly SST estimates (Good et al. 2020). Care must be taken when selecting or applying the wide range of satellite-derived SST products to account for differences in their representative depth and methods to account for factors including the cool skin, diurnal warm layer, and hourly variability.

Clouds are a particular challenge for retrieving satellite SST measurements over the tropical oceans. They block visible and infrared signals that provide the highest resolution SST (and ocean color) measurements, while also shading the surface from solar radiation and emitting infrared radiation in all directions and thereby modulating SST. Newer generations of passive microwave sensors (e.g., the ESA-proposed Copernicus Imaging Microwave Radiometer) aim to provide higher resolution (~15 km) measurements in the presence of clouds.

Mixed-layer depth

The depth of the ocean boundary layer, or mixed-layer depth (MLD), is of critical importance to coupled air-sea processes as it controls the amount of upper ocean heat that is available to the atmosphere. MLD can range from 1 to almost 100 m in the tropical Pacific and can vary by up to tens of meters within a day in response to surface forcing (winds, waves, surface cooling/heating, precipitation) and ocean dynamics. MLD is typically defined as the depth to which near-surface density is constant (e.g., well mixed); in the tropical Pacific, this is usually dominated by salinity, with temperature a major contributor. Observing MLD variations is thus a major challenge, as it requires high-resolution vertical profiles of both temperature and salinity. Although MLD cannot be directly measured with satellites, indirect methods have been developed to estimate MLD in a few specific situations. Fresh surface layers generated by rainfall produce stable layers O(0.1 to 1) meters thick that act as thin boundary layers, preventing mixing between the surface and below the layer. Similarly, ocean diurnal warm layers create stable layers O(1) meters thick. Recent efforts have shown that fresh layers can be predicted from satellite rain measurements and a simple model for the evolution of salinity profiles (Santos-Garcia et al. 2014). Sea surface salinity (SSS) estimates from the SMOS, Aquarius, and SMAP satellites have been used to detect the presence and strength of large rain-generated fresh layers and upper-ocean salinity stratification in river plumes; relating these to upper ocean structure is a subject of ongoing research. Efforts to simulate amounts of diurnal warming present in individual satellite SST retrievals using a combination of satellite-derived and numerical weather prediction model data (e.g., Merchant et al. 2019) can also yield estimates of the diurnal warm layer thickness. Recent efforts to estimate MLD by combining satellite measurements of SSS, SST, and sea surface height with in situ profiles have shown promising results in the tropical Pacific Ocean (Foster et al. 2021).

Surface currents and waves

Ocean surface velocity and waves are critical parameters for quantifying the oceanic component of the air-sea momentum flux. Present-day satellite missions do not measure ocean currents directly, but several products estimate geostrophic currents based on altimetric sea surface height and Ekman currents from surface winds (e.g., OSCAR, Globcurrent). Geostrophy breaks down at the equator, so these products have large uncertainties there—particularly the meridional velocity component (Johnson et al. 2007). Sequences of high-resolution satellite-derived SST have also been used to estimate surface currents using maximum cross correlation techniques (e.g., Bowen et al. 2002) and to improve altimetric-derived estimates (Ciani et al. 2020). Vertical current shear, which plays a major role in equatorial mixing, cannot be measured using satellite remote sensing techniques. Surface waves regulate the transfer of momentum between atmosphere and ocean yet have often been overlooked in studies of air-sea interaction in the tropics. Estimates of significant wave height are made using satellite altimeter data (e.g., the merged multi-satellite GlobWave project; Farquhar et al. 2013), but other important parameters such as directional wave spectra are not available.

The atmospheric boundary layer

Vertical structure

There is a striking lack of information over the tropical Pacific on the vertical structure of atmospheric motion, thermodynamics, atmospheric composition, clouds, and precipitation which, together, drive air-sea interaction and the global atmospheric circulation. Passive imaging, spectrometer, microwave, and IR satellite measurements of clouds, precipitation, water vapor and liquid water content, and aerosols are often column-integrated quantities rather than the vertically-resolved, concentration, size distribution, and composition information needed to comprehensively study convection or estimate radiative-cloud microphysics-aerosol feedbacks that drive weather and climate.

Marine atmospheric boundary layer (MABL) height can be estimated at sub-kilometer spatial resolution and ~100 m vertical resolution from spaceborne lidar or laser altimeters, but with very slow update cycles (e.g., 16 days for the CALIPSO mission). GPS-RO (radio occultation) methods are lower resolution (2°, > monthly) with similar vertical resolution (e.g., the COSMIC mission). More high-spatial resolution MABL height retrievals, with much quicker update cycles, are needed in cloudy and precipitating conditions that befall lidar techniques.

The vast majority of temperature and humidity observations from satellites are currently derived from passively collecting multi-spectral and hyperspectral infrared and microwave observations and from GPS-RO (see section 2 of Wolding et al. this issue). Multi-spectral microwave observations and hyperspectral IR observations are currently available on the Suomi National Polar-orbiting Partnership (NPP) and will be available onboard the Joint Polar Orbiting System (JPSS) satellite series over the next two decades. NPP observations have increased spatial resolution and improved vertical resolutions (~1 km) and accuracy (Smith et al. 2009; Iturbide-Sanchez et al. 2018) of atmospheric profiles compared to previous Advanced TIROS Operational Vertical Sounder satellites, but limitations still remain for profiling the MABL. Hyperspectral IR observations are ineffective below clouds, thus reducing the vertical resolution of the remaining microwave observation. Recent development of a hyperspectral microwave instrument (Aires et al. 2015) is a promising development that should improve vertical resolution if incorporated into future satellite missions. The recent completion of the six-satellite COSMIC-2 constellation (Schriener et al. 2019; Johnston et al. 2021) uses RO with higher vertical resolution profiles (~200 m) than the infrared and microwave sounders.

Surface wind stress

Surface winds are a critical driver of air-sea momentum and turbulent heat fluxes and ocean mixing. Passive microwave satellite radiometers sense surface roughness, which is converted to a scalar wind speed estimate via a radiative transfer model, giving spatial resolutions of 20–35 km. The scalar wind speed record has been continuous, with good spatial and temporal coverage, since 1996 (Bourassa et al. 2019). However, vector winds are needed to accurately estimate fluxes and characterize air-sea interaction; these are typically measured with scatterometers–active micro-wave radiometers. The existing scatterometer constellation currently achieves better than 25 km resolution every 6 hours; the International Ocean Vector Winds Science Team recommends at least one scatterometer fly in an equatorial orbit to improve tropical coverage (Bourassa et al. 2019). Both scalar and vector wind retrievals have large uncertainties in raining conditions.

Precipitation

Surface rain rate is critical for estimating the freshwater input to the ocean and the sensible heat flux due to rain (Gosnell et al. 1995). Rain rate can be estimated from satellite radar products at 5 km resolution with an approximate 1.5 day update cycle (GPM Dual-frequency Precipitation Radar radar) or from multi-satellite merged global products available at nominal 30 min and ~10 km resolution (CMORPH or IMERG). Though considered higher accuracy, satellite radar products cannot measure into the atmospheric boundary layer because the lowest clutter-free bin (1.5–2.5 km) is almost always above the top of the atmospheric mixed layer, and often above or at the subsidence inversion height. The result is that satellite precipitation radar data often do not include raining boundary layer cumulus clouds ubiquitous to the tropics and subtropics. Merged multi-satellite products are global and continuous in time, but show the best accuracy compared to in situ measurements of instantaneous rain rate when averaged over several hours to days, and have effective spatial resolutions closer to ~30 km due to their reliance on passive microwave radiometer input data (Wilheit et al. 1991; Chiu et al. 1993; Kummerow 1998). Thus, raining cells or their fine-scale details are missed when they are smaller than 30 km in dimension and evolve faster than 30–60 min.

Air-sea fluxes

Turbulent and net fluxes

Satellite-derived turbulent heat, moisture, and momentum surface fluxes are a challenge to compute from satellite observations based on bulk methods (e.g., Fairall et al. 1996a,b, 2003; Edson et al. 2013), which require accurate, high-resolution, collocated, and coincident in time retrievals of four input parameters: near-surface wind speed; temperature and humidity; and rain rate. Fluxes are calculated using match-ups of available satellite data, with gaps often filled with reanalysis products. Many satellite-based flux products have been produced; the longest record (since 1958) and most up to date (through 2020 at time of writing) global product of air-sea turbulent and net fluxes is OAFlux, with daily, 1° resolution (Yu 2007; Yu and Weller 2007; Objectively-Analyzed air-sea Fluxes). OAFlux also provides the meteorological and oceanic inputs used to calculate fluxes, including radiation (discussed in the next subsection). Errors and disagreements between different global satellite and reanalysis flux products were recently reviewed by Yu (2019). Random errors in input surface variables which result in air-sea flux uncertainties > 15 Wm^{-2}; differences in sampling time between parameters add additional uncertainties that can exceed 100 Wm^{-2} (Gentemann et al. 2020), particularly in regions of strong atmospheric and oceanic gradients. The indirect approaches used to retrieve the input parameters also lead to significant errors in turbulent fluxes (as discussed above). Finally, no satellite platform combines high-resolution and accurate measurements for all input parameters simultaneously, which is key in reducing flux errors to < 10 Wm^{-2} for spatial scales of < 25 km. Gentemann et al. (2020) proposed combining a microwave imager and hyperspectral sounder onboard a low-earth orbiting small satellite, which would bring turbulent heat and moisture surface flux estimates much closer to the 5 Wm^{-2} goal set forth by the 2017 Earth Science and Applications from the Space Decadal Survey (National Academies of Sciences 2018).

Radiative fluxes

Estimating the net surface heat flux and ocean buoyancy flux requires estimates of all components mentioned in the prior paragraph, plus the downwelling surface infrared (longwave) and solar (shortwave) fluxes. Many legacy historical surface radiation satellite products such as ISCCP and CERES do not provide data past 2017 and had long processing times (International Satellite Cloud Climatology Project, Clouds and the Earth's Radiant Energy System). Newer surface radiation products have higher spatial (⅛-1°) and temporal resolution (hourly, sub-daily) and near-real time latency (e.g., NOAA GSIP – GOES Surface and Insolation Product; NASA FLASHflux). All satellite-based surface radiation products are subject to errors in the radiative transfer model and its input data: aerosol optical depth, cloud optical depth, precipitation, atmospheric gas concentrations, surface albedo, atmospheric temperature and moisture, sea surface emissivity, and SST. Cloud coverage is often a leading source of error in surface solar flux products, followed by aerosols, whereas vertical profiles of temperature and moisture cause most errors in surface infrared products (Zhang et al. 1995, 2006). Upwelling solar heat flux can be estimated reliably from albedo and downwelling solar flux (Payne 1972). Upwelling infrared heat flux can be estimated as a function of skin SST and downwelling infrared heat flux (Fairall et al. 1996b).

Challenges and future missions

In addition to the challenges for specific variables described above, there are a number of general challenges for satellite measurements of the coupled MBL. We now realize the importance of small and fast processes (e.g., diurnal variability, localized atmospheric convective processes, sub-mesoscale ocean variations) in multi-scale interactions within the coupled tropical system, but struggle to observe these with satellites, whose spatial and temporal resolution is limited by physics and mission requirements. However, constellations of satellites (e.g., the Global Precipitation Mission or COSMIC-2) have the advantage of optimizing spatial and temporal coverage. Satellites generally measure individual variables and so capturing coupled processes necessarily requires combining a suite of satellite measurements. On timescales shorter than a few days, correctly matching the time and space signatures of multiple measurements can be problematic. Satellites cannot directly measure vertical ocean structure, advances in combining satellite measurements of the sea surface with vertical profiles from in situ platforms such as Argo floats show promise for capturing ocean vertical structure, particularly as data assimilating models and machine learning techniques improve.

The future of satellite observing is bright. The Investigation of Convective Updrafts (INCUS) and Atmosphere Observing System (AOS) missions, scheduled to launch in 2028-9, will measure the vertical motion of air and water vapor which, together, quantify the convective mass flux. These atmospheric parameters are needed to understand links between convective motion, clouds, precipitation, and their surrounding environment (also described by Wolding et al. this issue). Smaller and optimized satellite precipitation sensors aboard CubeSats or SmallSats are set to be launched soon and might provide precipitation information at higher resolution and closer to the sea surface than currently available (Blackwell et al. 2018). The Surface Water and Ocean Topography (SWOT) mission, launching in late 2022, will enable us to measure sea surface height (and hence to estimate geostrophic currents) on much smaller scales than is currently possible (Morrow et al. 2019). New and expanded satellite sounders, polarimetry, Differential Absorption Lidars, and Differential Absorption Radars, as well as other sensors in low earth orbit, show the promise of providing better vertical profiles of vector wind, air temperature, air humidity, liquid water, water vapor, more detailed aerosol information, as well as more estimates of MABL height. These are discussed further in Wolding et al. (2022 this issue) and Teixeira et al. (2021).

A number of proposed missions are also gaining community support. For instance, the Winds and

Currents Mission would make simultaneous measurements of surface winds and currents (Wineteer et al. 2020) and the Butterfly mission would measure smaller-scale air-sea turbulent heat and moisture fluxes with improved accuracy than currently available (Gentemann et al. 2021). If funded, these or similar missions would transform our ability to measure oceanic and atmospheric boundary layers, as well as the fluxes of heat, moisture, and momentum that are central to tropical Pacific dynamics.

Acknowledgements

Drushka was supported by NASA grant 80NSSC-18K1330. Thompson, Wick, and Jackson acknowledge a NOAA grant through the "Innovative Ocean Dataset/Product Analysis and Development for support of the NOAA Observing and Climate Modeling Communities" competition administered jointly through the NOAA Climate Observations and Monitoring program, NOAA Climate Variability and Predictability program, and NOAA Global Ocean Monitoring and Observing program office.

References

Aires, F., C. Prigent, E. Orlandi, M. Milz, P. Eriksson, S. Crewell, C. -C. Lin, and V. Kangas, 2015: Microwave hyperspectral measurements for temperature and humidity atmospheric profiling from satellite: The clear-sky case. *J. Geophys. Res. Atmos*., **120**, 11334–11351, https://doi.org/10.1002/2015JD023331.

Balaguru, K., G. R. Foltz, L. R. Leung, J. Kaplan, W. Xu, N. Reul, and B. Chapron, 2020: Pronounced impact of salinity on rapidly intensifying tropical cyclones. *Bull. Amer. Meteor. Soc*., **101**, E1497-E1511, https://doi.org/10.1175/BAMS-D-19-0303.1.

Blackwell, W. J., and Coauthors, 2018: An overview of the TROPICS NASA earth venture mission. *Quart. J. R. Meteor. Soc*., **144**, 16-26, https://doi.org/10.1002/qj.3290.

Bourassa, M. A., and Coauthors, 2019: Remotely sensed winds and wind stresses for marine forecasting and ocean modeling. *Front. Mar. Sci*., **6**, 1-28, https://doi.org/10.3389/fmars.2019.00443.

Bowen, M. M., W. J. Emery, J. L. Wilkin, P. C. Tildesley, I. J. Barton, and R. Knewtson, 2002: Extracting multiyear surface currents from sequential thermal imagery using the maximum cross-correlation technique. *J. Atmos. Oceanic Technol*., **19**, 1665-1676, https://doi.org/10.1175/1520-0426(2002)019<1665:EMSCFS>2.0.CO;2.

Ciani, D., M. -H. Rio, B. B. Nardelli, H. Etienne, and R. Santoleri, 2020: Improving the alitimeter-derived surface currents using sea surface temperature (SST) data: A sensitivity study to SST products. *Remote Sens*., **12**, 1601, https://doi.org/10.3390/rs12101601.

Chiu, L. S., A. T. C. Chang, and J. Janowiak, 1993: Comparison of monthly rain rates derived from GPI and SSMI/I using probability distribution functions. *J. Appl. Meteorol*., **32**, 323–334, https://doi.org/10.1175/1520-0450(1993)032<0323:COMRRD>2.0.CO;2.

Cronin, M. F., and Coauthors, 2020: Surface Radiation Community Consultation Working Group Report. *Evolving and Sustaining Ocean Best Practices Workshop IV, Proceedings, IOC Workshop Report*, Paris, France, UNESCO, **2**, 98-111, https://doi.org/10.25607/OBP-1036.

Da, N. D., G. R. Foltz, and K. Balaguru, 2020: A satellite-derived upper-ocean stratification data set for the tropical North Atlantic with potential applications for hurricane intensity prediction. *J. Geophys. Res.: Oceans*, **125**, https://doi.org/10.1029/2019JC015980.

Dash, P., and Coauthors, 2012: Group for high resolution sea surface temperature (GHRSST) analysis fields intercomparisons. Part 2: near-real time web-based level 4 SST quality monitor (L4-SQUAM). *Deep Sea Res. II*, **77–80**, 31–43, https://doi.org/10.1016/j.dsr2.2012.04.002.

DeMott, C. A., A. Subramanian, S. Chen, K. Drushka, Y. Fujii, A. Sutton, J. Sprintall, and D. Zhang, 2022: Focused observations for expanded comprehensions: advancing tropical Pacific coupled modeling and process understanding. *Bull. Amer. Meteor. Soc*., **103**, E1644-E1649, https://doi.org/10.1175/BAMS-D-22-0041.1.

Durre, I., X. Yin, R. S. Vose, S. Applequist, and J. Arnfield, 2018: Enhancing the Data Coverage in the Integrated Global Radiosonde Archive. *J. Atmos. Oceanic Technol*., **35**, 1753-1770, https://doi.org/10.1175/JTECH-D-17-0223.1.

Edson, J. B., and Coauthors, 2013: On the exchange of momentum over the open ocean. *J. Phys. Oceangr*., **43**, 1589–1610, https://doi.org/10.1175/JPO-D-12-0173.1.

Fairall, C. W., E. F. Bradley, J. S. Godfrey, G. A. Wick, J. B. Edson, and G. S. Young, 1996a: Cool-skin and warm-layer effects on sea surface temperature. *J. Geophys. Res*., **101**, 1295–1308, https://doi.org/10.1029/95JC03190.

Fairall, C. W., E. F. Bradley, D. P. Rogers, J. B. Edson, and G. S. Young, 1996: Bulk parameterization of air-sea fluxes for Tropical Ocean- Global Atmosphere Coupled-Ocean Atmosphere Response Experiment. *J. Geophys. Res*., **101**, 3747–3764, https://doi.org/10.1029/95JC03205.

Fairall, C. W., A. B. White, J. B. Edson, and J. E. Hare, 1997: Integrated shipboard measurements of the marine boundary layer. *J. Atmos. Oceanic Technol*., **14**, 338–359, https://doi.org/10.1175/1520-0426(1997)014<0338:ISMOTM>2.0.CO;2.

Fairall, C. W., E. F. Bradley, J. E. Hare, A. A. Grachev, and J. B. Edson, 2003: Bulk parameterization of air-sea fluxes: Updates and verification for the COARE algorithm. *J. Climate*, **16**, 571–591, https://doi.org/10.1175/1520-0442(2003)016<0571:BPOASF>2.0.CO;2.

Farquhar, C. R. and Coauthors, 2013: GlobWave: A Global wave data portal. EUMETSAT. https://www.eumetsat.int/media/8654.

Foster, D., D. J. Gagne, and D. B. Whitt, 2021: Probabilistic machine learning estimation of ocean mixed layer depth from dense satellite and sparse in situ observations. *Journal of Advances in Modeling Earth Systems*, **13**, 1-33, https://doi.org/10.1029/2021MS002474.

Gentemann, C. L. and Coauthors, 2020: FluxSat: Measuring the Ocean–Atmosphere Turbulent Exchange of Heat and Moisture from Space, *Remote Sens*., **12**, 1796, https://doi.org/10.3390/rs12111796.

Gentemann, C. L., and Coauthors, 2021: Butterfly: a satellite mission to reveal the oceans' impact on our weather and climate. *Zenodo*, https://doi.org/10.5281/zenodo.5120586.

Good, S., and Coauthors, 2020: The current configuration of the OSTIA system for operational production of foundation sea surface temperature and ice concentration analyses. *Remote Sens*., **12**, 720, https://doi.org/10.3390/rs12040720.

Gosnell, R., C. W. Fairall, and P. J. Webster, 1995: The sensible heat of rainfall in the tropical ocean. *J. Geophys. Res*., **100**, 18437– 18442, https://doi.org/10.1029/95JC01833.

Iturbide-Sanchez, F., S. R. Santos da Silva, Q. Liu, K. L. Pryor, M. E. Pettey, and N. R. Nalli, 2018: Toward the Operational Weather Forecasting Application of Atmospheric Stability Products Derived From NUCAPS CrIS/ATMS Soundings, IEEE Trans. *Geosci. Remote Sens*., **56**, 4522-4545, https://doi.org/10.1109/TGRS.2018.2824829.

O'Carroll, A. G., and Coauthors, 2019: Observational Needs of Sea Surface Temperature. *Front. Mar. Sci*., **6**, 1-27, https://doi.org/10.3389/fmars.2019.00420.

Johnson, E. S., F. Bonjean, G. S. Lagerloef, J. T. Gunn, and G. T. Mitchum, 2007: Validation and error analysis of OSCAR sea surface currents. *J. Atmos. Oceanic Technol*., **24**, 688-701, https://doi.org/10.1175/JTECH1971.1.

Kummerow, C., 1998: Beamfilling errors in passive microwave rainfall retrievals. *J. Appl. Meteorol*., **37**, 356–370, https://doi.org/10.1175/1520-0450(1998)037<0356:BEIPMR>2.0.CO;2.

Martin, M. and Coauthors, 2012: Group for high resolution sea surface temperature (GHRSST) analysis fields inter-comparisons. Part 1: a GHRSST multi-product ensemble (GMPE). *Deep-Sea Res. II*, **77–80**, 21–30, https://doi.org/10.1016/j.dsr2.2012.04.013.

Merchant, C. J., and Coauthors, 2019: Satellite-based time-series of sea-surface temperature since 1981 for climate applications. *Scientific Data*, **6**, 1-18, https://doi.org/10.1038/s41597-019-0236-x.

Morrow, R., and Coauthors, 2019: Global observations of fine-scale ocean surface topography with the Surface Water and Ocean Topography (SWOT) mission. *Front. Mar. Sci*., **6**, 232, https://doi.org/10.3389/fmars.2019.00232.

National Academies of Sciences, Engineering, and Medicine. 2018. *Thriving on Our Changing Planet: A Decadal Strategy for Earth Observation from Space*. Washington, DC: The National Academies Press. https://doi.org/10.17226/24938.

Payne, R. E., 1972: Albedo of the Sea Surface. *J. Atmos. Sci*., **29**, 959-970, https://doi.org/10.1175/1520-0469(1972)029<0959:AOTSS>2.0.CO;2.

Santos-Garcia, A., M. M. Jacob, W. L. Jones, W. E. Asher, Y. Hejazin, H. Ebrahimi, and M. Rabolli, 2014: Investigation of rain effects on Aquarius Sea Surface Salinity measurements. *J. Geophys. Res. Oceans*, **119**, 7605– 7624, https://doi.org/10.1002/2014JC010137.

Schreiner, W. S., and Coauthors, 2020: COSMIC-2 radio occultation constellation: First results. *Geophys. Res. Lett*., **47**, 1-7, https://doi.org/10.1029/2019GL086841.

Smith, W. L., and Coauthors, 2009: Technical Note: Evolution, current capabilities, and future advance in satellite nadir viewing ultra-spectral IR sounding of the lower atmosphere. *Atmos. Chem. Phys*., **9**, 5563-5574, https://doi.org/10.5194/acp-9-5563-2009.

Teixeira, J., and Coauthors, 2021: The NASA PBL Incubation Study Team Report: Toward A Global Planetary Boundary Layer Observing System. NASA PBL Incubation Study Workshop Report, 134, https://science.nasa.gov/science-pink/s3fs-public/atoms/files/NASA_PBL_Incubation_Final_Report_2.pdf.

Vazquez-Cuervo, J., S. Castro, M. Steele, C. Gentemann, J. Gomez-Valdes, W. Tang, 2022: Comparison of GHRSST SST analysis in the Arctic Ocean and Alaskan coastal waters using Saildrones. *Remote Sens*., **14**, 692, https://doi.org/10.3390/rs14030692.

Wick, G. A., and S. Castro, 2020: Assessment of extreme diurnal warming in operational geosynchronous satellite sea surface temperature products. *Remote Sens*., **12**, 3771, https://doi.org/10.3390/rs12223771.

Wilheit, T. T., A. T. Chang, and L. S. Chiu, 1991: Retrieval of monthly rainfall indices from microwave radiometric measurements using probability distribution functions. *J. Atmos. Oceanic Tech*., **8**, 118–136, https://doi.org/10.1175/1520-0426(1991)008<0118:ROMRIF>2.0.CO;2.

Wineteer, A., and Coauthors, 2020: Measuring winds and currents with Ka-band doppler scatterometry: An airborne implementation and progress towards a spaceborne mission. *Remote Sens*., **12**, 1021, https://doi.org/10.3390/rs12061021.

Yu, L., and R. A. Weller, 2007: Objectively Analyzed Air–Sea Heat Fluxes for the Global Ice-Free Oceans (1981–2005). *Bull. Amer. Meteor. Soc*., **88**, 527-540, https://doi.org/10.1175/BAMS-88-4-527.

Yu, L., 2007: Global Variations in Oceanic Evaporation (1958–2005): The Role of the Changing Wind Speed. *J. Climate*, **20**, 5376-5390, https://doi.org/10.1175/2007JCLI1714.1.

Yu, L., 2019: Global Air–Sea Fluxes of Heat, Fresh Water, and Momentum: Energy Budget Closure and Unanswered Questions. *Annu. Rev. Mar. Sci*., **11**, 227-248, https://doi.org/10.1146/annurev-marine-010816-060704.

Zhang, Y. C., W. B. Rossow, and A. A. Lacis, 1995: Calculation of surface and top of atmosphere radiative fluxes from physical quantities based on ISCCP data sets: 1. Method and sensitivity to input data uncertainties. *J. Geophys. Res*., **100**, 1149–1165, https://doi.org/10.1029/94JD02747.

Zhang, Y. C., W. B. Rossow, and P. W. Stackhouse, 2006: Comparison of different global information sources used in surface radiative flux calculation: Radiative properties of the near-surface atmosphere. *J. Geophys. Res*., **111**, D13106, https://doi.org/10.1029/2005JD006873.

Use of adjoint sensitivity to advance process understanding and identify observing needs in the tropical Pacific

Yosuke Fujii[1], Ariane Verdy[2], Shuhei Masuda[3], Helen Pillar[4], Matthew Mazloff[2], Bruce Cornuelle[2], Patrick Heimbach[4], Aneesh Subramanian[5], Takuma Yoshida[1]

[1]Japan Meteorological Agency / Meteorological Research Institute
[2]University of California, San Diego / Scripps Institution of Oceanography
[3]Japan Agency for Marine-Earth Science and Technology
[4]University of Texas at Austin
[5]University of Colorado

Adjoint models are an essential tool for performing four-dimensional variational (4DVAR) data assimilation (e.g., Rabier et al. 1993; Stammer et al. 2002; Sugiura et al. 2008; Hoteit et al. 2010). They are also used for inferring space and time-resolved sensitivities in a numerical model of oceanic metrics to perturbations (e.g., Fukumori et al. 2004; Masuda et al. 2010), and evaluation of singular vectors to identify instable modes of the system (e.g., Fujii et al. 2008; Zana et al. 2011). Sensitivity experiments using adjoint models can be used to evaluate and design oceanic observation systems (e.g., Köhl and Stammer 2004; Cummings et al. 2014; Loose et al. 2021). This article introduces three studies which evaluate the sensitivity of ocean general circulation models using adjoint models and offers insights into understanding and evaluation of observing needs in the tropical Pacific.

Adjoint sensitivity study based on the Tropical Pacific Ocean State Estimate

A regional configuration of the MIT general circulation model (MITgcm) is constrained to fit observational data from the Tropical Pacific Observing System (TPOS). Data assimilation is accomplished iteratively through the adjoint method (4DVAR), resulting in a physically-realistic estimate of the ocean state. The Tropical Pacific Ocean State Estimate (TPOSE.3) provides overlapping 4-month state estimates from 2010 to 2020 with a 1/3˚ horizontal resolution (see Verdy et al. 2017 for details).

In Verdy et al. (2017), the TAO mooring data were not assimilated but instead used as an independent dataset to assess the skill of TPOSE.3 and to identify the timescales resolved by the current observing and modeling system. On timescales between 20 and 100 days, TPOSE.3 provides a better fit to TAO temperature observations than an objectively mapped Argo product (Roemmich and Gilson 2009), demonstrating the advantage of allowing the MITgcm to serve as a dynamical interpolator in the model-data synthesis. However, neither the state estimate nor the Argo product showed much skill on timescales less than 20 days, suggesting that the TAO mooring array has the potential to bring important higher-frequency information to the state estimate.

Accepting this result implies that observations from the TPOS array are key to representing sub-20-day variability with deterministic skill. However, the dynamical model of TPOSE must also be able to simulate these signals. We have recently enhanced the model resolution to 1/6˚ (TPOSE.6), which has sharpened the simulation of features such as tropical instability waves (TIWs) and Tsuchiya jets. As an example, Figure 1(a) shows that TPOSE.6 represents TIWs; with a 4-month assimilation window, these must come from the model dynamics. Figure 1(b) also indicates that the amplitudes of the zonal jets are increased and the Tsuchiya jets around 5°S and 5°N are better reproduced in the higher-resolution state estimate.

Withholding experiments require the specification of a design strategy (acquired variables/times/locations) and so best serve as network evaluation tools. Although these evaluations are useful for identifying important network elements (e.g., Carrier et al. 2016; Fujii et al. 2019), a clear dynamical explanation of observation impacts is often missing. Adjoint-based methods offer the opportunity for rigorous and dynamics-based observing network design. Recent work by Loose et al. (2020) and Loose and Heimbach (2021) provides a focused assessment of network value as efficacy in detecting and correcting the simulation of key quantities of interest (QoIs). Their approach maps the linear sensitivity of targeted QoIs to changes in the 3D velocity,

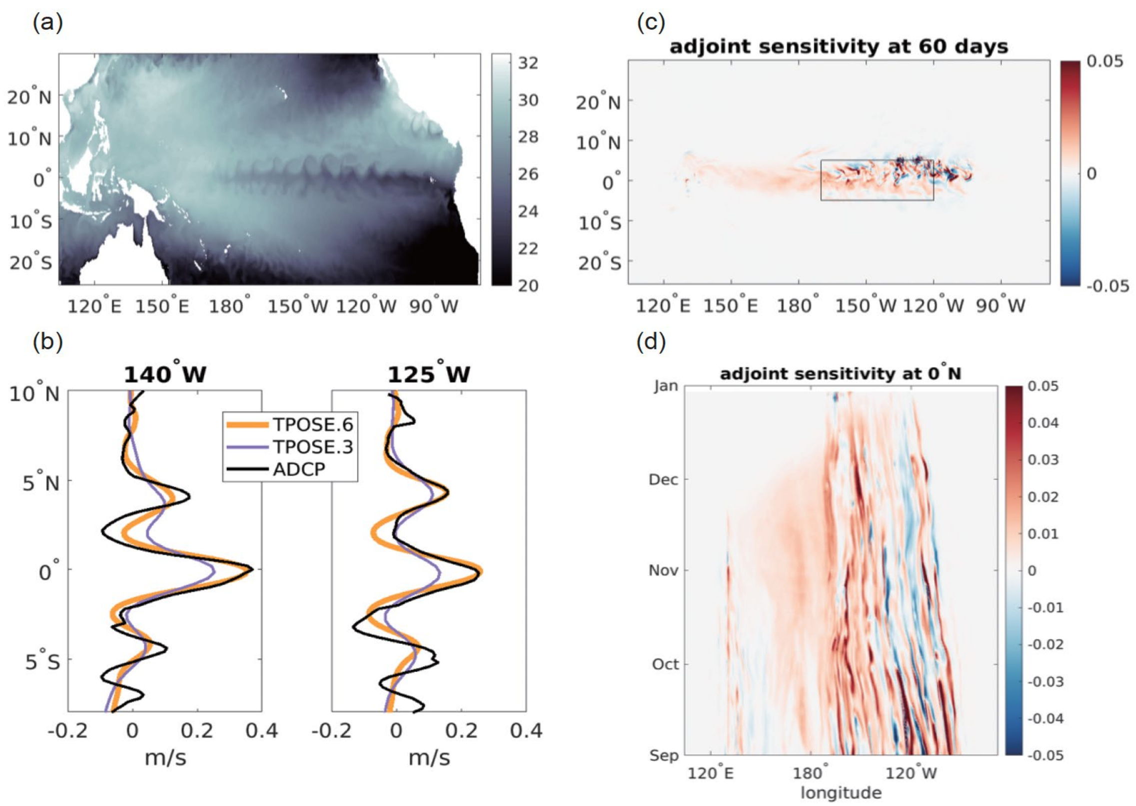

Figure 1. Results of the Tropical Pacific Ocean State Estimation and associated adjoint sensitivity study. (a) SST snapshot on October 31, 2014, in TPOSE.6 showing TIWs. (b) Zonal speed at 200 m vs latitude at 140°W and 125°W in TPOSE.6 (orange), TPOSE.3 (purple), and from ADCP observations (black; Johnson et al. 2002). (c) Snapshots of adjoint sensitivity of SST in the Niño 3.4 region (black box) on December 31, 2015, to zonal wind stress perturbations 60 days earlier in TPOSE.6. (d) Time-longitude Hovmöller diagram of the sensitivity along the equator during a 4-month adjoint run. Red colors indicate time/location of increased eastward wind stress resulting in SST warming. Units are oC / day / (N/m^2).

temperature, salinity, and surface forcing (e.g., the model state and inputs). These linear sensitivity maps are akin to "heat maps" generated by Layer-wise Relevance Propagation for interpretable machine learning (McGovern et al. 2019; Samek et al. 2021) and quantify variables and regions that impact the QoIs.

Adjoint experiments have been conducted in TPOSE.6 to map the sensitivity of Niño 3.4 SST to atmospheric forcing perturbations (Figures 1c and 1d). As explained by Zhang et al. (2011), downwelling Kelvin waves excited by westerly wind anomalies in the western equatorial Pacific can reach the Niño 3.4 region on timescales of 2–3 months, explaining the largely positive sensitivity extending westward along the equatorial Pacific. In contrast to Zhang et al. (2011) which used higher viscosities in the adjoint model to filter nonlinearities from TIWs, our sensitivities show small-scale structures eastward of 180˚E and within ±5˚ of the Equator, indicative of TIWs (e.g., see Figure 2 in Chelton et al. 2000). Inspecting the time-space evolution of these sensitivities reveals westward propagation at phase speeds of ~0.5 ms^{-1} consistent with observations (cf. Chelton et al. 2000, Figure 5). These sensitivity maps reveal mechanisms that may underpin Niño 3.4 SST variability. The magnitude of the variability depends on the extent that zonal wind anomalies project onto these patterns. Whether these wind-driven responses can be captured by the current observing system is determined by quantifying the extent that the observations project onto these QoI sensitivity patterns.

Possible methods to design the Argo array based on adjoint sensitivity

Masuda and Hosoda (2014) demonstrated some case studies for an optimal design of the Argo float network. They employed adjoint sensitivity analysis along with a four-dimensional fluctuating oceanic current system to identify the key regions that drifting profiling floats should intensively monitor. They chose "heat content" as a scientific benchmark to validate the "optimal" system.

An adjoint code was used to define the ambient sensitivity of the oceanic heat content to a subtle change in the water temperature within the Pacific Basin. The model has a horizontal resolution of 1˚ and is capable of multi-decadal sensitivity analyses. Figure 2 shows the distribution of the calculated products averaged over the upper 2000 m of the water column. The geographical patterns show the high "sensitivity" areas of the change in the heat content during 10-year period to small perturbations in modeled water temperature. Relatively high positive values appear near the equatorial region, in the central part of the southern subtropical region centered at 40˚S, 120˚W, and in the western subtropical region along 13˚N. Additionally, the values in the Kuroshio Extension region west of 170˚W around 40˚N are relatively high. Such large values highlight regions that are most important for monitoring.

A regularly arranged deployment of in-situ instrumentation is not necessarily the most effective method for monitoring basin-scale oceanic heat content variations over a decadal timescale. A configuration and monitoring frequency based on the alternative shown in Figure 2 may be more efficient. It should be noted that the configuration can be specifically adjusted according to the targeted climate variation, that is the change in the upper ocean heat content. A non-biased configuration will be desirable for fundamental ocean monitoring.

Masuda and Hosoda (2014) showed the effectiveness of the proposed "optimal" observation designed to monitor the decadal evolution of heat content in the entire Pacific region. Two sets of 1652 grid points, which represented a rectangular region of the Pacific Ocean from 60˚S to 60˚N and from 120˚E to 70˚W, were used. This value (1652) corresponds to the number of oceanic observation sites spaced in intervals of 3˚ of latitude by 3˚ of longitude across the region as an Argo network analogy. The first set followed a conventional deployment pattern on a regularly assigned grid (e.g., every 3˚ in both latitude and longitude).

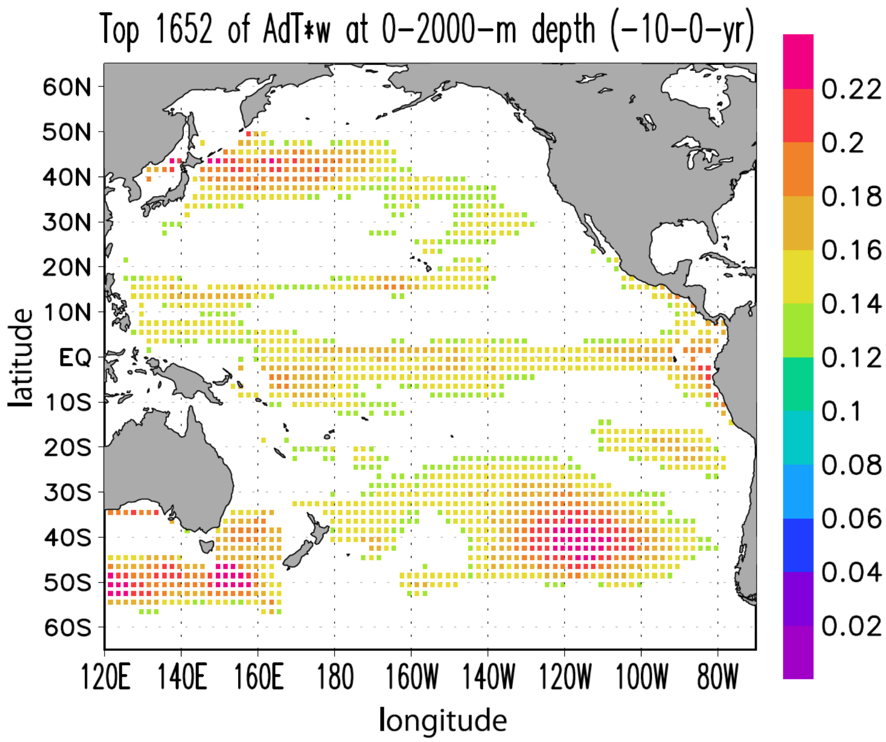

Figure 2. Modified sensitivity calculated as the product of sensitivity values and the square root of the temperature error variance. Plot shows the 1652 highest sensitivity values to a decadal heat content change, where the values are averaged over the upper 2000 m of the water column within an adjoint time window of 10 years. Units are °C. From Masuda and Hosoda 2014, CC.

The other represented a systematic deployment consisting of the 1652 grid points shown in Figure 2.

The total value of the observational sensitivity derived from the "optimal" observing system is 1.21 times that of the conventional one. Thus, intensive deployments in key regions may enhance the estimation accuracy of the heat content change in the entire Pacific Basin by 20% without increasing the necessary resources. However, their model spatio-temporal resolution is too low to imitate an Argo float behavior. Taken together with the fact that the proposed values and distributions are from a case study using an ideal experiment, the quantitative reality of the system would be low. Consequently, the potential of this approach to design a new global ocean observation network remains unclear but holds promise for specific scientific targets.

Monitoring the array modes in the global ocean data assimilation system in JMA

JMA updated the coupled atmosphere-ocean prediction system for operational subseasonal-to-seasonal predictions in February 2022. The system initializes the oceanic part of the coupled model using a 4DVAR global ocean data assimilation system constructed from the ocean model used in Urakawa et al. (2020). It has a 1˚× 0.5˚ (zonal × meridional) resolution with meridional refinement to 0.3˚ near the equator. The 4DVAR is based on Usui et al. (2015). It uses 10-day assimilation windows and optimizes analysis increments gradually added to the temperature and salinity fields in the first five days to fit the model trajectory to the data (in-situ temperature and salinity, satellite altimetry, and objective SST mapping) observed in the following five days.

In the 4DVAR system, JMA regularly calculates approximated eigen vectors of the preconditioned Hessian matrix of the cost function, I+B1/2MTHTR-1HMB1/2 scaled by B1/2, where B and R are the background and observation error co-variance matrices, M is the tangent linear model, H is the linearized observation operator, and I is the identity matrix. The vectors are estimated from the search directions and the difference vectors of the gradient based on the adjoint model which are calculated in minimization of the cost function by a quasi-Newton method (Fujii and Kamachi 2003; Fujii 2005), and are equivalent to reduced-rank array modes (Moore et al. 2017, 2021). Eigen vectors of the Hessian matrix are also equivalent to the right singular vectors of the observ-ability matrix (Zou et al. 1992), R-1/2HMB1/2, and therefore reflect characteristics of the singular vectors of the tangent linear model M, as well as being affected by the observation operator H. The relationship between the singular vectors and analysis increments is discussed in Johnson et al. (2005).

Figure 3 shows an example of the leading array modes in the JMA system. Generally, the first several modes have few coherent signals in some specific areas while the number of signals

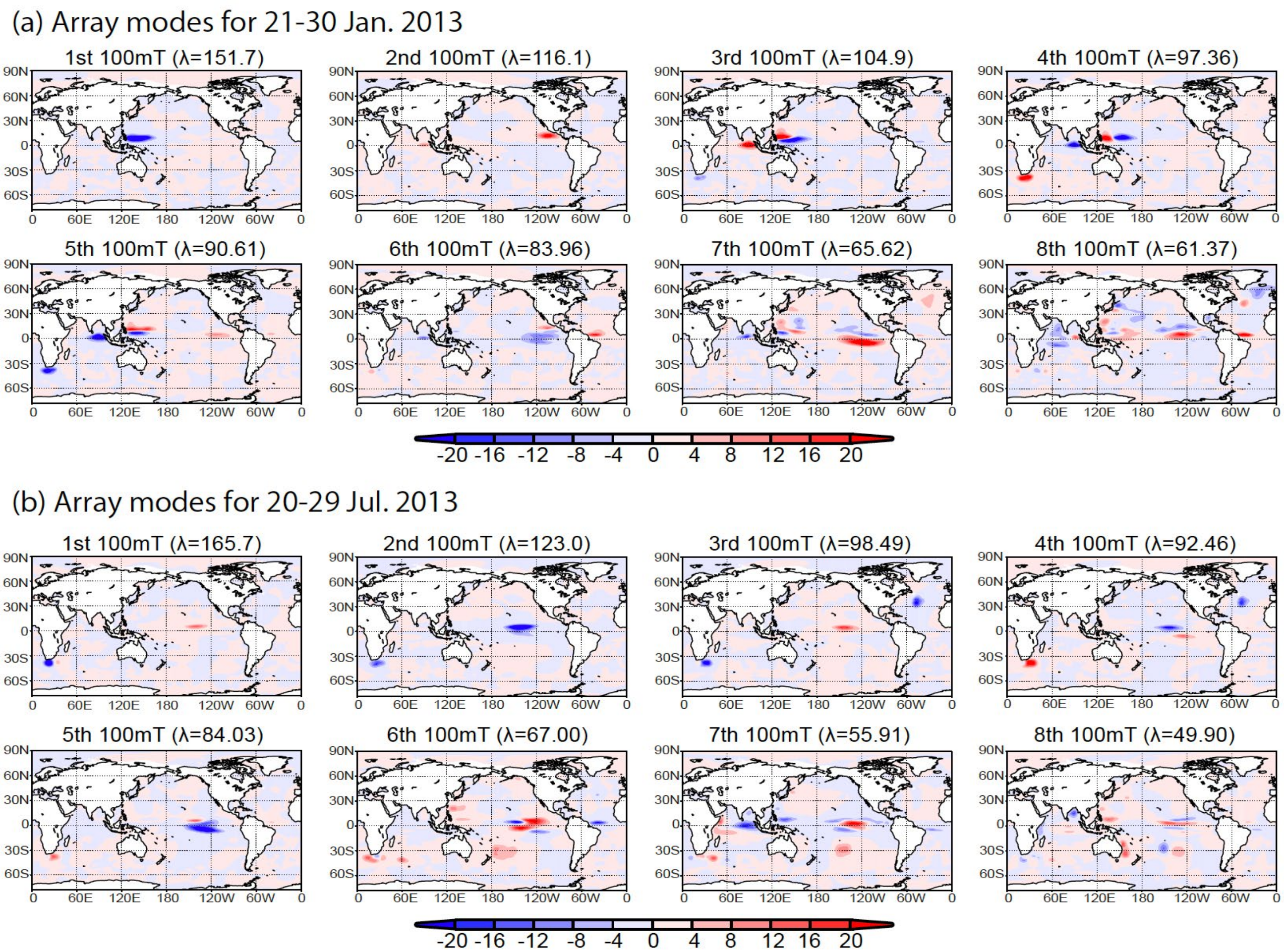

Figure 3. Analysis increments of temperature at 100 m depth corresponding to the leading eight array modes (Units in 10–3˚C) for (a) January 21–30, 2013, and (b) July 20–29, 2013, estimated in the JMA's global ocean 4DVAR system. The eigen value corresponding to each mode is denoted on the top of the panel. Courtesy of Yosuke Fujii.

increases with the order of the modes. The patterns of the array modes are, then, different for different assimilation cycles. As all the modes depicted here have singular values sufficiently larger than two, they significantly affect the analysis increments (Hénaff et al. 2009).

Coherent signals are found around the eastern equatorial Pacific and Indian Oceans, Philippine Sea, and regions of western boundary currents and their extensions. These signals indicate the areas where observation data have high impacts in the assimilation system. Considering the highly uniform distribution of Argo, altimetry, and SST data in the global ocean, the signals seem to reflect unstable modes of the tangent linear model, or perturbations which develop rapidly in the assimilation cycle. The signals around the eastern equatorial Pacific tend to have their peaks away from the equatorial bands, which indicates the importance of off-equatorial observations. In addition, the third, fourth, and fifth modes for 21–30 January imply a physically close connection between temperature variations of eastern equatorial Indian Ocean and Philippine Sea. Monitoring of array modes thus offers some insights on the impacts of observation data and areas where disturbance tends to develop.

Summary

The studies highlighted above demonstrate the potential of adjoint sensitivity applications to explore physical mechanisms underlying ocean variability and to identify observing needs in the tropical Pacific. It is a virtue of adjoint sensitivity calculations that they directly reflect model physics and, therefore, physical interpretation is feasible. In particular, adjoint sensitivity provides physical insight even if systematic model errors hinder meaningful quantitative results. It is, in fact, not straightforward to evaluate the sensitivity in a region where air-sea interactions play a significant role, such as in the tropical Pacific, without an adjoint model of a coupled atmosphere-ocean model. We expect, nevertheless, that recent progress in methodology, including studies on array modes and QoIs, will make a significant contribution to improving the tropical Pacific observing network.

Meanwhile, the OceanPredict Observing System Evaluation Task Team has submitted a UN Decade project “Synergistic Observing Network for Ocean Prediction” (SynObs). SynObs expects that adjoint sensitivity applications will be a key effort to achieve the goal of improving the global and the tropical ocean observing network to get more information from observation data.

Acknowledgements

This work was partly supported by JSPS KAKENHI Grants 17H00728, and 17H04579, and by NOAA/OAR/CPO Grant #NA21OAR4310255.

References

Carrier, M. J., H. E. Ngodock, P. Muscarella, and S. Smith, 2016: Impact of assimilating surface velocity observations on the model sea surface height using the NCOM-4DVAR. *Mon. Wea. Rev*., **144**, 1051-1068, https://doi.org/10.1175/MWR-D-14-00285.1.

Chelton, D. B., F. J. Wentz, C. L. Gentemann, R. A. de Szoeke, and M. G. Schlax, 2000: Satellite microwave SST observations of transequatorial tropical instability waves. *Geophys. Res. Lett*., **27**, 1239-1242, https://doi.org/10.1029/1999GL011047.

Cummings, J. A., and O. M. Smedstad, 2014: Ocean data impacts in global HYCOM. *J. Atmos. Oceanic Technol*, **31**, 1771–1791, https://doi.org/10.1175/JTECH-D-14-00011.1.

Fujii, Y., 2005: Preconditioned Optimizing Utility for Large-dimensional analyses (POpULar). *J. Oceanogr*., **61**, 167-181, https://doi.org/10.1007/s10872-005-0029-z.

Fujii, Y., and M. Kamachi, 2003: A nonlinear preconditioned quasi-Newton method without inversion of a first-guess covariance matrix in variational analyses. *Tellus*, **55A**, 450-454, https://doi.org/10.3402/tellusa.v55i5.12110.

Fujii, Y., and Coauthors, 2019: Observing system evaluation based on ocean data assimilation and prediction systems: On-going challenges and a future vision for designing and supporting ocean observational networks. *Front. Mar. Sci*., **6**, 417, https://doi.org/10.3389/fmars.2019.00417.

Fujii, Y., H. Tsujino, N. Usui, H. Nakano, and M. Kamachi, 2008: Application of singular vector analysis to the Kuroshio large meander. *J. Geophys. Res*., **113**, C07026, https://doi.org/10.1029/2007JC004476.

Fukumori, I., T. Lee, B. Cheng, and D. Menemenlis, 2004: The origin, pathway, and destination of NINO3 water estimated by a simulated passive tracer and its adjoint, *J. Phys. Oceanogr*., **34**, 582–604, https://doi.org/10.1175/2515.1.

Hoteit, I., B. Cornuelle, and P. Heimbach, 2010: An eddy-permitting, dynamically consistent adjoint-based assimilation system for the tropical Pacific: Hindcast experiments in 2000. *J. Geophys. Res*., **115**, C03001, https://doi.org/10.1029/2009jc005437.

Johnson, C., B. J. Hoskins, and N. K. Nichols, 2005: A singular vector perspective of 4D-Var: Filtering and interpolation, *Q. J. R. Meteorol. Soc*., **131**, 1–19, https://doi.org/10.1256/qj.03.231.

Johnson, G. C., B. M. Sloyan, W. S. Kessler, and K. E. McTaggart, 2002: Direct measurements of upper ocean currents and water properties across the tropical Pacific during the 1990s. *Prog. Oceanogr*., **52**, 31–61, https://doi.org/10.1016/S0079-6611(02)00021-6.

Köhl, A., and D. Stammer, 2004: Optimal Observations for Variational Data Assimilation. *J. Phys. Oceanogr*., **34**, 529–542, https://doi.org/10.1175/2513.1.

Le Hénaff, M., P. De Mey, and P. Marsaleix 2009: Assessment of observational networks with the Representer Matrix Spectra method—application to a 3D coastal model of the Bay of Biscay, *Ocean Dyn*., **59**, 3–20, https://doi.org/10.1007/s10236-008-0144-7.

Loose, N., P. Heimbach, H. R. Pillar, and K. H. Nisancioglu, 2020: Quantifying Dynamical Proxy Potential Through Shared Adjustment Physics in the North Atlantic. *J. Geophys. Res*., **125**, e2019RG000654, https://doi.org/10.1029/2020jc016112.

Loose, N., and P. Heimbach, 2021: Leveraging Uncertainty Quantification to Design Ocean Climate Observing Systems. *J. Adv. Model. Earth Syst*., **13**, e2020MS002386, https://doi.org/10.1029/2020MS002386.

Masuda, S., and Coauthors, 2010: Simulated rapid warming of abyssal North Pacific waters. *Science*, **329**, 319–322, https://doi.org/10.1126/science.1188703.

Masuda, S., and S. Hosoda, 2014: Effective Design of Profiling Float Network for Oceanic Heat-Content Monitoring. *Sci. World J*., **2014**, 1-6, https://doi.org/10.1155/2014/340518.

McGovern, A., R. Lagerquist, D. J. Gagne II, G. E. Jergensen, K. L. Elmore, C. R. Homeyer, and T. Smith, 2019: Making the Black Box More Transparent: Understanding the Physical Implications of Machine Learning. *Bull. Amer. Meteor. Soc*., **100**, 2175–2199, https://doi.org/10.1175/bams-d-18-0195.1.

Moore, A. M., J. Levin, H. G. Arrango, and C. A. Edwards 2017: Reduced-rank array modes of the California Current observing system. *J. Geophys. Res*., **123**, 452-465, https://doi.org/10.1002/2017JC013172.

Moore, A. M., J. Levin, H. G. Arrango, and J. Wilkin 2021: Assessing the performance of an ocean observing, analysis and forecast system for the Mid-Atlantic Bight using array modes. *Ocean Modelling*, **164**, https://doi.org/10.1016/j.ocemod.2021.101821.

Rabier, F., P. Courtier, J. Pailleux, O. Talagrand, and D. Vasiljevic, 1993: A comparison between four-dimensional variational assimilation and simplified sequential assimilation relying on three-dimensional variational analysis. *Q. J. R. Meteorol. Soc*., **119**, 845-880, https://doi.org/10.1002/qj.49711951213.

Roemmich, D., and J. Gilson, 2009: The 2004–2008 mean and annual cycle of temperature, salinity, and steric height in the global ocean from the Argo Program. *Prog. Oceanogr*., **82**, 81-100, https://doi.org/10.1016/j.pocean.2009.03.004.

Samek, W., G. Montavon, S. Lapuschkin, C. J. Anders, and K. R. Müller, 2021: Explaining deep neural networks and beyond: A review of methods and applications. *Proceedings of the IEEE*, 109, 247-278 pp., https://doi.org/10.1109/JPROC.2021.3060483.

Stammer, D., and Coauthors, 2002: Global ocean circulation during 1992–1997, estimated from ocean observations and a general circulation model. *J. Geophys. Res*., **107**, C9, 3118, https://doi.org/10.1029/2001JC000888.

Sugiura, N., T. Awaji, S. Masuda, T. Mochizuki, T. Toyoda, T. Miyama, H. Igarashi, and Y. Ishikawa, 2008: Development of a four-dimensional variational coupled data assimilation system for enhanced analysis and prediction of seasonal to interannual climate variations. *J. Geophys. Res*., **113**, C10017, https://doi.org/10.1029/2008JC004741.

Urakawa, L. S., H. Tsujino, H. Nakano, K. Sakamoto, G. Yamanaka, and T. Toyoda, 2020: The sensitivity of a depth-coordinate model to diapycnal mixing induced by practical implementations of the isopycnal tracer diffusion scheme. *Ocean Modelling*, **154**, 101693, https://doi.org/10.1016/j.ocemod.2020.101693.

Usui, N., Y. Fujii, K. Sakamoto, and M. Kamachi, 2015: Development of a Four-Dimensional Variational Assimilation System toward Coastal Data Assimilation around Japan. *Mon. Wea. Rev*., **143**, 3874-3892, https://doi.org/10.1175/MWR-D-14-00326.1.

Verdy, A., B. Cornuelle, M. R. Mazloff, and D. L. Rudnick, 2017: Estimation of the Tropical Pacific Ocean State 2010-13. *J. Atmos. Oceanic Technol*., **34**, 1501-1517, https://doi.org/10.1175/JTECH-D-16-0223.1.

Zanna, L., P. Heimbach, A. M. Moore, and E. Tziperman, 2011: Optimal Excitation of Interannual Atlantic Meridional Overturning Circulation Variability. *J. Climate*, **24**, 413-427, https://doi.org/10.1175/2010JCLI3610.1.

Zhang, X., B. Cornuelle, and D. Roemmich, 2011: Adjoint sensitivity of the Nino-3 surface temperature to wind forcing. *J. Climate*, **24**, 4480–4493, https://doi.org/10.1175/2011JCLI3917.1.

Zou, X., I. M. Navon, and F. X. Le Dimet, 1992: Incomplete observations and control of gravity waves in variational data assimilation. *Tellus*, **44A**, 273–296, https://doi.org/10.3402/tellusa.v44i4.14961.

The in-situ tropical Pacific Ocean operational observing system

Elizabeth J. Thompson[1], Kyla Drushka[2], Brandon Wolding[1,3]

[1]NOAA Physical Sciences Lab
[2]University of Washington
[3]University of Colorado Boulder / Cooperative Institute for Research in Environmental Sciences

Introduction

This article summarizes the tropical Pacific Ocean operational observing system in terms of routine, operational, and/or long-time series records (Figure 1, Table 1). We discuss physical oceanographic, meteorological, and air-sea interface data types. These are summarized in Figure 1, Table 1, and discussed in the next section, "Operational Datasets."

Field campaign data taken in the tropical Pacific Ocean from ships, aircraft, and autonomous platforms collect valuable data during intensive operations periods. However, data archive location and availability vary from experiment to experiment. Field campaign data are not discussed here.

Operational datasets

Argo profiling floats

The international global Argo profiling float array is the largest source of global ocean data in terms of vertical profiles (Figure 2). The University of California, San Diego runs the Argo Program Office, and Argo data are served by Global Data Assembly Centers (GDACS) in France and the US. Argo floats transmit data when they surface, make a downward vertical profile of temperature, salinity (conductivity), and depth (and additional biogeochemical properties, for some floats) between the surface and about 1000 m, drift freely with 1000 m ocean currents for approximately 9 days, descend to 2000 m, make an upward vertical profile of the ocean of the same variables, then start the cycle over at the surface. The goal is for an Argo float to visit every 1000 x 1000 km box every 3 months. Some areas are covered more densely than others due to natural convergence or sheltering by coastlines and currents. For instance, the equatorial region requires a constant resupplying of drifters to maintain consistent Argo data coverage. There is also a notable lack of Argo vertical profiles within the seas of the Maritime Continent, where virtually no Argo data have been collected. Although most of the Argo float network samples only to 2000 m, floats from the Deep Argo mission collect profiles down to 6,000 m depth. The current and future capabilities of the Argo array are discussed by Roemmich et al. (2019).

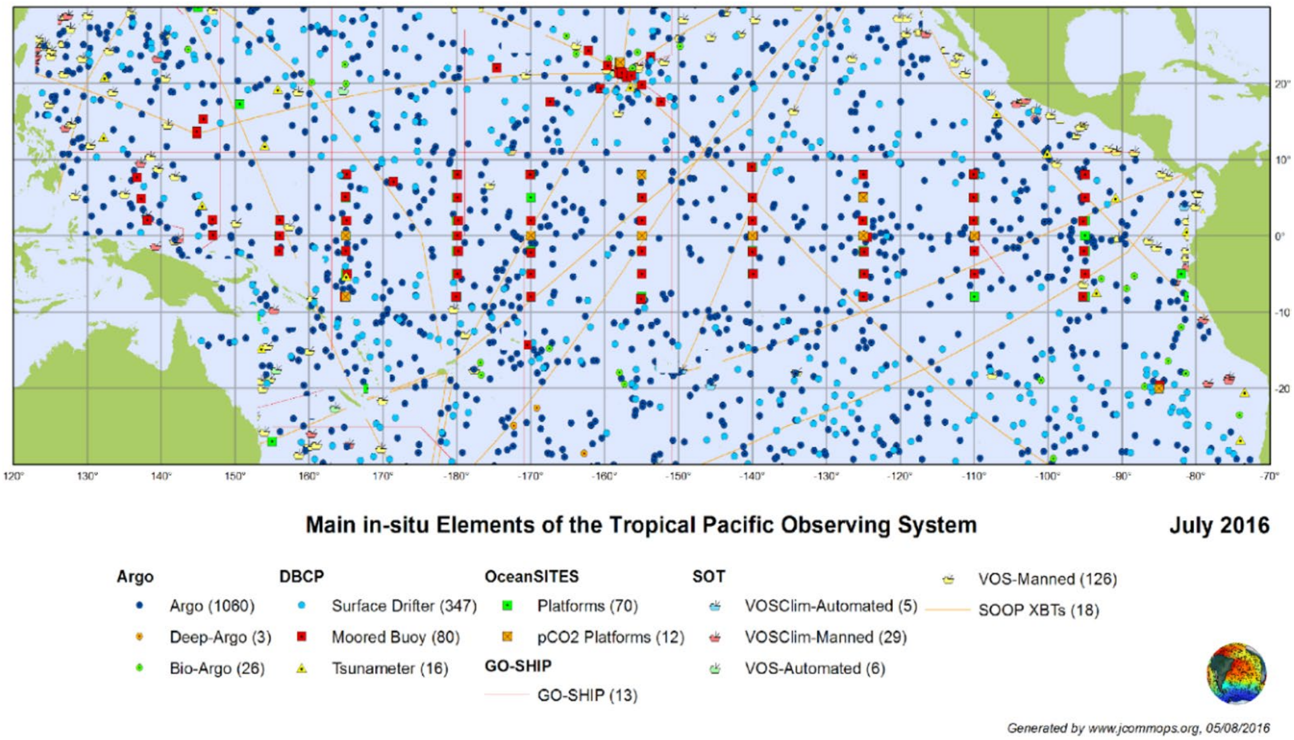

Figure 1. Tropical Pacific in-situ Observing System from TPOS 2020 first report (Cravatte et al. 2016).

Ocean Vertical Profiles	Surface Data: Ocean, Atmosphere, Interface	Atmosphere Vertical Profiles
Argo profiling floats	Meteorology and near-surface oceanographic measurements from research vessels and voluntary observing ships. SAMOS repository for all ship data	NOAA Integrated Global Radiosonde Archive
XBTs launched from ships along repeat transects	AOML global surface drifter program	Dropsondes
AXBTs launched from aircraft	CDIP surface buoys	
TRITON/TAO moorings	Ocean Reference Station (OceanSITES) moorings	
Ocean Reference Station (Ocean SITES) moorings	Tide gauge networks	
GO-SHIP	Moorings or buoys with surface data also served through NDBC	
Repeat Glider transects	Saildrones	

Table 1. Summary of operational in-situ measurements in the tropical Pacific Ocean.

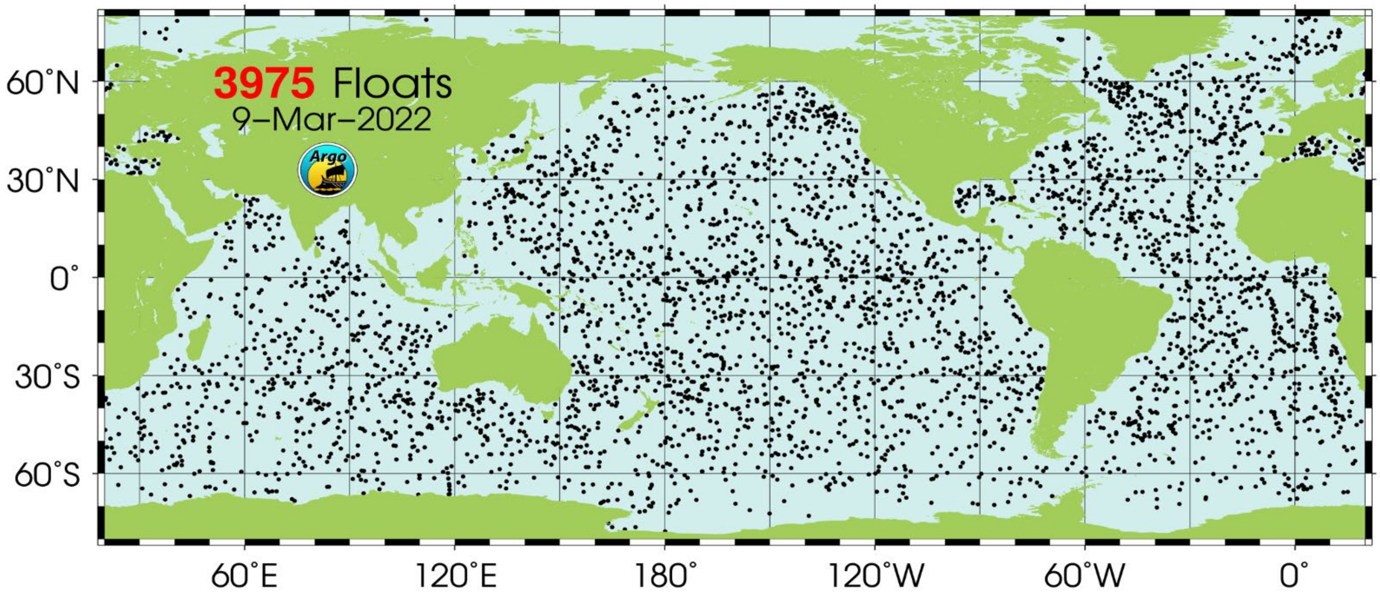

Figure 2. Global array of Argo profiling ocean drifters. Courtesy of Argo Program Office.

XBT and AXBT expendables

Two additional sets of ocean vertical temperature profile data come from expendable sensors. EXpendable BathyThermographs (XBTs) are launched from repeat ship transects, research ships, and ships of opportunity. The XBT network is maintained by NOAA Atlantic Oceanographic and Meteorological Lab (AOML). Airborne EXpendable BathyThermographs (AXBTs) are launched from aircraft as part of NOAA hurricane surveillance flights in the eastern Pacific Ocean, as well as some opportunistic US field program research flights in the Pacific. These data are archived at the NOAA National Center of Environmental Information (NCEI).

TAO / TRITON moorings

The Tropical Atmosphere Ocean (TAO) / Triangle Trans-Ocean Buoy Network (TRITON) instrumented mooring array is currently operated through the NOAA National Buoy Data Center (NDBC) in partnership with the Japan Agency for Marine-Earth Science and Technology (JAMSTEC). Figure 3 shows all moorings that have been deployed since the mid-1990s, though not all are reporting and not all variables are recorded at all stations. Planning is ongoing to upgrade the TAO array through the Tropical Pacific Observing System (TPOS) effort. Presently, these buoys provide ocean vertical profiles of temperature, salinity, and currents. Buoys at 0°W, 140°W and 110°W (discontinued) have Oregon State University χ-pods for measuring the turbulent dissipation rate. Surface meteorology is also measured: rain rate is available at some buoys while most buoys measure surface air temperature and humidity; sea level pressure; and vector wind. Solar and infrared downwelling radiative fluxes are measured at some buoys. A recent Ocean Best Practices Workshop report detailed the challenges and opportunities of obtaining more surface in-situ radiative fluxes across tropical oceans (Cronin et al. 2020). When all these meteorological parameters are measured

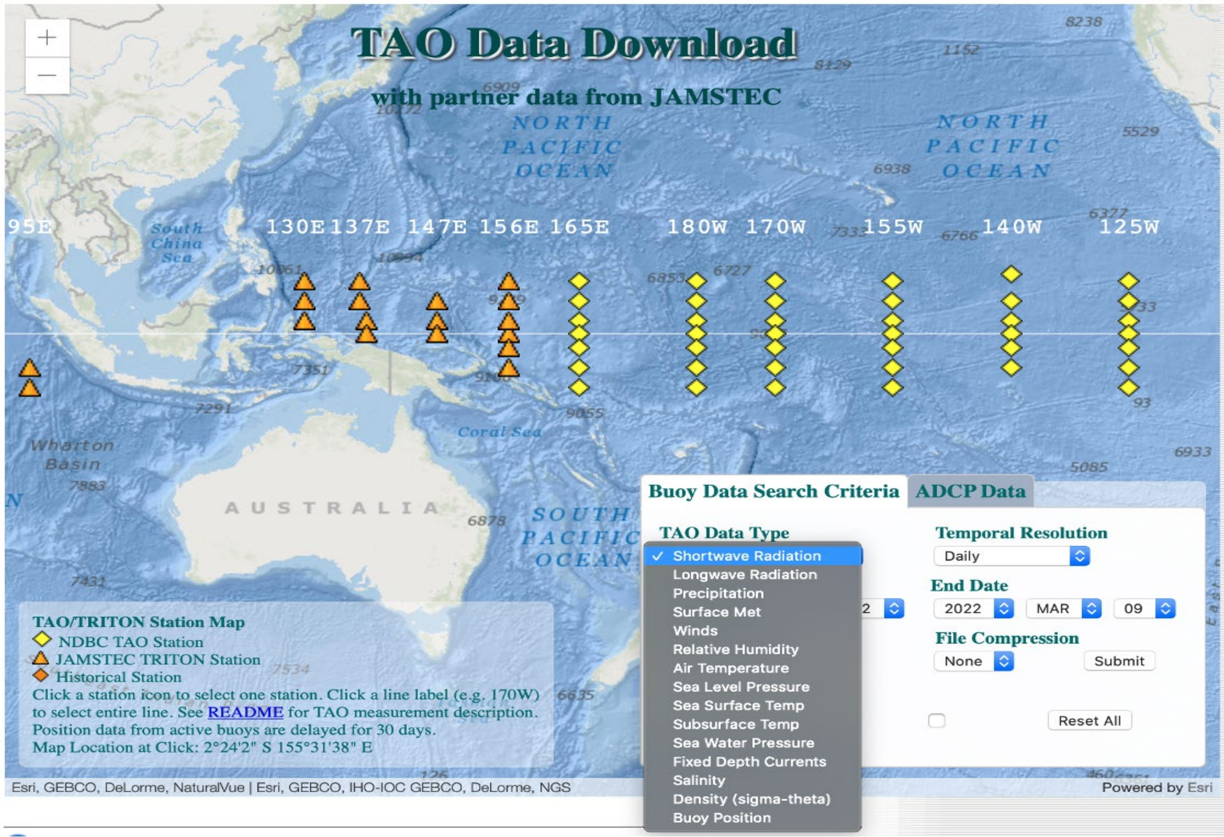

Figure 3. TAO mooring locations and potential data fields available at some buoys for certain time periods. Courtesy of the NOAA National Buoy Data Center.

at the same buoy along with at least near-surface ocean temperature (current and salinity improve estimates but are not technically required), these inputs can be used to estimate the surface net, sensible, latent, and momentum fluxes from bulk algorithms such as COARE (Fairall et al. 1996a,b, 2003; Edson et al. 2013).

Ocean Reference Station (OceanSITES) moorings

The NOAA Global Ocean Monitoring and Observing (GOMO) program maintains data from several Ocean Reference Stations (OceanSITES). These moorings offer deep ocean salinity, temperature, and current profiles as well as surface buoys for near-surface ocean, meteorological, and air-sea flux data. Unlike the operational TAO array, the OceanSITES instrument packages are expanded with several redundant sensors and the buoys are serviced for repairs, full equipment replacements, and calibrations. In the tropical Pacific, the Woods Hole Oceanographic Institution Hawaii Ocean Timeseries (HOT) Site (WHOTS) buoy is located near Hawaii and the Kuroshio Extension Observatory (KEO) is deployed in the Kuroshio Extension Region just east of Japan. The KEO is maintained by the NOAA Pacific Marine Environmental Lab (PMEL). The WHOTS buoy is part of the HOT network of oceanographic moorings and ship records collected around Hawaii since 1987. The OceanSITEs data are publicly available but purposefully withheld from the Global Telecommunications System responsible for collecting and assimilating observations into global numerical prediction models because they are designed to serve as independent benchmarks for model evaluation.

GO-SHIP

The Global Ocean Ship-Based Hydrographic Investigations Program (GO-SHIP) refers to additional ship-based repeat datasets collected on vertical profiles of temperature, salinity, conductivity, pressure, and currents, as well as ocean carbon data.

Repeat Glider Transects (Solomon Sea)

Ocean gliders have repeated horizontal transects of vertical profiles across the Solomon Sea from 2007 to present, between eastern Papua New Guinea and the Solomon Islands. This forms one of the only public, in-situ, long-term datasets of physical oceanography in the Maritime Continent (Figure 2). As the glider transits horizontally, it pitches up and down to collect vertical profiles of temperature, salinity, and velocity, from which horizontal transport is inferred (Kessler et al. 2019a,b, 2021).

SAMOS reporting of surface ocean, atmosphere, and radiation data from ships

All ships in the University-National Oceanographic Laboratory System (UNOLS) and NOAA fleets automatically report their near-surface oceanographic, near-surface meteorological, and radiative flux data through the Shipboard Automated Meteorological and Oceanographic System (SAMOS) operated through Florida State University. These data can be used to calculate surface air-sea bulk fluxes using the COARE bulk flux algorithm (Fairall et al. 1996a,b, 2003; Edson et al. 2013). The SAMOS ocean, meteorology, and air-sea flux database grows as research cruises are performed, repeat maintenance cruises are performed to service mooring arrays, and during transects between field experiments.

Global Surface Drifter Array

The NOAA Atlantic Oceanic and Meteorological Lab (AOML) manages the Global Drifter Array or Global Drifter Program (GDP), with contributions from many countries. The array consists of ~1,300 satellite-tracked drifters (Figure 4). Buoys sense SST, sea level pressure, and ocean surface wave height/direction in real time. The buoys are drogued at 15 m depth, and their positions are used to estimate ocean mixed-layer currents (Elipot et al. 2016).

CDIP surface buoys

The University of California San Diego's Coastal Data Information Program (CDIP) buoys report significant wave height, peak wave period, peak wave direction, and sea surface temperature (Figure 5). Two CDIP buoys exist in the tropical western Pacific on the southern tip of the Mariana Islands, seven CDIP buoys are deployed near Hawaii, and one buoy is deployed near American Samoa (Figure 5). Commercial wave buoys and drifters such as SOFAR, Nortek, and Datawell may also have data coverage over the Pacific. Though their data may be shared with global numerical weather prediction centers for input and data assimilation, these data are not publicly available.

Tide Gauges

NOAA collects and provides sea level height data at several Pacific stations (Figure 6) through the Center for Operational Oceanographic Products and Services, which has collected these data for over 150 years. Very few of these stations also collect other oceanographic or meteorological measurements.

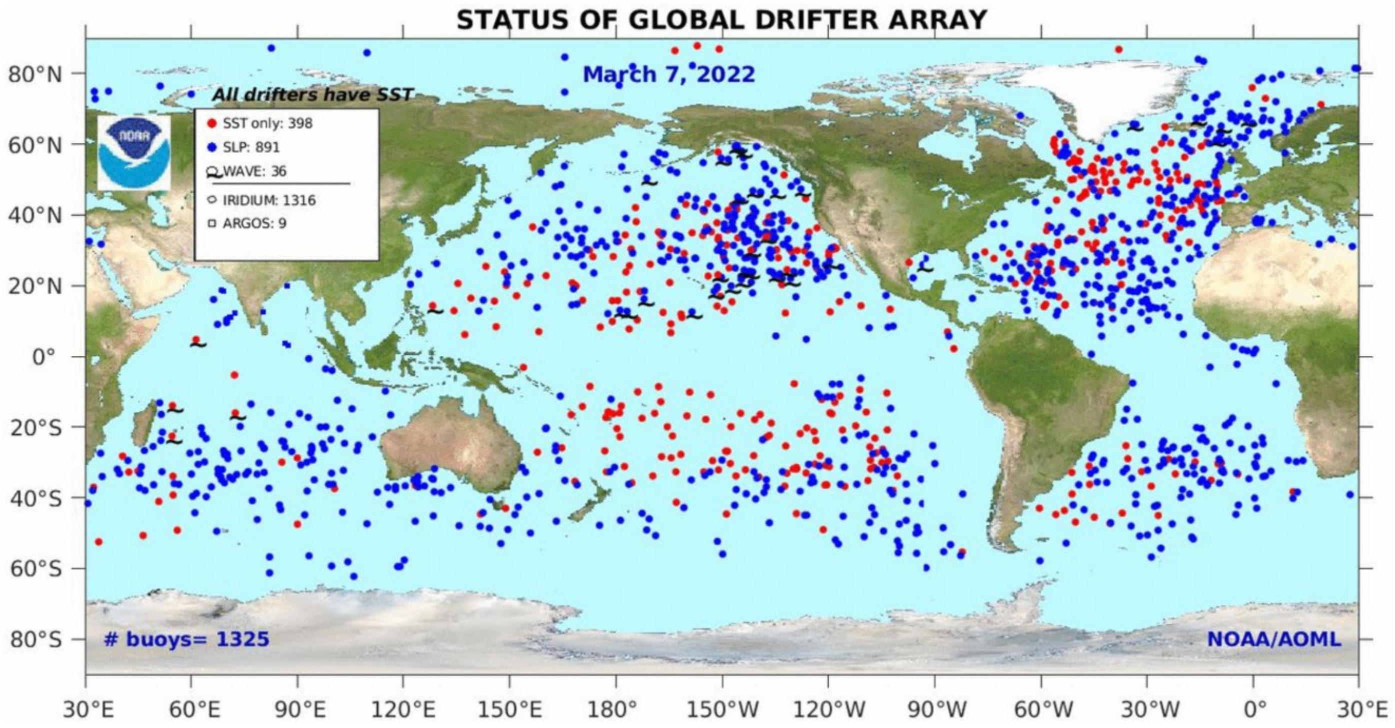

Figure 4. Status of the Global Drifter Array operated through NOAA AOML. Courtesy of the Global Drifter Program.

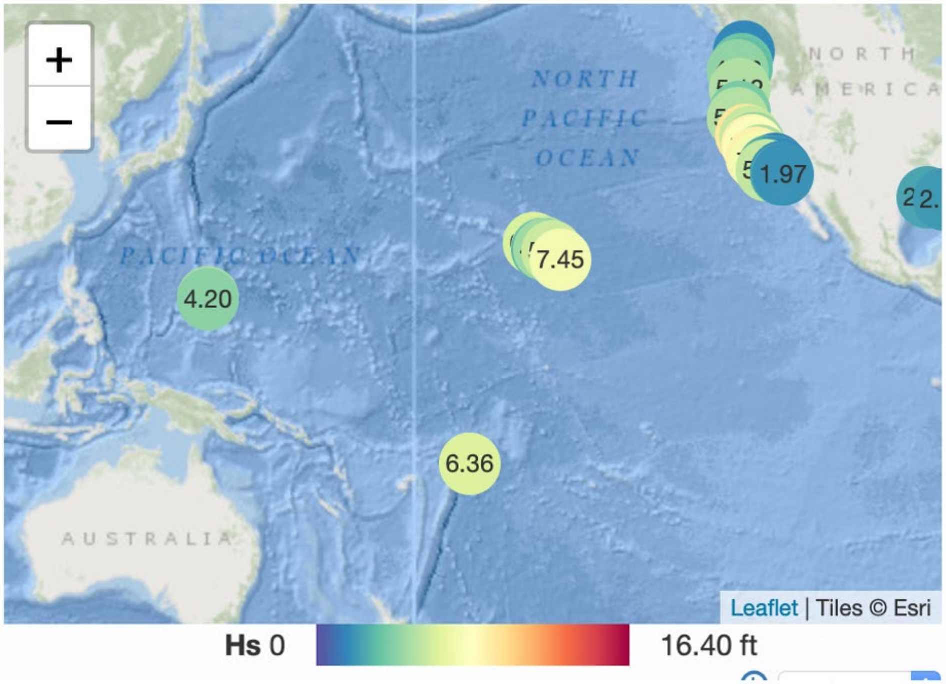

Figure 5. Locations of CDIP buoys with shading indicating significant wave height, Hs. Courtesy of the Coastal Data Information Program.

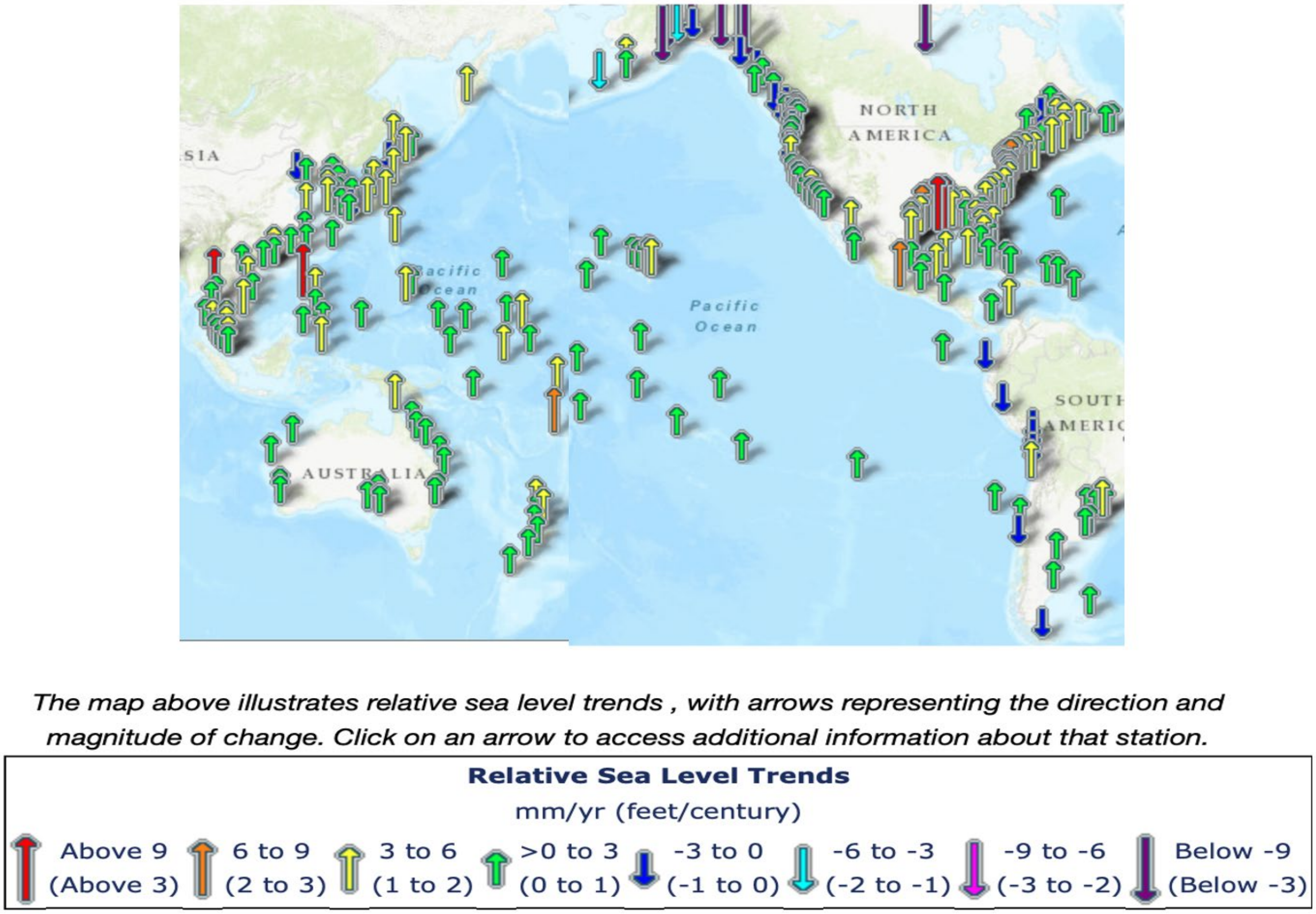

Figure 6. Tide gauges reporting to NOAA.

NDBC surface stations and moorings

Some additional islands in the western Pacific collect surface and ocean meteorological data that report to the NOAA NDBC (Figure 7, which also shows buoys from Figures 2–6). More island data may be available upon request or through specific country websites.

Saildrones

Saildrones missions in the Pacific Ocean have been carried out since 2017 (Meinig et al. 2019). Saildrones collect data of surface meteorology including radiative fluxes, near-surface ocean ocean properties, and sometimes vertical profiles of currents. These data can currently be used to calculate bulk air-sea fluxes. Efforts are ongoing to measure direct eddy covariance fluxes of momentum from Saildrones (Cronin et al. 2019). Not all saildrone vehicles have the same instrument package or capabilities. The Pacific Ocean Saildrone data are maintained at NOAA PMEL.

Atmospheric vertical profiles

NOAA maintains and distributes the Integrated Global Radiosonde Archive (IGRA), a collection of historical and near-real-time radiosonde and pilot balloon observations that provide high vertical resolution, quality-controlled records

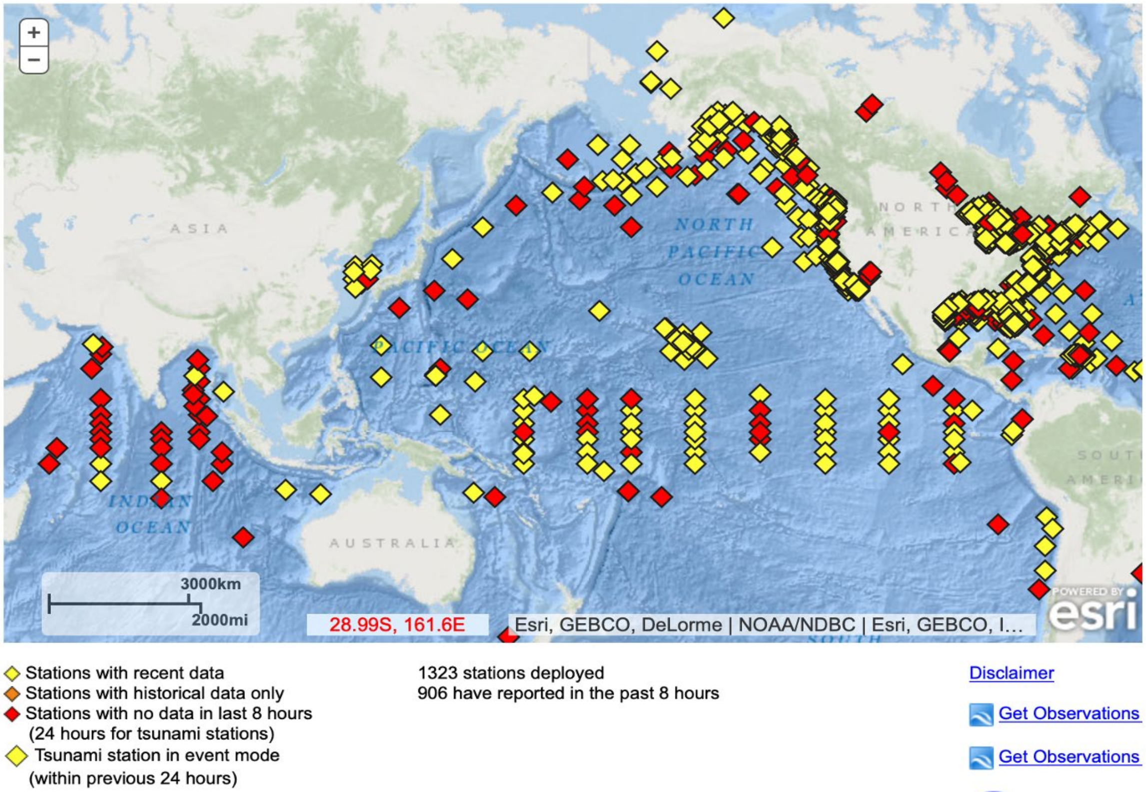

Figure 7. NDBC archive of ocean buoys consisting of TAO/TRITON, CDIP, ORS/OceanSITES buoy arrays (Figures 2–6) and a few additional buoys.

of temperature, relative humidity, dewpoint depression, wind direction, and wind speed (Durre et al. 2006; Durre et al 2018). Additionally, IGRA provides sounding-derived moisture and stability parameters for each sounding with suitable resolution and input fields. While this archive is expansive (Figure 8), records from small islands within the tropical belt (Figure 8, red markers) are extremely limited, particularly in the central and eastern Pacific Ocean. The presence of land can impact the marine character of these records, even over small tropical islands. For example, the remote equatorial western Pacific island of Nauru, which measures only 6 km long by 4 km wide, has

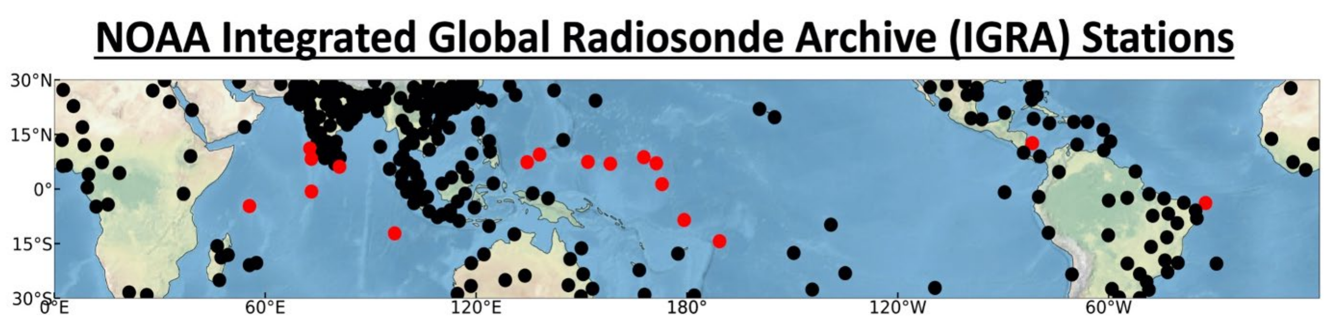

Figure 8. NOAA IGRA stations, where red markers indicate "small island" stations within the tropical belt ±15°), are defined as stations whose nearest corresponding 0.25° ERA5 reanalysis grid point has a land fraction less than 10%.

been shown to impact atmospheric boundary layer structure and generate cloud streets that can extend hundreds of kilometers downwind (Long and McFarlane 2012). The lack of in-situ soundings representative of marine environments in the tropical Pacific results in a void of records suitable for the calibration/validation of space-based observations and the validation of models and reanalysis.

References

Cravatte, S., and Coauthors, 2016: First Report of TPOS 2020. GOOS-215, 200 pp, https://tropicalpacific.org/tpos2020-project-archive/reports/.

Cronin, M. F., and Coauthors, 2019: Air-sea fluxes with a focus on heat and momentum. OceanObs'19. *Front. Mar. Sci*., **6**, https://doi.org/10.3389/fmars.2019.00430.

Durre, I., R. S. Vose, and D. B. Wuertz, 2006: Overview of the Integrated Global Radiosonde Archive. *J. Climate*, **19**, 53-68, https://doi.org/10.1175/JCLI3594.

Durre, I., X. Yin, R. S. Vose, S. Applequist, and J. Arnfield, 2018: Enhancing the Data Coverage in the Integrated Global Radiosonde Archive. *J. Atmos. Oceanic Technol*., **35**, 1753-1770, https://doi.org/10.1175/JTECH-D-17-0223.1.

Edson, J. B., and Coauthors, 2013: On the exchange of momentum over the open ocean. *J. Phys. Oceanogr*., **43**, 1589–1610, https://doi.org/10.1175/JPO-D-12-0173.1.

Elipot, S., R. Lumpkin, R. C. Perez, J. M. Lilly, J. J. Early, and A. M. Sykulski, 2016: A global surface drifter data set at hourly resolution. *J. Geophys. Res.: Oceans*, **121**, 2937-2966, https://doi.org/10.1002/2016JC011716.

Fairall, C. W., A. B. White, J. B. Edson, and J. E. Hare, 1997: Integrated shipboard measurements of the marine boundary layer. *J. Atmos. Oceanic Technol*., **14**, 338–359, https://doi.org/10.1175/1520-0426(1997)014<0338:ISMOTM>2.0.CO;2.

Fairall, C. W., E. F. Bradley, J. S. Godfrey, G. A. Wick, J. B. Edson, and G. S. Young, 1996a: Cool-skin and warm-layer effects on sea surface temperature. *J. Geophys. Res*., **101**, 1295–1308, https://doi.org/10.1029/95JC03190.

Fairall, C. W., E. F. Bradley, D. P. Rogers, J. B. Edson, and G. S. Young, 1996b: Bulk parameterization of air-sea fluxes for Tropical Ocean-Global Atmosphere Coupled-Ocean Atmosphere Response Experiment. *J. Geophys. Res*., **101**, 3747–3764, https://doi.org/10.1029/95JC03205.

Fairall, C. W., E. F. Bradley, J. E. Hare, A. A. Grachev, and J. B. Edson, 2003: Bulk parameterization of air-sea fluxes: Updates and verification for the COARE algorithm. *J. Climate*, **16**, 571–591, https://doi.org/10.1175/1520-0442(2003)016<0571:BPOASF>2.0.CO;2.

Kessler, W. S., and H. G. Hristova, 2019: Solomon Sea volume transport time-series measured by glider [Data set]. Scripps Institution of Oceanography Instrument Development Group, https://doi.org/10.21238/S8SPRAY2718A.

Kessler, W. S., H. G. Hristova, and R. E. Davis, 2019: Equatorward western boundary transport from the South Pacific: Glider observations, dynamics and consequences. *Prog. Oceanogr*., **175**, 208-225, https://doi.org/10.1016/j.pocean.2019.04.005.

Kessler, W. S., and H. G. Hristova, 2021: Climatology of Solomon Sea currents, temperature and salinity measured by glider [Data set]. Scripps Institution of Oceanography Instrument Development Group, https://doi.org/10.21238/S8SPRAY2718B.

Long, C. N., and S. A. McFarlane, 2012: Quantification of the Impact of Nauru Island on ARM Measurements. *J. Appl. Meteor. Climatol*., **51**, 628-636, https://doi.org/10.1175/JAMC-D-11-0174.1.

Meinig, C., and Coauthors, 2019: Public–private partnerships to advance regional ocean-observing capabilities: a saildrone and NOAA–PMEL case study and future considerations to expand to global scale observing. *Front. Mar. Sci*., **6**, 1-15, https://doi.org/10.3389/fmars.2019.00448.

Roemmich, D., and Coauthors, 2019: On the future of Argo: a global, full-depth, multi-disciplinary array. *Front. Mar. Sci*., **6**, 1-28, https://doi.org/10.3389/fmars.2019.00439.

Want to learn more? Dive into each of the TPOS 2020 Project reports:

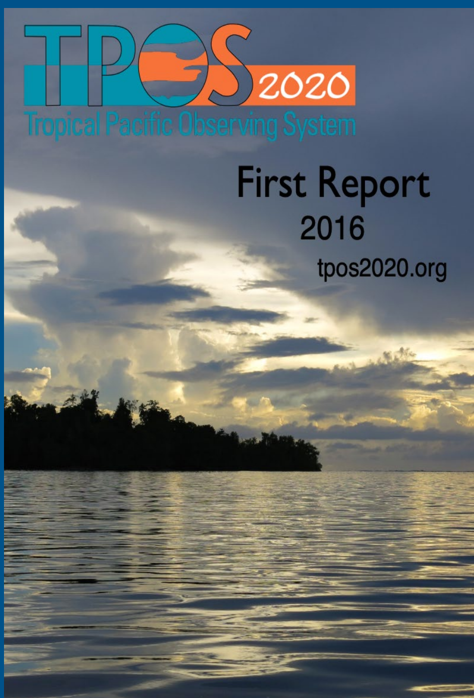

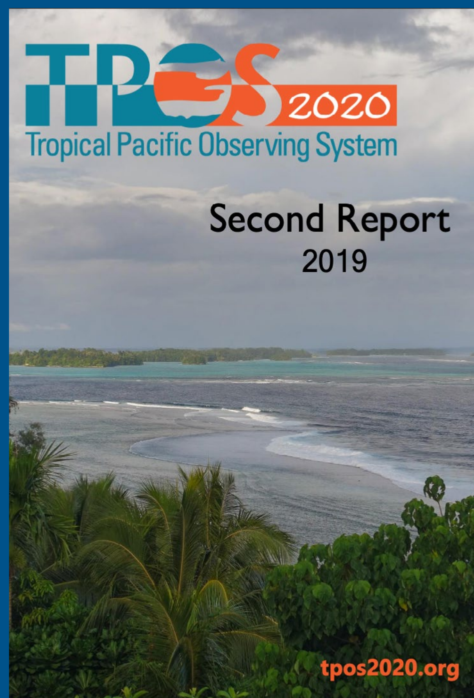

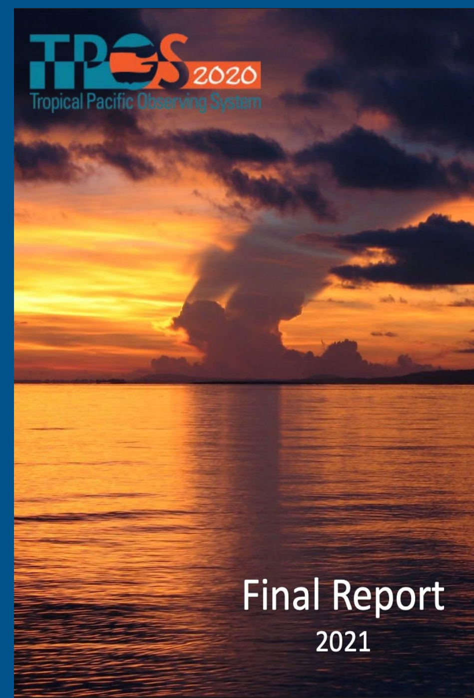

https://tropicalpacific.org/tpos2020-project-archive/reports/

usclivar.org
uscpo@usclivar.org
@usclivar.bsky.social

US Climate Variability and Predictability (CLIVAR) Program

US CLIVAR acknowledges support from these US agencies:

This material was developed with federal support of NASA (80NSSC17M0007), NOAA (NA11OAR4310213), NSF (AGS-1502208), and DOE (DE-SC0016332). Any opinions, findings, conclusions, or recommendations expressed in this material are those of the authors and do not necessarily reflect the views of the sponsoring agencies.